UNIVERSITY OF CALIFORNIA
RIVERSIDE

Moldless Hydrogel Scaffold for 3D Cell Culture

A Thesis submitted in partial satisfaction
of the requirements for the degree of

Master of Science

in

Bioengineering

by

Alexander Robert Brunelle

June 2017

Thesis Committee:
Dr. Jin Nam, Chairperson
Dr. Boris Hyle Park
Dr. William Grover

The Thesis of Alexander Robert Brunelle is approved:

Committee Chairperson

University of California, Riverside

ACKNOWLEDGEMENTS

I would like to thank my faculty advisor, Dr. Jin Nam, for his continuous support and guidance. Without his valuable expertise in biomechanical signaling, stem cell research and biomaterials, I would not be where I am today. He has helped me to become a better student, engineer and researcher.

I would also like to thank the other members my Thesis Defense Committee, Dr. B. Hyle Park and Dr. William Grover, for volunteering their time and agreeing to evaluate my work as a graduate student.

Finally, I would like to thank my loving family. Thank you, Mom and Dad, for always supporting me and pushing me to be better in every aspect. And to my wonderful fiancée Jessie, you have been my rock for the last ten years. I will never be able to repay you for your support, and your compassion, as I endeavored to graduate.

ABSTRACT OF THE THESIS

Moldless Hydrogel Scaffold for 3D Cell Culture

by

Alexander Robert Brunelle

Master of Science, Graduate Program in Bioengineering
University of California, Riverside, June 2017
Dr. Jin Nam, Chairperson

Many fabrication methods for scaffolds made with biodegradable polymers and hydrogels have shown promise for tissue engineering applications. Utilizing both, a hybrid scaffold can be manufactured with extracellular matrix-like topography and improved mechanical stability. Hybrid scaffolds often require complicated, multistep construction protocols and the use of a mold to contain hydrogel solutions until they gel. However, by electrospinning a thermo-sensitive hydrogel, poly (ethylene glycol)-poly (N-isopropylacrylamide) (PEG-PNIPAAm), blended with a hydrophobic, biodegradable polymer, poly (ε-caprolactone) (PCL), a microfibrous, 3-dimensional (3D) scaffold was fabricated for *in vitro* cell seeding and tissue morphogenesis applications. PEG-PNIPAAm hydrogels were optimized for the lowest critical concentration (5 wt. %) by increasing the free-radical polymerization reaction concentration of the starting materials. The resulting hybrid scaffold was further optimized for the ideal blending ratio of PEG-PNIPAAm/PCL

(13:9), scaffold porosity (90%) and average fiber diameter (11 μm) that allowed for uniform cell seeding, and subsequent encapsulation of cells within the hydrogel. With a single-step process, cells were seeded uniformly within the hybrid scaffold while the PEG-PNIPAAm was dissolved by the cell/media solution. Dissolved PEG-PNIPAAm surrounding the seeded cells and filled the scaffold's pore volume without the use of a mold to contain it. When incubated at 37 °C, the seeded cells were encapsulated within the hybrid scaffold by the thermo-sensitive hydrogel. The electrospun, hydrophobic PCL fiber network remained as a structural support, increasing the compressive, elastic and viscoelastic properties of the scaffold above both pure PEG-PNIPAAm and pure PCL scaffolds. Culturing of mesenchymal stem cells (MSCs) within the hybrid scaffolds for two weeks, under a model chondrogenic differentiation system, exhibited increased chondrogenic gene expression and proteoglycan deposition compared to pure PCL controls with similar scaffold porosity and fiber diameters. The addition of a customizable thermo-sensitive hydrogel, like PEG-PNIPAAm, within a 3D-structured, PCL network produced a hybrid scaffold with many potential applications for tissue morphogenesis.

TABLE OF CONTENTS

LIST OF TABLES

LIST OF FIGURES

CHAPTER 1. LITERATURE REVIEW

1.1. Tissue Engineering

Cell and tissue necrosis is invariably irreversible. While clinical treatments for tissue replacement such as prosthetics and allografts exist, complications commonly arise requiring further research into more promising alternatives. The process of tissue engineering is a novel technique which hopes to better understand and control cell development and repair.

Prosthetics primarily utilize non-organic biomaterials (metal/ceramic) to replace damaged or diseased tissue. Superior mechanical strength makes them attractive as an option for load-bearing tissue replacements, such as orthopedic tissue[1-2]. Their material composition can have serious adverse side-effects such as host-immune rejection, corrosion and attrition[3]. Additionally, their non-organic constitution prevents their use for replacing tissue that requires more complicated physiological function. Recent developments into soft tissue prosthetics have produced potentials for simple replacements of organs involving fluidic movement including a continuous-flow total artificial heart. Biomaterials capable of both performing complex physiological functions and reacting in real-time to chemical

and physical changes remains impossible without incorporating natural tissue[4]. Therefore, implants utilizing living cells remains the most promising option for tissue replacement.

To date, the standard method for replacing a patient's failing/damaged organ with living tissue is the transplantation of an organ from a donor. Since the first successful kidney allograft in 1954, organ transplants have become commonplace. Today, the request for organ donations greatly exceeds the number of available organs[5]. Graft rejection, systemic infection and sepsis are some of the more severe side effects seen with allografts and xenografts[6-7]. Autografts reduce the occurrence of graft rejection, but are only transplantable from non-essential locales, such as skin, bone and cartilage[8-11]. The inadequate supply of grafting material and severe side effects associated with it prompted the scientific community to facilitate in vitro/in vivo morphogenesis using a more available resource, pluripotent stem cells.

The successful harvest of embryonic stem cells (ESCs) provided significant breakthroughs for tissue engineering. Possessing proliferative and pluripotent properties, they are capable of dividing numerous times and differentiating into all three germ layers (endoderm, mesoderm and ectoderm)[12]. New methods have found and isolated multipotent adult somatic stem cells, like mesenchymal stem cells (MSCs), and have induced pluripotency in already differentiated adult tissue (iPSCs)[13-14]. The potential of autologous stem cell harvesting for patient-specific tissue grafts reduces the possibility of the host rejection because the tissue is

cultured from cells originating from the same organism. Currently, it takes a few million iPSCs with controlled differentiation to even potentially produce a fully operational organ. With the continued development of iPSCs, the availability of treatment for life threatening illness and waiting times for transplant lists can be significantly reduced.

Researchers have determined three fundamental components necessary for successful tissue morphogenesis. By seeding cells capable of differentiating the desired phenotype into a structural, 3-dimensional (3D) scaffold and supplying chemical and biological signals that direct and maintain phenotypic characteristics, cells will proliferate and form the tissue morphology desired for implantation (**Fig. 1.1**). While biological signaling of pluripotent cells has been predominately dictated from studies of natural tissue, stem cells and cellular signaling pathways, the ideal biomaterials for tissue scaffolding remains contested.

This chapter will discuss the potential implantable biomaterials currently available for tissue engineering. Their benefits and consequences of constituents, fabrication methods and their potential applications are compared here in. Finally, the use of hybrid scaffolds and the method of electrospinning biocompatible polymers, and their applications, are discussed in detail.

1.2. Biocompatible Tissue Scaffolds

Studies of biomaterials used in vivo have helped to identify desirable characteristics for tissue scaffolds that best operate like native cell substrates.

Potential biomaterials must illicit little to no adverse reaction from the host's immune system. Additionally, utilized biomaterials should be absorbed by the host thereby preventing additional surgery. Cytotoxic by-products may also occur, and must be taken into consideration. Scaffolding used for cell seeding and infiltration must also provide cells with adequate porosity and attachment points. For cells to successfully replace implants, additional surface area from increased pore volumes can be advantageous. Like native extracellular matrices (ECMs), interconnected porous scaffolds provide cells with 3-D motility and superior fluid dynamics for nutrient diffusion[15-16].

1.1.1. Biodegradable Polymers

Cells utilize ECM, organic polymer chains as a substrate for their cell attachment and motility[17]. They are made up of hydrophilic polysaccharide and polypeptide polymer chains with porous, 3D structures. Cells can produce their own ECM by intracellular synthesis or recycling pre-existing substrates and reorganizing them for improved functionality. Research also shows that cells can be internally manipulated by the mechanical characteristics of the surrounding ECM[18]. Therefore, many scaffolds have used polymers as a scaffolding for cells to most resemble the native tissue and influence the cell's signaling pathways. Polymer-based scaffolds are made by polymerizing naturally-derived or synthetic polymers for scaffold fabrication.

Natural Polymers

Natural polymers (collagen, chitosan, hyaluronic acid, etc.) are

advantageous because they are synthesized from ECM derivatives and already have the desirable biocompatibility suitable for an acceptable scaffold[19-21]. Yet, their natural components also make them easily degraded and provides insufficient mechanical properties for load-bearing tissue. Natural polymers have hydrophilic properties which result in rapid dissolution in aqueous conditions, preventing them from providing implanted cells with a continuously stable scaffolding for their gradual morphogenesis without further modification.

Synthetic Polymers

Synthetic polymers are a viable alternative for biodegradable, polymer-based scaffolds. Unlike natural polymers, synthetic polymer chains can easily be modified, providing a desirable versatility in scaffold design. Their degradation and mechanical properties can be tailored by incorporating hydrophobic monomers, allowing slower degradation for prolonged tissue development and preventing dissociation in aqueous solutions for improved stability and strength[22]. This improves scaffold designed for cell infiltration since their porosity can be dictated during fabrication without dissolving or collapsing after implantation/seeding.

Common synthetic polymers used for tissue scaffolding include polyester-based chains such as poly (glycolide) (PGA), poly (lactide) (PLA) and poly (lactide-co-glycolide) (PLGA)[23-25]. Though PGA is a synthetic polymer, it degrades into glycolic acid, which can be utilized by the cells they support for metabolic nourishment[26]. Similarly, PLA is degraded into lactic acid, a common byproduct of

metabolic fermentation. Concentrated accumulation of acidic byproducts can lead to tissue damage, especially with PLA and PGA, where their degradation occurs faster than the absorption of their by-products[27]. Furthermore, PGA and PLA are brittle polymers which undergo plastic deformation[28]. The property of elastic deformation must be considered for tissue engineering scaffolds that would be subject to repetitive strain. Its importance is particularly relevant with orthopedic implants as research shows that cyclic strain can facilitate articular cartilage rejuvenation and direct chondrogenic differentiation[29-31]. PGA and PLA can be incorporated into other polymer scaffolds made from co- and terpolymers, supplying their benefits to polymers with better mechanical properties, like poly (**ε**-caprolacetone) (PCL)[32].

PCL is commonly used for tissue scaffolds[33-35]. It has a prolonged degradation rate, making it more appropriate for orthopedic implants than either PGA or PLA[36-37]. Studies have shown PCL can even stand up to cyclic strain common for musculoskeletal tissue[38]. It is also dissolvable in many organic solvents, beneficial for scaffold fabrication into desirable shapes and structures. Its degradation occurs due to gradual esterification of its polymer chains, shortening the molecular weight for easy macrophage phagocytosis[39]. Studies into the longevity of PCL in vivo report intact implants after two years[40]. Copolymerization with PLA or PGA has also shown to significantly increase its degradation[41]. PCL is hydrophobic and therefore prevents rapid dissociation and allows it to maintain its mechanical strength during tissue morphogenesis. Cell attachment onto PCL is

difficult without first functionalizing its surface. Once additional polar functional groups are made with methods like plasma etching, PCL can be coated with polypeptide chains for better cell attachment[42-43]. Methods to increase the hydrophilicity of 3D PCL scaffolds, like using hydrophilic polymers, or hydrogels, helps to support fluid transport and cell infiltration.

1.1.2. Hydrogels

Like other biodegradable polymers, hydrogels act as ECM-like networks for cell motility and support. Hydrogels can be used as two-dimensional (2D) substrates or as 3D scaffolds for cell cultures or tissue morphogenesis. Natural ECM-derived hydrogels, such as collagen and chitosan, are commonly used as hydrogels because they are exceptionally hydrophilic, especially before crosslinking[44-46]. Poly (ethylene glycol) (PEG), PLGA and poly (N-isopropylacrylamide) (PNIPAAm) are synthetic polymers that can be used as hydrogels, also due to their hydrophilicity[47-50]. Hydrogels are generally preferred over other polymer options because their highly porous structures (>90%) are made of nanoscopic polymer fibers similar in size to natural ECM. Their ability to remain in solution before crosslinking also allows them to be injected into the body rather than requiring surgical implantation[51]. Hydrogels have also been used to encapsulate and slowly diffuse drugs for prolonged drug release studies[52-54]. Regardless of the hydrogel polymer constituents, they all require crosslinking to prevent immediate dissociation in aqueous conditions. The choice in hydrogel

depends on the application in mind and the desired method for crosslinking. Like natural polymers scaffolds, the drawbacks with hydrogels are an increased degradation and limited mechanical capabilities. However, both can be tailored by increasing the crosslinking density[55-57]. Other important considerations when choosing a hydrogel include its swelling ratio, biodegradability, degradation rate and incorporation of cell attachment sites.

Crosslinking chains act as tethers, connecting separate polymer chains to one another. Shortening the length of crosslinking chains or increasing the density can restrict the swelling ratio of a hydrogel and thus limit the pore size and overall porosity[58]. This can also increase the rigidity of the hydrogel since the crosslinking chains restrict free-flowing viscoelastic movement of the polymer when strain is applied[59-61]. Increased crosslinking hydrogels also prolongs its degradation due to the multiple connections made between polymer chains, increasing the number of chains requiring cleavage for dissociation[60, 62-63].

Physically Crosslinked Hydrogels

Physically crosslinked gels are the result of environmental stimulation of the polymer chains. Both temperature and pH sensitive hydrogels can be utilized for tissue scaffolding or drug release nanoparticles[64-67]. The mechanics of gelation is a result of changes in the hydrophobic nature of the polymer chain by ionic or temperature changes in the environment. For instance, PNIPAAm is classified as a reverse thermosensitive hydrogel because at temperatures below its lower

critical solution temperature (LCST) it is hydrophilic and remains in solution. However, when temperature increases past its LCST, PNIPAAm's amide groups undergo a conformational change that promote hydrophobic attraction and aggregation, overpowering the hydrogen bonds previously formed with the solvent (**Fig. 1.2a**)[68]. Ionic hydrogels, such as poly (acrylic acid) (PAA), are affected by changes in solvent pH depending on its molecular weight[69]. Within acidic solutions, the anionic polymer PAA forms a globular conformation, while basic solvents cause it to swell (**Fig. 1.2b**).

Chemically Crosslinked Hydrogels

Covalent bonds can be used to crosslink polymer chains. This process can occur either during or after initial polymerization. The covalent bonding of polymer chains can occur with a variety of methods, including photopolymerization (**Fig. 1.3**) and chemically substituting existing monomer moieties for polymer chains with reactive ends (**Fig. 1.4**)[49, 70-72]. For 3D cell encapsulation with a hydrogel, crosslinking usually occurs after cells have been seeded in the hydrogel, while it is still dissolved in solution. This is because the decrease in porosity for stiffer hydrogels would limit the infiltration of cells entering the scaffold after crosslinking. The chain length of the crosslinking polymer can be modified to allow for increased pore size, or the polymer backbone can also be combined with an environmentally sensitive hydrogel chain, which would remain swollen under the specific conditions[73-74]. However, the methods for chemically crosslinking require initiators,

most of which are cytotoxic or produce harmful byproducts[75-76]. As a result, chemically crosslinking is best performed prior to cell seeding and should have any unreacted materials or byproducts removed with purifying washes. The disadvantage then becomes the limitation of scaffold mechanical properties to allow for larger pore sizes for cell seeding. Therefore, methods have been investigated combining the strengths of both physical and chemical hydrogels.

Since physical crosslinking acts as the mechanism for gelation, chemical cross linkers can supply hydrophilic chains that help to retain water as a gel [74]. The result resembles an interconnected polymer network that swells, when dissolved, and aggregates into small hydrophobic regions connected by hydrophilic chains, when it gels (**Fig. 1.5**). Similar effects are seen with the polymerization of environmentally sensitive and insensitive monomers along the same chain[77]. Crosslinking hydrophilic chains affects the gelation conditions of environmentally sensitive hydrogels. When the hydrophilic crosslinking chains swell in aqueous solutions, environmentally sensitive chains can become too far apart to aggregate when stimulated (below the critical concentration).

Regardless of their degree of crosslinking, hydrogels are still unable to compete with the mechanical strength of non-dissolvable polymers, like PCL. Current research efforts have produced unique hybrid scaffolds ideal for multiple tissue engineering applications requiring load-bearing scaffolds.

1.2. Electrospinning

The technique of electrospinning was patented in 1934 as a novel method to produce a porous network of non-woven polymer fibers[78]. Its resemblance to natural ECM (**Fig. 1.6(a)**) makes electrospun fibers (**Fig. 1.6(b)**) an attractive method for fabricating scaffolds utilized in tissue engineering. Other scaffolding designs, such as polymer films and 3D-printed structures, are unable to produce porous structures like electrospun scaffolds. Films made with hydrophobic polymers provide no pores, while 3D-printed scaffolds are limited by their printing resolution and are unable to produce the same porosity as electrospun fibers. Increased porosity provides electrospun scaffolds with a high surface-to-volume ratio improving the cells ability to adhere to multiple points, and supporting integrin-dependent pathways with attached cells. Electrospun scaffolds can be fabricated for 2D and 3D cell attachment, depending on the fiber size. The diameters of electrospun fibers can range from 10 nm to 10 μm and help control the pore sizes for 3D cell seeding and motility[79-80]. The fibrous polymers scaffolds can be tailored to desired specifications by manipulating environmental parameters and intrinsic solution properties during spinning.

1.2.1. Electrospinning Setup and Fundamental Theory

In a traditional electrospinning setup, a polymer solution is placed inside of a syringe, and is ejected through a capillary nozzle, charged by a high voltage source, and aimed at a grounded or oppositely charged collector (**Fig. 1.7**). The

polymer solution is then launched through the capillary nozzle at a predetermined rate by a syringe pump. Without charging the nozzle, the solution forms a droplet, its shape held by the surface tension of the solvent, and falls as a drip when the force of gravity overcomes its surface tension. The voltage source charges the nozzle and the collector and creates an electric field between them, inducing a charge onto the polymer solution's surface as it is being expelled[81-82]. The induced charge causing a repulsive force on the solution by the nozzle and an attractive force by the collector. The combined repulsion and attraction overpowers the surface tension and forces the droplet's hemispherical shape to elongate into a cone, known as the Taylor Cone. The Taylor Cone ends in a thin jet of polymer solution that ejects continuously. Still charged by the electric field, the thin jet whips through the air toward the collector. Centripetal forces cause further elongation of the polymer fiber. Simultaneously, the volatile solvent evaporates, solidifying the polymer fiber before it lands randomly on the collector. Over time, the fibers pile up on the collector to form a randomly non-woven scaffold. The amount of charge required to electrospin a polymer solution depends on several parameters, including: the characteristics of the polymer solution, the humidity, temperature and airflow of the surrounding environment, the flow rate of the ejecting solution and the distance needed to travel from the nozzle tip to the collector.

1.2.2. Tailoring Fiber Diameter and Morphology

Once a polymer solution is selected for electrospinning, many parameters

must be optimized for the desired fiber morphology and diameter. Cylindrical fibers are the preferred morphology for electrospun fibers, because of their uniform shape and resulting pore size (**Fig. 1.8(a)**). Undesirable morphologies include ribbons (**Fig. 1.8(b)**), where the flat fibers form compact scaffolds with small pore sizes because of their wide, two-dimensional structure, and beads (**Fig. 1.8(c)**), which appear as extraordinarily thin fibers connecting large spherical aggregates of polymer[83-86]. Nanometer sized cylindrical fibers more closely resemble natural ECM and are ideal for 2D cell scaffolds. However, micrometer size fibers produce larger pores, and are more beneficial for 3D cells scaffolds with uniform cell attachment without additional steps to increase pore size. Larger fibers produce greater residual charge which repulse fibers just reaching the collector causing greater distances between fibers.

Tailoring Solution Properties for Optimized Electrospun Fibers

As the process of electrospinning requires generating an electric field that counters the surface tension of the polymer solution, properties that affect the surface tension are important for optimizing the polymer solution. A solution's viscosity is directly proportional to the magnitude of its surface tension. A charged viscous fluid will be able to resist the forces of an electric field and gravity more than a less viscous fluid. The viscosity of a solution will increase with higher concentrations of dissolved polymer. Therefore, the viscosity of the solvent and the concentration of the polymers within the fluid will affect the electrostatic forces

necessary to create a Taylor cone[87-88]. When the electric field is not adjusted according to the solutions viscosity, viscous solutions will form beads (**Fig. 1.8(c)**) due to the increased surface tension, and less viscous solutions will form multiple Taylor Cones and fiber diameters will be reduced[89-90].

The storage of an electric charge within the solvent and its conductivity is also thought to play a role during electrospinning. Increasing the dielectric constant of a solution by adding another solvent with a higher dielectric constant, results in smaller fiber diameters[91]. The higher conductivity of the mixed solvent increases the magnitude of the electric field forces, resulting in lower surface tension.

Morphology and fiber topography can also be affected by the properties of the dissolved polymers. Ribbons are believed to be the result of hollow fibers forming when the polymer collects at the surface, like a shell. When the solvent evaporates, the polymer shell solidifies, and then collapses, as the remaining solvent inside the tube evaporates as well[84]. The phase separation of the polymer from the solvent also affects the surface of formed fibers. Local regions of concentrated polymer with similar regions of concentrated solvent can form during convective evaporation and the thermodynamics of the solution become unstable[92-93]. Evaporation of the solvent leaves nanoscopic pits in regions with low polymer concentrations.

Tailoring Environmental Parameters for Optimized Electrospun Fibers

During electrospinning, fibers only form if the solvent evaporates before

reaching the collector. As the solvent is evaporating, the drying polymer fibers are also being elongated. When the rate of evaporation is slow, the electrostatic repulsion of the drying fibers decreases and will result in thick, possibly wet, fibers. While the solvent's intrinsic properties play a role in the rate of its evaporation, the environment around the electrospinning fiber can also affect it. Although, surface tension holds the solvent molecules at its surface together, the equilibrium of liquid and vaporized solvent at the surface of the solution is additionally affected by extrinsic factors. Increasing temperatures can lead to a rise in the kinetic energy of the molecules at the solvent's surface and thereby prevents condensation into the solution[94-95]. Humidity, a higher concentration of water in the air can decrease the rate of evaporation[94].

The flow rate of the ejected polymer solution changes the surface tension forces at the needle tip[79, 96]. The increase of fluid at the tip diffuses the charge from the electric field across a larger volume and decreases the electrostatic repulsion from the needle. The voltage at the tip and the collector must be adjusted to prevent beading of the fibers. Therefore, adjusting the flow rate has a greater effect on the fiber morphology than its diameter.

The distance between the tip and the collector contributes to the size of the fiber diameter. When electrospinning solvents with slow evaporation rates, increasing the distance to the collector can increase the amount of time given for evaporation and elongation. The further the fibers must travel, the longer its exposure to flowing air and the thinner the diameters can become. Distance also

affects the strength of the electric field. Therefore, the voltages must be increased with greater distances. Similar fiber diameters seen with traditional distances (>10 cm) and voltage gaps can be achieved with lower voltages at smaller distances (500 μm), provided a minimum distance is maintained proportional to the length of the Taylor Cone[97-98].

While many adjustable parameters are intimately connected to the strength of the electric field, the voltage that can be applied has limitations. It is possible for higher voltages to result in branching of the Taylor Cone[99]. The increased repulsion forces exerted on the polymer jet is believed to cause multiple Taylor Cones, and subsequently, non-uniform fiber diameters in the scaffold. Therefore, electrospinning can only be achieved by maintaining a delicate balance of all the parameters affecting a solution's surface tension and the electric field[79].

Electrospinning is not limited to only hydrophobic polymers like PCL. Any polymer can be electrospun given the right solvent and parameters, including hydrophilic hydrogels. Examples of electrospun fiber mats composed of hydrogel polymers have been explored, such as PNIPAAm, PEG, PLGA and gelatin[100-103]. Creating electrospun fibers from hydrogels does not improve their porosity or mechanical characteristics. Instead, the electrospinning hydrogels improves their rate of dissolution within aqueous media. Hydrogels normally require hours to dissolve even when ground into powders. By electrospinning them into nanometer or micrometer sized fibers, their surface area to volume ratio increases and subsequently so does their dissolution rates. However, once introduced to an

aqueous solution, even thick 3D scaffolds collapse and lose their structure permanently. Recent research efforts have explored unique hybrid scaffolds which incorporate hydrophobic and hydrophilic polymers together within a single scaffold. Their design makes them ideal for multiple tissue engineering applications requiring load-bearing scaffolds while incorporating ECM-like porosity and topography.

1.3. Hybrid Scaffolds

Hybrid scaffolds incorporating both hydrogels and non-dissolvable polymers have been developed as potential tissue scaffolds. Specifically, non-dissolvable polymers are utilized to provide a structural foundation and enhance the scaffold's mechanical properties, while hydrogels are incorporated to provide the scaffold with a biomimetic surface topography for improved cell attachment and motility, while maintaining significant porosity. Attempts at producing hybrid scaffolds have utilized unique fabrication techniques, including: biological 3D-printing and electrospinning.

3D printing has recently emerged as a popular means of digitally designing devices with reasonable detail for a variety of applications. Printers dispense liquid or heated materials, like polymers, in organized patterns, creating functional devices. Multiple types of material are generally used for 3D printing, including: plastics, like nylon and resin, and metals, like steel, gold and titanium. Printer resolution varies between models, however some can create structures with a

resolution around 5 μm[104]. Biological 3D printers can even construct 3D-printed structures with cells already within the scaffolding solutions (**Fig. 1.6**)[105-106]. In this way, hybrid scaffolds can be fabricated already with seeded cells. However, the resolution of the scaffolds they produce are still much larger than scaffolds fabricated with different techniques. While electrospun fibrous scaffolds can produce ECM-like fiber meshes with nanoscopic fiber diameters and highly interconnected pore volumes, 3D-printers can only create macroscale, with micrometer-wide channel-like pores. To reduce the volume of empty fluid in their pores, some 3D-printed scaffolds have printed hydrogels within them that more accurately represents the environment in the human body[107]. These scaffolds still commonly use non-porous, hydrophobic polymers as a structural backbone because of their mechanical benefits. This results in non-uniform cell seeding and ultimately extends the time needed for the cells infiltration and the replacement of the non-porous structures by growing tissue. The resolution of a printer also restricts the level of detail that can currently be used to design scaffold topography. ECMs provide a mesh like substrate for multiple cell attachments to many individual polymer fibers, often in different orientations, adding to the strength of cell adhesion. However, nano-sized detail is required to produce similar topography on the surface of a fabricated scaffold. Unlike 3D-printers, electrospun fibers provide the appropriate resolution for biomimetic scaffold topography and pore size.

Electrospun fibers are advantageous in the fabrication of hybrid scaffolds.

Xu et al. combines sheets of PCL electrospun fibers with bio-3D-printed hydrogels infused with cells, to create multi-layered, 3D scaffolds for chondrocyte tissue implants[108]. While this technique improves the porosity of its structural PCL component, and allows for easier cell infiltration compared to solid 3D-printed PCL scaffolds, the beaded fiber morphology decreases the pore sizes, preventing optimal cell motility into the scaffold. Electrospun fibers can be divided into sections and mixed with hydrogels improving their mechanical moduli by almost double[109]. Disadvantageously, the cut fibers do not form an interconnected network. With other electrospun scaffolds, individual fibers support the surrounding fibers, improving the stability of the structure. Other methods for incorporating hydrogels with electrospun fibers includes saturating the porous scaffolds with dissolved hydrogels and then crosslinking them, electrospinning hydrogels blended with hydrophobic polymers or creating core shell fibers with hydrogels coating the outside of individual fibers as a shell. Kai et al electrospun PCL with gelatin hydrogels as both a blend and as a coaxial fiber[110]. The coaxial fibers improved the strength of the scaffold over the blended fibers, and significantly prolonged its dissociation over just gelatin. Predominately, these intertwined, electrospun, hybrid scaffolds are only made with nanometer diameter fibers and result in limited pore size preventing 3D cell seeding.

1.4. Conclusions

With the continual growth of the tissue engineering field, there is an ever-

increasing variety in available scaffolds. Yet, since its inception, electrospinning has presided as an authoritative method for fabricating biomimetic scaffolds. Electrospun scaffolds provide researchers with the versatility and customizability to fine-tune their scaffolds for a multitude of applications. 2D scaffolds have been unable to effectively facilitate tissue morphogenesis. Therefore, 3D scaffolds are necessary to engineer higher caliber artificial tissue grafts. While hydrogels can be used as 3D scaffolds, their low mechanical characteristics cannot support tissue that requires a certain level of load-bearing strength, such as bone or cartilage. Conversely, electrospun, hydrophobic polymers, superior mechanical moduli, may lack the porosity and the structural resemblance to natural ECM seen with hydrogels. Their fiber diameters must be increased to form larger pores for 3D cell infiltration.

Methods for hybrid scaffold fabrication provide researchers with the means to incorporate both hydrogels and hydrophobic, supportive polymers together within the same scaffold. This promising technique removes the limitations of the individual scaffold types, expanding their potential for novel tissue scaffolds for supporting novel types of tissue. Predominately used for soft, non-load-bearing tissue morphogenesis, hydrogels can now be provided the mechanical support necessary for growing tissues that experience significant strain. Similarly, hydrophobic polymers, made porous for 3D cell seeding, can incorporate hydrogels to provide hydrophilic nano-sized substrates for improved motility and attachment. In these chapters, the synthesis of a novel hybrid scaffold design is

described that provides cells seeded within it a customizable and reliable structure for successful tissue growth. The optimization covered in these chapters, explores the use of our hybrid scaffold in chondrogenic tissue development, and suggests an ability to be easily modified for successful stem cell differentiation toward other cell lineages.

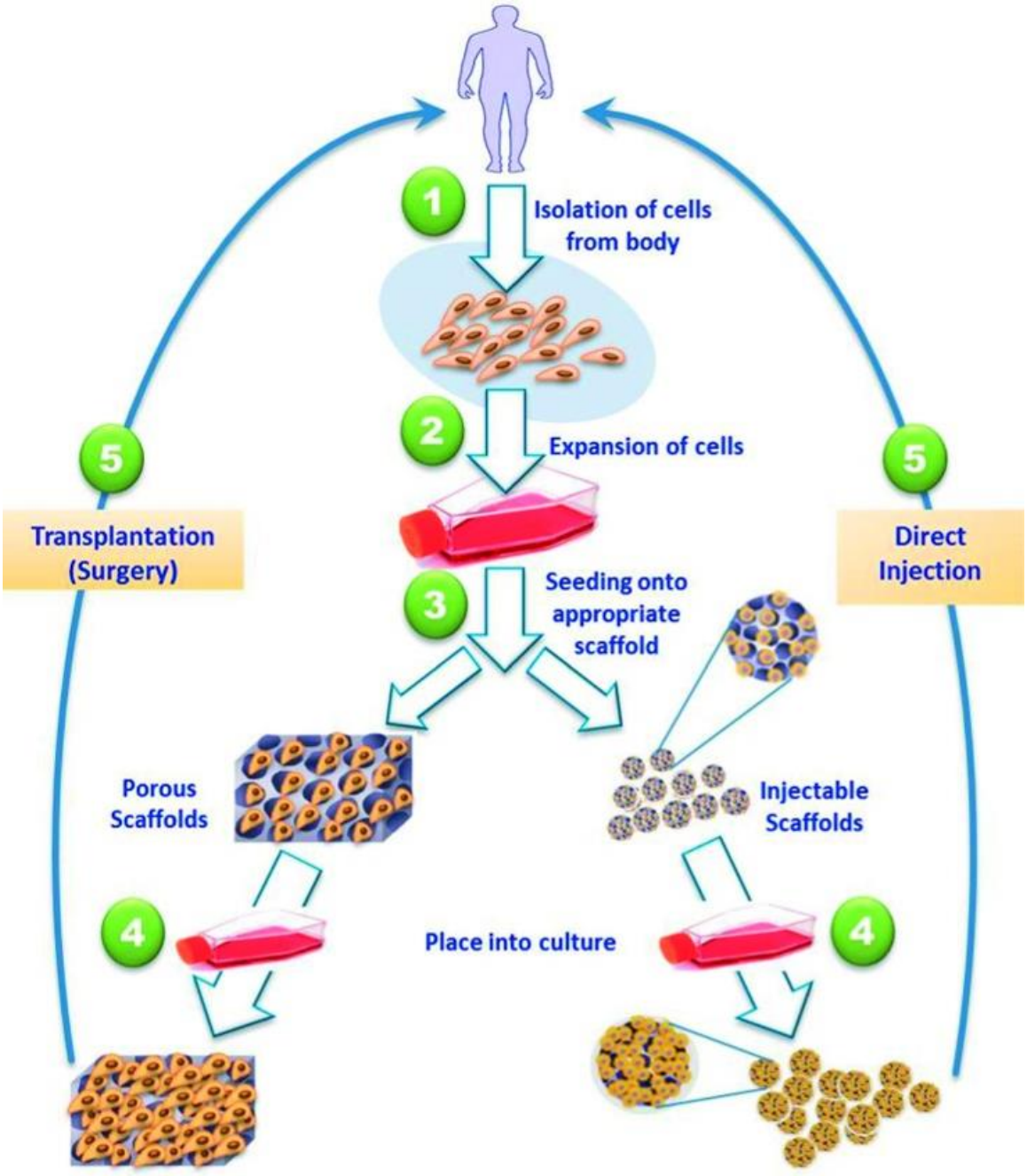

Figure 1.1. Autologous tissue transplants. Cells from the same organism can be utilized for tissue engineering by: (1) isolating cells from the host's body, (2) expanding them in culture, (3) seeding them onto an appropriate scaffold for the desired method of implantation, (4) re-culturing them and (5) transplanting or injecting them back into the host (taken from [111]).

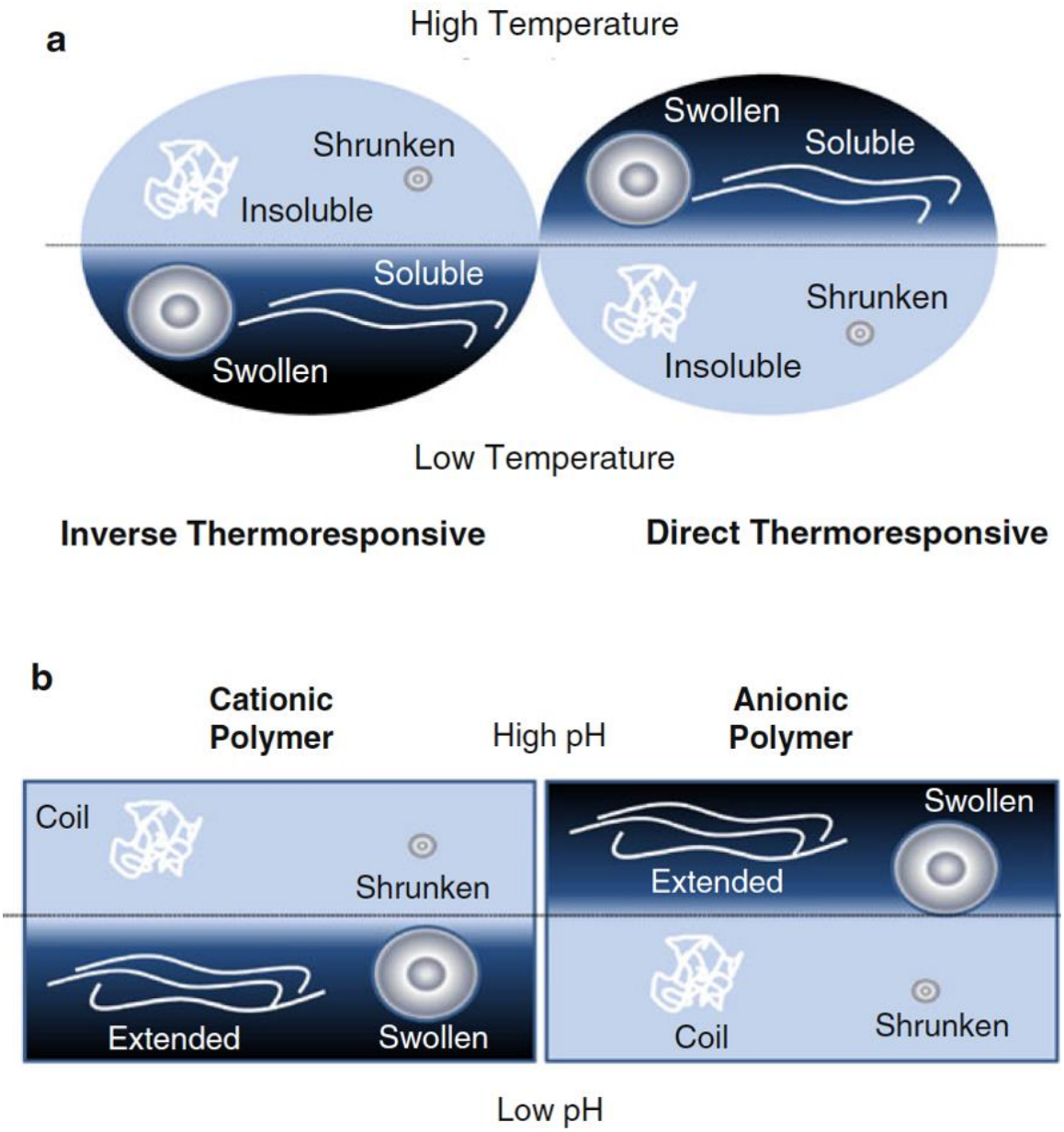

Figure 1.2. Physical Hydrogels. Environmentally-sensitive hydrogels can be affected by (a) temperature or (b) pH. Inverse/Reverse thermoresponsive hydrogels shrink to form gels at higher temperatures and anionic polymers form gels in acidic solutions (taken from [68]).

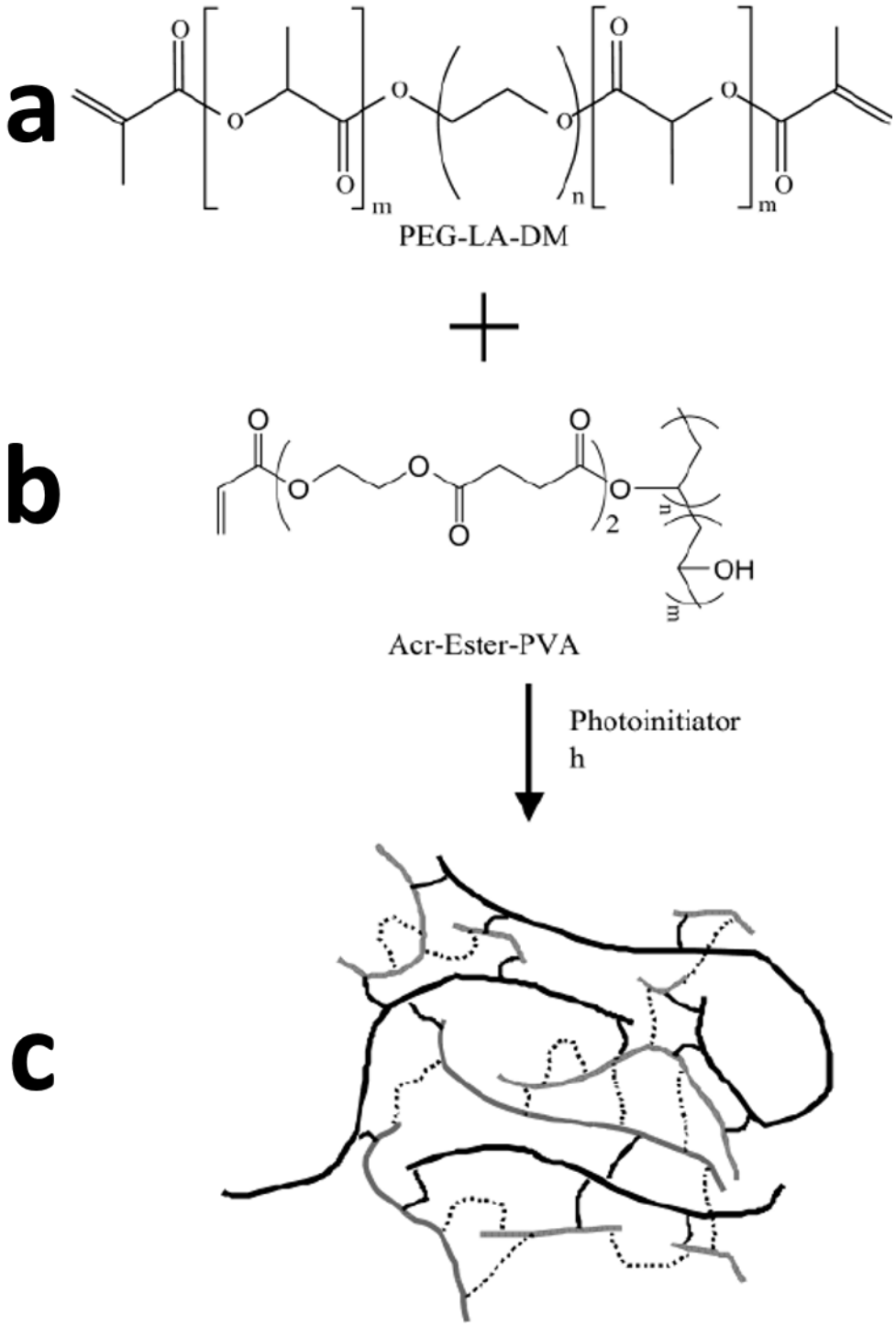

Figure 1.3. Photopolymerization. PEG-PLA-dimethylacrylate and crosslinking polymer, 5-ester-acrylate-Poly (vinyl alcohol) (PVA) are photopolymerized resulting in crosslinked hydrogel formation, irreversibly connecting polymer chains together. (taken from [112]).

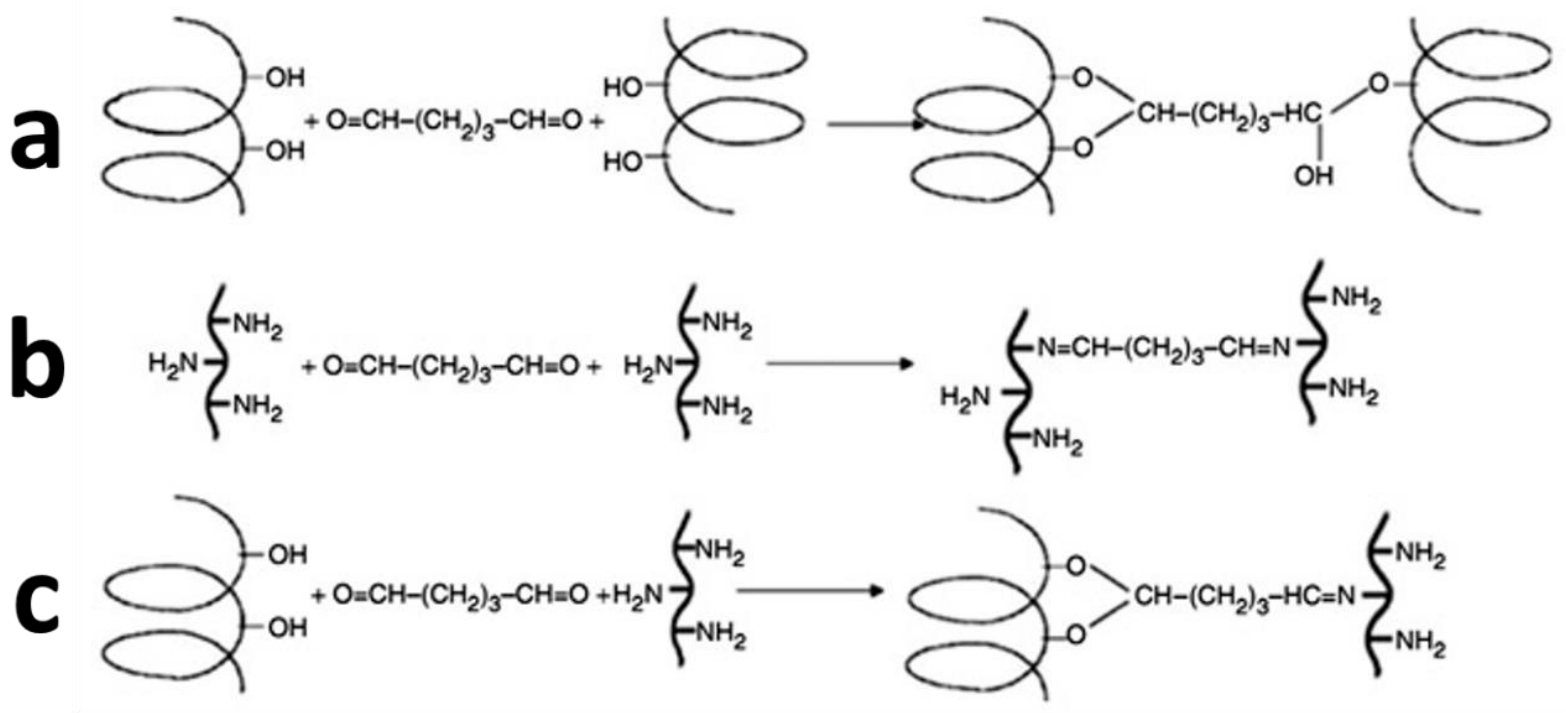

Figure 1.4. Chemical crosslinking with glutaraldehyde. Aldehyde groups chemically bind with (a) alcohol and (b, c) amine groups to form crosslinked polymer chains. (taken from [113]).

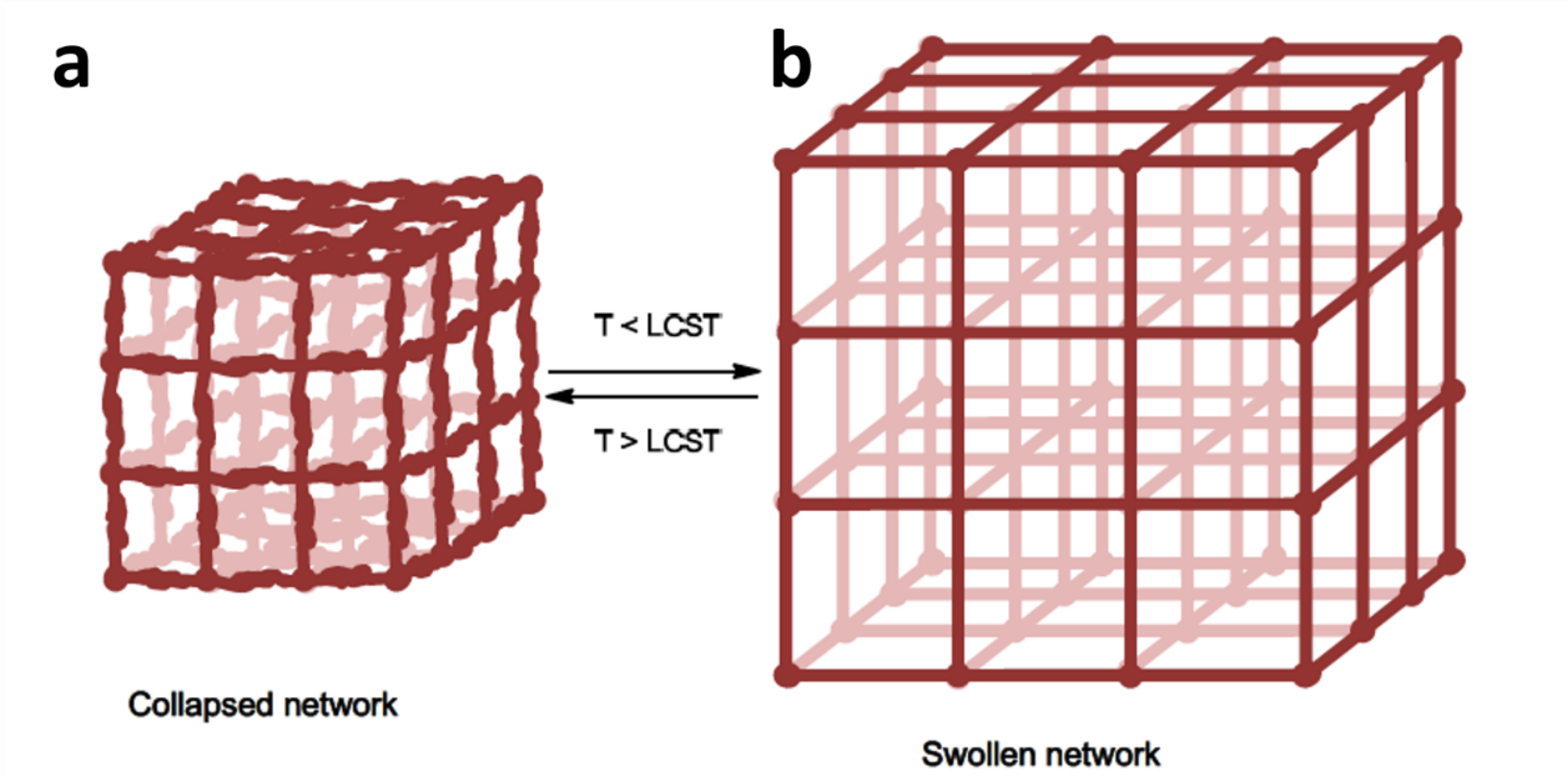

Figure 1.5. Swelling characteristics of crosslinked, reverse thermo-sensitive hydrogels. Reverse thermosensitive hydrogels networks are made up of hydrophobic regions crosslinked/connected by hydrophilic regions. They (a) contract when the surrounding temperature is above their inherent LCST, due to conformational changes in polymer chains, reducing their water content volume. (b) When temperatures fall below their LCST, they swell, increasing their water volume (taken from [67]).

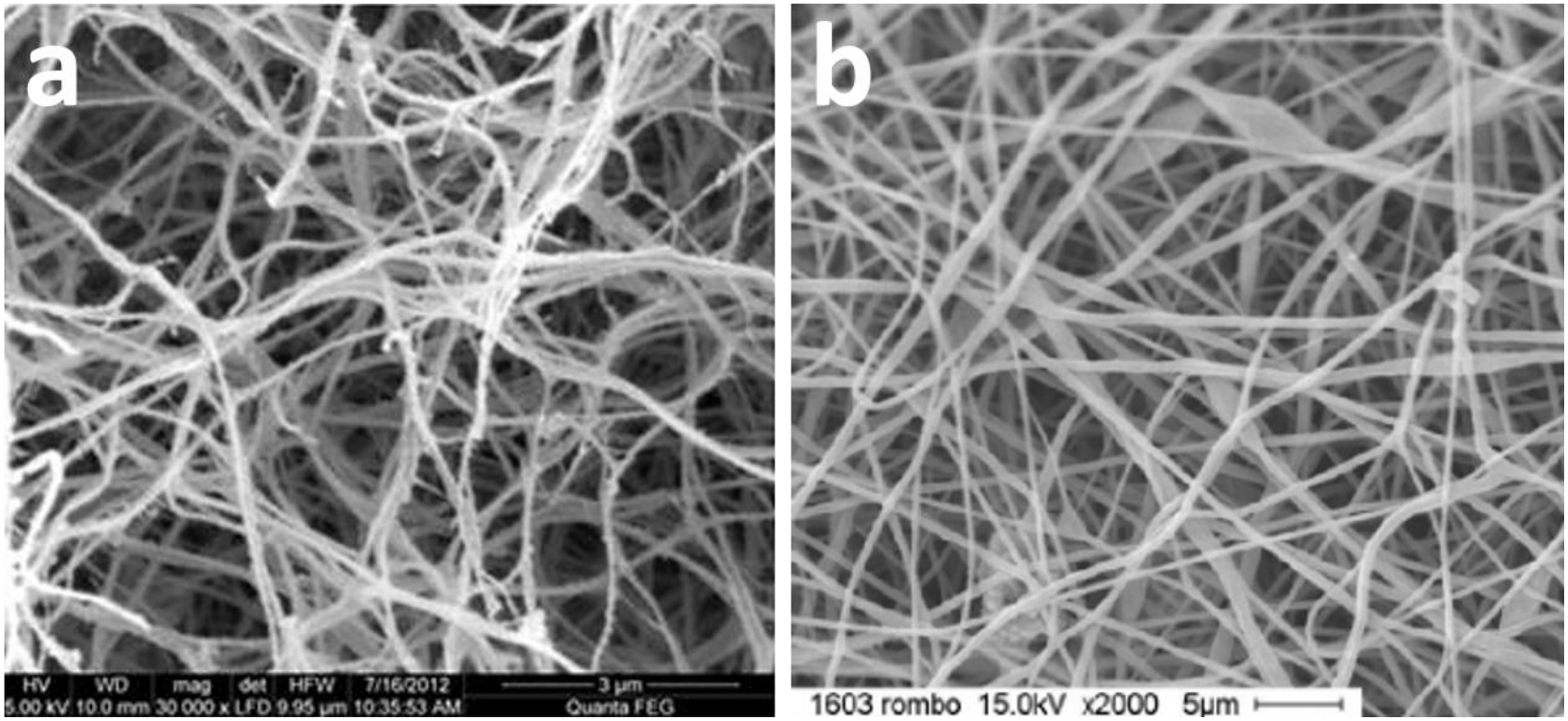

Figure 1.6. Comparison of natural extracellular matrix structure to electrospun scaffolds. (a) Fibrin clot extracellular matrix is shown here as a representative image of decellularized ECM for comparison to (b) poly (vinylidene fluoride) (PVDF) electrospun fibers. ECM and electrospun fibers both form polymer fibrous networks. Scale bar = (a) 3 μm and (b) 5 μm. (taken from [114] and [115]).

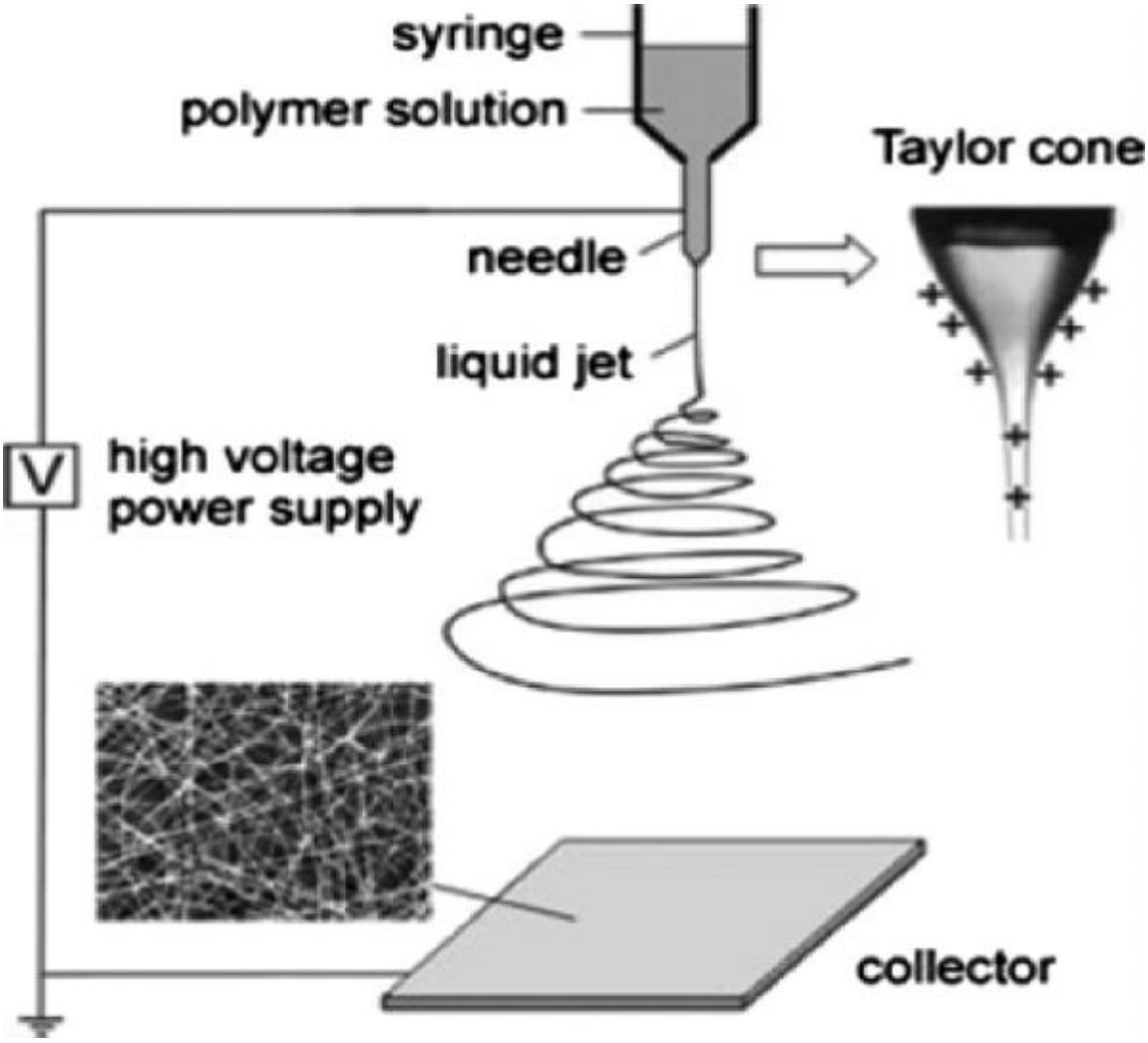

Figure 1.7. Traditional Electrospinning Setup. Polymer solution inside a syringe is dispensed through a negatively charged needle tip, at a set velocity. Negatively charged needle tip, repels charges on polymer solution's surface, overpowering its surface tension and elongating the solution into a Taylor Cone. Positively charged collector plate attracts charged polymer "fibers", as electrostatic forces within the region of instability and the region of elongation cause Taylor Cone to whip around in a circle. Fibers moving through the air are dried by convection and elongated by centripetal forces. Fibers collect in a random, non-woven arrangement upon the collector plate. (taken from [116]).

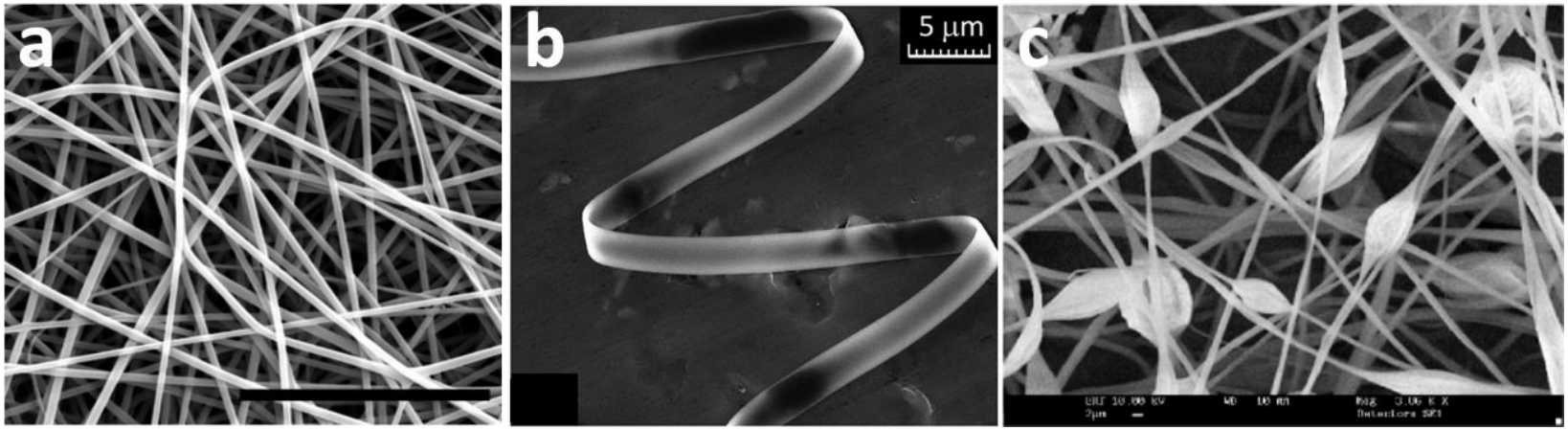

Figure 1.8. Common fiber morphologies. Ideal cylindrical electrospun fibers, with uniform fiber shape and scaffold porosity, Scale bar = 5 µm (taken from [117]). Ribbon-shaped electrospun fibers, believed to be caused from rapid evaporation and collapse of polymer fibers, scale bar = 5 µm (taken from [118]). Beaded fiber morphology, caused by strong surface tension forces by the solvent pulling the polymers together into beads, Scale bar = 2 µm (taken from [119]).

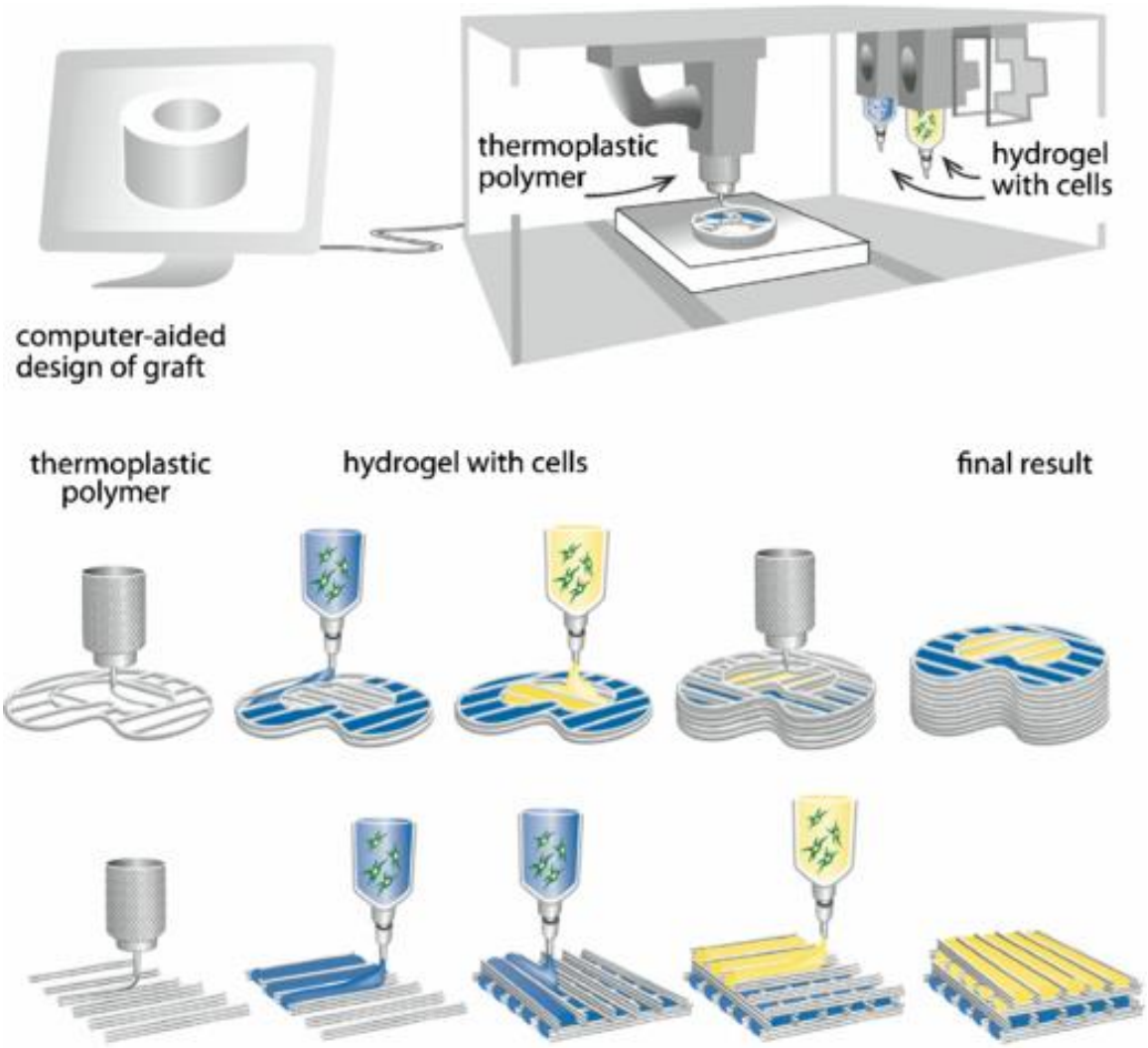

Figure 1.9. 3D-printed scaffold components and process. Model of object is made using computer software and information of the design is shared with printer. Device is printed in layers and uses structural material (gray) for support while it dries. Bio-printers can also print hydrogels (yellow) with cells already in them for ready to go tissue implants. (taken from [120]).

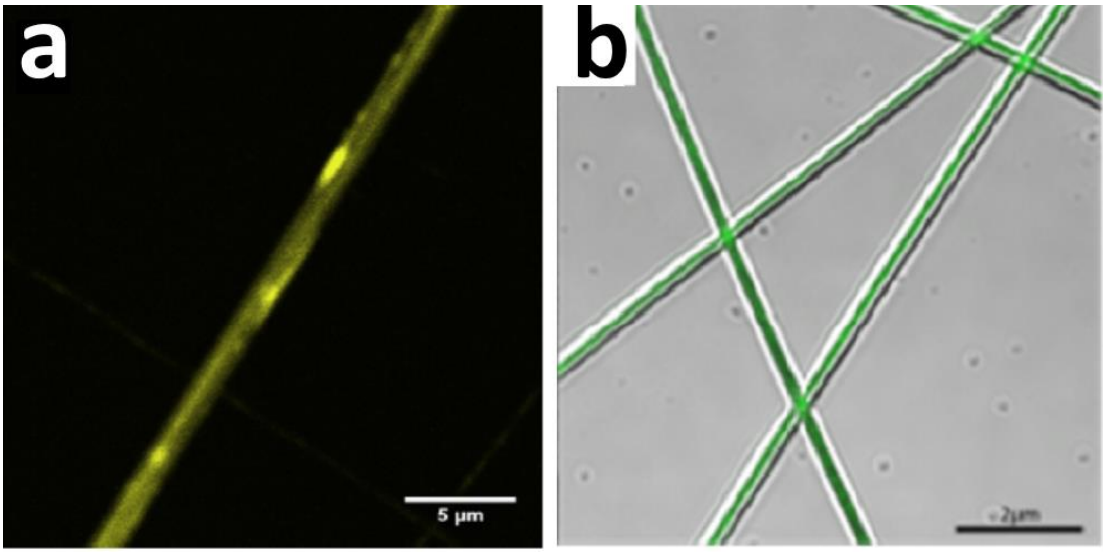

Figure 1.10. Hybrid electrospun scaffolds. (a) Blended fibers, made with hydrogel and hydrophobic polymer mixed together were electrospun loaded with fluorescent dye to visualize different polymers. (b) Core-Shell electrospun fibers have electrospun two polymers on the same fiber: one in the core and the other the shell. Fluorescence dye illustrates the separation of core vs shell (taken from [121] and [122]).

References

1. Park, J., *Biomaterials science and engineering*. Springer Science & Business Media: **2012**.

2. Hench, L. L., Bioceramics: from concept to clinic. *Journal of the american ceramic society* **1991,** *74* (7), 1487-1510.

3. Hench, L. L.; Ethridge, E., Biomaterials: an interfacial approach. *Academic Press, Inc., 1972* **1972**, 385.

4. Fukamachi, K.; Horvath, D. J.; Massiello, A. L.; Fumoto, H.; Horai, T.; Rao, S.; Golding, L. A., An innovative, sensorless, pulsatile, continuous-flow total artificial heart: device design and initial in vitro study. *The Journal of Heart and Lung Transplantation* **2010,** *29* (1), 13-20.

5. Port, F. K.; Dykstra, D. M.; Merion, R. M.; Wolfe, R. A., Trends and results for organ donation and transplantation in the United States, 2004. *American Journal of transplantation* **2005,** *5* (4p2), 843-849.

6. Platt, J. L.; Fischel, R. J.; Matas, A. J.; Reif, S. A.; Bolman, R. M.; Bach, F. H., Immunopathology of hyperacute xenograft rejection in a swine-to-primate model. *Transplantation* **1991,** *52* (2), 214-220.

7. Cowan, P. J.; Tector, A. J., The Resurgence of Xenotransplantation. *American Journal of transplantation* **2017**.

8. Rawlinson, J., Morbidity after anterior cervical decompression and fusion. The influence of the donor site on recovery, and the results of a trial of surgibone compared to autologous bone. *Acta neurochirurgica* **1994,** *131* (1), 106-118.

9. Kraeutler, M. J.; Bravman, J. T.; McCarty, E. C., Bone–patellar tendon–bone autograft versus allograft in outcomes of anterior cruciate ligament reconstruction: a meta-analysis of 5182 patients. *The American journal of sports medicine* **2013,** *41* (10), 2439-2448.

10. Gomoll, A. H.; Minas, T., The quality of healing: articular cartilage. *Wound Repair and Regeneration* **2014,** *22* (S1), 30-38.

11. Morimoto, N.; Mahara, A.; Jinno, C.; Ogawa, M.; Kakudo, N.; Suzuki, S.; Kusumoto, K.; Fujisato, T.; Yamaoka, T., An evaluation of the engraftment and the blood flow of porcine skin autografts inactivated by high hydrostatic pressure. *Journal of Biomedical Materials Research Part B: Applied*

Biomaterials **2016**.

12. Itskovitz-Eldor, J.; Schuldiner, M.; Karsenti, D.; Eden, A.; Yanuka, O.; Amit, M.; Soreq, H.; Benvenisty, N., Differentiation of human embryonic stem cells into embryoid bodies compromising the three embryonic germ layers. *Molecular medicine* **2000,** *6* (2), 88.

13. Jiang, Y.; Jahagirdar, B. N.; Reinhardt, R. L.; Schwartz, R. E.; Keene, C. D.; Ortiz-Gonzalez, X. R.; Reyes, M.; Lenvik, T.; Lund, T.; Blackstad, M., Pluripotency of mesenchymal stem cells derived from adult marrow. *Nature* **2002,** *418* (6893), 41-49.

14. Takahashi, K.; Tanabe, K.; Ohnuki, M.; Narita, M.; Ichisaka, T.; Tomoda, K.; Yamanaka, S., Induction of pluripotent stem cells from adult human fibroblasts by defined factors. *cell* **2007,** *131* (5), 861-872.

15. Ishii, O.; Shin, M.; Sueda, T.; Vacanti, J. P., In vitro tissue engineering of a cardiac graft using a degradable scaffold with an extracellular matrix–like topography. *The Journal of thoracic and cardiovascular surgery* **2005,** *130* (5), 1358-1363.

16. Holzwarth, J. M.; Ma, P. X., Biomimetic nanofibrous scaffolds for bone tissue engineering. *Biomaterials* **2011,** *32* (36), 9622-9629.

17. Hood, J. D.; Cheresh, D. A., Role of integrins in cell invasion and migration. *Nature Reviews Cancer* **2002,** *2* (2), 91-100.

18. Giancotti, F. G.; Ruoslahti, E., Integrin signaling. *Science* **1999,** *285* (5430), 1028-1033.

19. Kuo, C. K.; Ma, P. X., Ionically crosslinked alginate hydrogels as scaffolds for tissue engineering: part 1. Structure, gelation rate and mechanical properties. *Biomaterials* **2001,** *22* (6), 511-521.

20. Yoo, H. S.; Lee, E. A.; Yoon, J. J.; Park, T. G., Hyaluronic acid modified biodegradable scaffolds for cartilage tissue engineering. *Biomaterials* **2005,** *26* (14), 1925-1933.

21. Peng, C. K.; Yu, S. H.; Mi, F. L.; Shyu, S. S., Polysaccharide-based artificial extracellular matrix: Preparation and characterization of three-dimensional, macroporous chitosan and chondroitin sulfate composite scaffolds. *Journal of Applied Polymer Science* **2006,** *99* (5), 2091-2100.

22. Gunatillake, P. A.; Adhikari, R., Biodegradable synthetic polymers for tissue engineering. *Eur Cell Mater* **2003,** *5* (1), 1-16.

23. Chu, C. R.; Coutts, R. D.; Yoshioka, M.; Harwood, F. L.; Monosov, A. Z.; Amiel, D., Articular cartilage repair using allogeneic perichondrocyteseeded biodegradable porous polylactic acid (PLA): A tissue-engineering study. *Journal of biomedical materials research* **1995,** *29* (9), 1147-1154.

24. Karp, J. M.; Shoichet, M. S.; Davies, J. E., Bone formation on two-dimensional poly (DL-lactide-co-glycolide)(PLGA) films and three-dimensional PLGA tissue engineering scaffolds in vitro. *Journal of Biomedical Materials Research Part A* **2003,** *64* (2), 388-396.

25. Cao, H.; Kuboyama, N., A biodegradable porous composite scaffold of PGA/β-TCP for bone tissue engineering. *Bone* **2010,** *46* (2), 386-395.

26. Chu, C., The in-vitro degradation of poly (glycolic acid) sutures—effect of pH. *Journal of Biomedical Materials Research Part A* **1981,** *15* (6), 795-804.

27. Taylor, M.; Daniels, A.; Andriano, K.; Heller, J., Six bioabsorbable polymers: in vitro acute toxicity of accumulated degradation products. *Journal of applied biomaterials* **1994,** *5* (2), 151-157.

28. Engelberg, I.; Kohn, J., Physico-mechanical properties of degradable polymers used in medical applications: a comparative study. *Biomaterials* **1991,** *12* (3), 292-304.

29. Guilak, F.; Butler, D. L.; Goldstein, S. A., Functional tissue engineering: the role of biomechanics in articular cartilage repair. *Clinical orthopaedics and related research* **2001,** *391*, S295-S305.

30. Angele, P.; Schumann, D.; Angele, M.; Kinner, B.; Englert, C.; Hente, R.; Füchtmeier, B.; Nerlich, M.; Neumann, C.; Kujat, R., Cyclic, mechanical compression enhances chondrogenesis of mesenchymal progenitor cells in tissue engineering scaffolds. *Biorheology* **2004,** *41* (3-4), 335-346.

31. Carter, D. R.; Beaupré, G. S.; Wong, M.; Smith, R. L.; Andriacchi, T. P.; Schurman, D. J., The mechanobiology of articular cartilage development and degeneration. *Clinical orthopaedics and related research* **2004,** *427*, S69-S77.

32. Broz, M.; VanderHart, D. L.; Washburn, N., Structure and mechanical properties of poly (D, L-lactic acid)/poly (ε-caprolactone) blends. *Biomaterials* **2003,** *24* (23), 4181-4190.

33. Iooss, P.; Le Ray, A.-M.; Grimandi, G.; Daculsi, G.; Merle, C., A new injectable bone substitute combining poly (ε-caprolactone) microparticles with biphasic calcium phosphate granules. *Biomaterials* **2001,** *22* (20),

2785-2794.

34. Marletta, G.; Ciapetti, G.; Satriano, C.; Perut, F.; Salerno, M.; Baldini, N., Improved osteogenic differentiation of human marrow stromal cells cultured on ion-induced chemically structured poly-ε-caprolactone. *Biomaterials* **2007,** *28* (6), 1132-1140.

35. Porter, J. R.; Henson, A.; Ryan, S.; Popat, K. C., Biocompatibility and Mesenchymal Stem Cell Response to Poly (ε-Caprolactone) Nanowire Surfaces for Orthopedic Tissue Engineering. *Tissue Engineering Part A* **2009,** *15* (9), 2547-2559.

36. Pitt, C. G.; Chasalow, F.; Hibionada, Y.; Klimas, D.; Schindler, A., Aliphatic polyesters. I. The degradation of poly (ε-caprolactone) in vivo. *Journal of Applied Polymer Science* **1981,** *26* (11), 3779-3787.

37. Pitt, G.; Gratzl, M.; Kimmel, G.; Surles, J.; Sohindler, A., Aliphatic polyesters II. The degradation of poly (DL-lactide), poly (ε-caprolactone), and their copolymers in vivo. *Biomaterials* **1981,** *2* (4), 215-220.

38. Horner, C. B.; Hirota, K.; Liu, J.; Maldonado, M.; Park, B. H.; Nam, J., Magnitude-Dependent and Inversely-related Osteogenic/Chondrogenic Differentiation of Human Mesenchymal Stem Cells Under Dynamic Compressive Strain. *Journal of Tissue Engineering and Regenerative Medicine* **2016**.

39. Woodward, S. C.; Brewer, P.; Moatamed, F.; Schindler, A.; Pitt, C., The intracellular degradation of poly (ε-caprolactone). *Journal of Biomedical Materials Research Part A* **1985,** *19* (4), 437-444.

40. Sun, H.; Mei, L.; Song, C.; Cui, X.; Wang, P., The in vivo degradation, absorption and excretion of PCL-based implant. *Biomaterials* **2006,** *27* (9), 1735-1740.

41. Huang, M.-H.; Li, S.; Vert, M., Synthesis and degradation of PLA–PCL–PLA triblock copolymer prepared by successive polymerization of ε-caprolactone and dl-lactide. *Polymer* **2004,** *45* (26), 8675-8681.

42. Duan, Y.; Wang, Z.; Yan, W.; Wang, S.; Zhang, S.; Jia, J., Preparation of collagen-coated electrospun nanofibers by remote plasma treatment and their biological properties. *Journal of Biomaterials Science, Polymer Edition* **2007,** *18* (9), 1153-1164.

43. Yan, D.; Jones, J.; Yuan, X.-Y.; Xu, X.-H.; Sheng, J.; Lee, J. C.; Ma, G.-Q.; Yu, Q.-S., Plasma treatment of random and aligned electrospun pcl

nanofibers. *Journal of Medical and Biological Engineering* **2013,** *33* (2), 171-178.

44. Jin, R.; Teixeira, L. M.; Dijkstra, P. J.; Karperien, M.; Van Blitterswijk, C.; Zhong, Z.; Feijen, J., Injectable chitosan-based hydrogels for cartilage tissue engineering. *Biomaterials* **2009,** *30* (13), 2544-2551.

45. Helary, C.; Bataille, I.; Abed, A.; Illoul, C.; Anglo, A.; Louedec, L.; Letourneur, D.; Meddahi-Pelle, A.; Giraud-Guille, M. M., Concentrated collagen hydrogels as dermal substitutes. *Biomaterials* **2010,** *31* (3), 481-490.

46. Zhao, W.; Jin, X.; Cong, Y.; Liu, Y.; Fu, J., Degradable natural polymer hydrogels for articular cartilage tissue engineering. *Journal of Chemical Technology and Biotechnology* **2013,** *88* (3), 327-339.

47. Patrick Jr, C.; Chauvin, P.; Hobley, J.; Reece, G., Preadipocyte seeded PLGA scaffolds for adipose tissue engineering. *Tissue engineering* **1999,** *5* (2), 139-151.

48. Grinberg, V. Y.; Dubovik, A. S.; Kuznetsov, D. V.; Grinberg, N. V.; Grosberg, A. Y.; Tanaka, T., Studies of the thermal volume transition of poly (N-isopropylacrylamide) hydrogels by high-sensitivity differential scanning microcalorimetry. 2. Thermodynamic functions. *Macromolecules* **2000,** *33* (23), 8685-8692.

49. Burdick, J. A.; Anseth, K. S., Photoencapsulation of osteoblasts in injectable RGD-modified PEG hydrogels for bone tissue engineering. *Biomaterials* **2002,** *23* (22), 4315-4323.

50. Place, E. S.; George, J. H.; Williams, C. K.; Stevens, M. M., Synthetic polymer scaffolds for tissue engineering. *Chemical Society Reviews* **2009,** *38* (4), 1139-1151.

51. Chen, J. P.; Cheng, T. H., Thermo-Responsive Chitosan-graft-poly (N-isopropylacrylamide) Injectable Hydrogel for Cultivation of Chondrocytes and Meniscus Cells. *Macromolecular bioscience* **2006,** *6* (12), 1026-1039.

52. Huang, X.; Lowe, T. L., Biodegradable thermoresponsive hydrogels for aqueous encapsulation and controlled release of hydrophilic model drugs. *Biomacromolecules* **2005,** *6* (4), 2131-2139.

53. Hamidi, M.; Azadi, A.; Rafiei, P., Hydrogel nanoparticles in drug delivery. *Advanced drug delivery reviews* **2008,** *60* (15), 1638-1649.

54. Bhattarai, N.; Gunn, J.; Zhang, M., Chitosan-based hydrogels for controlled, localized drug delivery. *Advanced drug delivery reviews* **2010,** *62* (1), 83-99.

55. Kong, H. J.; Alsberg, E.; Kaigler, D.; Lee, K. Y.; Mooney, D. J., Controlling degradation of hydrogels via the size of crosslinked junctions. *Advanced materials* **2004,** *16* (21), 1917-1921.

56. Cha, C.; Kohman, R. H.; Kong, H., Biodegradable polymer crosslinker: independent control of stiffness, toughness, and hydrogel degradation rate. *Advanced Functional Materials* **2009,** *19* (19), 3056-3062.

57. Neffe, A. T.; Gebauer, T.; Lendlein, A. In *Tailoring of mechanical properties of diisocyanate crosslinked gelatin-based hydrogels*, MRS Proceedings, Cambridge Univ Press: **2013**; pp 3-8.

58. Vernengo, J.; Fussell, G.; Smith, N.; Lowman, A., Evaluation of novel injectable hydrogels for nucleus pulposus replacement. *Journal of Biomedical Materials Research Part B: Applied Biomaterials* **2008,** *84* (1), 64-69.

59. Caycik, S.; Jagger, R., The effect of cross-linking chain length on mechanical properties of a dough-molded poly (methylmethacrylate) resin. *Dental Materials* **1992,** *8* (3), 153-157.

60. Pilipchuk, S. P.; Vaicik, M. K.; Larson, J. C.; Gazyakan, E.; Cheng, M. H.; Brey, E. M., Influence of crosslinking on the stiffness and degradation of dermis-derived hydrogels. *Journal of Biomedical Materials Research Part A* **2013,** *101* (10), 2883-2895.

61. Bartnikowski, M.; Wellard, R. M.; Woodruff, M.; Klein, T., Tailoring hydrogel viscoelasticity with physical and chemical crosslinking. *Polymers* **2015,** *7* (12), 2650-2669.

62. Rault, I.; Frei, V.; Herbage, D.; Abdul-Malak, N.; Huc, A., Evaluation of different chemical methods for cros-linking collagen gel, films and sponges. *Journal of materials science: materials in medicine* **1996,** *7* (4), 215-221.

63. Wu, X.; Black, L.; Santacana-Laffitte, G.; Patrick, C. W., Preparation and assessment of glutaraldehyde-crosslinked collagen–chitosan hydrogels for adipose tissue engineering. *Journal of Biomedical Materials Research Part A* **2007,** *81* (1), 59-65.

64. Brannon-Peppas, L.; Peppas, N. A., Equilibrium swelling behavior of pH-sensitive hydrogels. *Chemical Engineering Science* **1991,** *46* (3), 715-722.

65. Aguilar, M.; Elvira, C.; Gallardo, A.; Vázquez, B.; Román, J., Smart polymers and their applications as biomaterials. *Topics in tissue engineering* **2007,** *3* (6).

66. Kim, M. S.; Park, S. J.; Chun, H. J.; Kim, C.-H., Thermosensitive hydrogels for tissue engineering. *Tissue Engineering and Regenerative Medicine* **2011,** *8* (2), 117-123.

67. Ward, M. A.; Georgiou, T. K., Thermoresponsive polymers for biomedical applications. *Polymers* **2011,** *3* (3), 1215-1242.

68. Omidian, H.; Park, K., Hydrogels. In *Fundamentals and applications of controlled release drug delivery*, Springer: **2012**, pp 75-105.

69. Swift, T.; Swanson, L.; Geoghegan, M.; Rimmer, S., The pH-responsive behaviour of poly (acrylic acid) in aqueous solution is dependent on molar mass. *Soft matter* **2016,** *12* (9), 2542-2549.

70. Nguyen, K. T.; West, J. L., Photopolymerizable hydrogels for tissue engineering applications. *Biomaterials* **2002,** *23* (22), 4307-4314.

71. Mansur, H. S.; Sadahira, C. M.; Souza, A. N.; Mansur, A. A., FTIR spectroscopy characterization of poly (vinyl alcohol) hydrogel with different hydrolysis degree and chemically crosslinked with glutaraldehyde. *Materials Science and Engineering: C* **2008,** *28* (4), 539-548.

72. Hennink, W.; Van Nostrum, C. F., Novel crosslinking methods to design hydrogels. *Advanced drug delivery reviews* **2012,** *64*, 223-236.

73. Yakushiji, T.; Sakai, K.; Kikuchi, A.; Aoyagi, T.; Sakurai, Y.; Okano, T., Effects of cross-linked structure on temperature-responsive hydrophobic interaction of poly (N-isopropylacrylamide) hydrogel-modified surfaces with steroids. *Analytical Chemistry* **1999,** *71* (6), 1125-1130.

74. Comolli, N.; Neuhuber, B.; Fischer, I.; Lowman, A., In vitro analysis of PNIPAAm–PEG, a novel, injectable scaffold for spinal cord repair. *Acta biomaterialia* **2009,** *5* (4), 1046-1055.

75. Sung, H. W.; Huang, D. M.; Chang, W. H.; Huang, R. N.; Hsu, J. C., Evaluation of gelatin hydrogel crosslinked with various crosslinking agents as bioadhesives: in vitro study. *Journal of Biomedical Materials Research Part A* **1999,** *46* (4), 520-530.

76. Mironi-Harpaz, I.; Wang, D. Y.; Venkatraman, S.; Seliktar, D., Photopolymerization of cell-encapsulating hydrogels: crosslinking efficiency

versus cytotoxicity. *Acta biomaterialia* **2012,** *8* (5), 1838-1848.

77. Shim, W. S.; Kim, J.-H.; Park, H.; Kim, K.; Kwon, I. C.; Lee, D. S., Biodegradability and biocompatibility of a pH-and thermo-sensitive hydrogel formed from a sulfonamide-modified poly (ε-caprolactone-co-lactide)–poly (ethylene glycol)–poly (ε-caprolactone-co-lactide) block copolymer. *Biomaterials* **2006,** *27* (30), 5178-5185.

78. Anton, F., Process and apparatus for preparing artificial threads. Google Patents: **1934**.

79. Fridrikh, S.; Yu, J.; Brenner, M.; Rutledge, G., Nonlinear whipping behavior of electrified fluid jets. ACS Publications: **2003**.

80. Eichhorn, S. J.; Sampson, W. W., Statistical geometry of pores and statistics of porous nanofibrous assemblies. *Journal of the Royal Society Interface* **2005,** *2* (4), 309-318.

81. Doshi, J.; Reneker, D. H., Electrospinning process and applications of electrospun fibers. *Journal of electrostatics* **1995,** *35* (2-3), 151-160.

82. Reneker, D. H.; Chun, I., Nanometre diameter fibres of polymer, produced by electrospinning. *Nanotechnology* **1996,** *7* (3), 216.

83. Fong, H.; Chun, I.; Reneker, D., Beaded nanofibers formed during electrospinning. *Polymer* **1999,** *40* (16), 4585-4592.

84. Koombhongse, S.; Liu, W.; Reneker, D. H., Flat polymer ribbons and other shapes by electrospinning. *Journal of Polymer Science Part B: Polymer Physics* **2001,** *39* (21), 2598-2606.

85. Lee, K.; Kim, H.; Bang, H.; Jung, Y.; Lee, S., The change of bead morphology formed on electrospun polystyrene fibers. *Polymer* **2003,** *44* (14), 4029-4034.

86. Rajzer, I.; Menaszek, E.; Kwiatkowski, R.; Planell, J. A.; Castano, O., Electrospun gelatin/poly (ε-caprolactone) fibrous scaffold modified with calcium phosphate for bone tissue engineering. *Materials Science and Engineering: C* **2014,** *44*, 183-190.

87. Yarin, A. L.; Koombhongse, S.; Reneker, D. H., Taylor cone and jetting from liquid droplets in electrospinning of nanofibers. *Journal of Applied physics* **2001,** *90* (9), 4836-4846.

88. Higuera, F., Flow rate and electric current emitted by a Taylor cone. *Journal*

of Fluid Mechanics **2003,** *484*, 303-327.

89. Son, W. K.; Youk, J. H.; Lee, T. S.; Park, W. H., Electrospinning of ultrafine cellulose acetate fibers: studies of a new solvent system and deacetylation of ultrafine cellulose acetate fibers. *Journal of Polymer Science Part B: Polymer Physics* **2004,** *42* (1), 5-11.

90. Fernández de La Mora, J., The fluid dynamics of Taylor cones. *Annu. Rev. Fluid Mech.* **2007,** *39*, 217-243.

91. Wannatong, L.; Sirivat, A.; Supaphol, P., Effects of solvents on electrospun polymeric fibers: preliminary study on polystyrene. *Polymer International* **2004,** *53* (11), 1851-1859.

92. Megelski, S.; Stephens, J. S.; Chase, D. B.; Rabolt, J. F., Micro-and nanostructured surface morphology on electrospun polymer fibers. *Macromolecules* **2002,** *35* (22), 8456-8466.

93. Casper, C. L.; Stephens, J. S.; Tassi, N. G.; Chase, D. B.; Rabolt, J. F., Controlling surface morphology of electrospun polystyrene fibers: effect of humidity and molecular weight in the electrospinning process. *Macromolecules* **2004,** *37* (2), 573-578.

94. Zampetti, E.; Muzyczuk, A.; Macagnano, A.; Pantalei, S.; Scalese, S.; Spinella, C.; Bearzotti, A., Effects of temperature and humidity on electrospun conductive nanofibers based on polyaniline blends. *Journal of Nanoparticle Research* **2011,** *13* (11), 6193-6200.

95. Yang, G.-Z.; Li, H.-P.; Yang, J.-H.; Wan, J.; Yu, D.-G., Influence of Working Temperature on The Formation of Electrospun Polymer Nanofibers. *Nanoscale research letters* **2017,** *12* (1), 55.

96. Wong, S., An investigation of process parameters to optimize the fiber diameter of electrospun vascular scaffolds through experimental design. **2010**.

97. He, J.-H.; Wu, Y.; Zuo, W.-W., Critical length of straight jet in electrospinning. *Polymer* **2005,** *46* (26), 12637-12640.

98. Sun, D.; Chang, C.; Li, S.; Lin, L., Near-field electrospinning. *Nano letters* **2006,** *6* (4), 839-842.

99. Reneker, D. H.; Yarin, A. L.; Fong, H.; Koombhongse, S., Bending instability of electrically charged liquid jets of polymer solutions in electrospinning. *Journal of Applied physics* **2000,** *87* (9), 4531-4547.

100. Deitzel, J.; Kleinmeyer, J.; Hirvonen, J.; Tan, N. B., Controlled deposition of electrospun poly (ethylene oxide) fibers. *Polymer* **2001,** *42* (19), 8163-8170.

101. Zhang, Y.; Ouyang, H.; Lim, C. T.; Ramakrishna, S.; Huang, Z. M., Electrospinning of gelatin fibers and gelatin/PCL composite fibrous scaffolds. *Journal of Biomedical Materials Research Part B: Applied Biomaterials* **2005,** *72* (1), 156-165.

102. Okuzaki, H.; Kobayashi, K.; Yan, H., Non-woven fabric of poly (N-isopropylacrylamide) nanofibers fabricated by electrospinning. *Synthetic metals* **2009,** *159* (21), 2273-2276.

103. Gentile, P.; Chiono, V.; Carmagnola, I.; Hatton, P. V., An overview of poly (lactic-co-glycolic) acid (PLGA)-based biomaterials for bone tissue engineering. *International journal of molecular sciences* **2014,** *15* (3), 3640-3659.

104. Smith, C. M.; Stone, A. L.; Parkhill, R. L.; Stewart, R. L.; Simpkins, M. W.; Kachurin, A. M.; Warren, W. L.; Williams, S. K., Three-dimensional bioassembly tool for generating viable tissue-engineered constructs. *Tissue engineering* **2004,** *10* (9-10), 1566-1576.

105. Murphy, S. V.; Atala, A., 3D bioprinting of tissues and organs. *Nature biotechnology* **2014,** *32* (8), 773-785.

106. Gu, B. K.; Choi, D. J.; Park, S. J.; Kim, M. S.; Kang, C. M.; Kim, C.-H., 3-dimensional bioprinting for tissue engineering applications. *Biomaterials research* **2016,** *20* (1), 12.

107. Kang, H.-W.; Lee, S. J.; Ko, I. K.; Kengla, C.; Yoo, J. J.; Atala, A., A 3D bioprinting system to produce human-scale tissue constructs with structural integrity. *Nature biotechnology* **2016,** *34* (3), 312-319.

108. Xu, T.; Binder, K. W.; Albanna, M. Z.; Dice, D.; Zhao, W.; Yoo, J. J.; Atala, A., Hybrid printing of mechanically and biologically improved constructs for cartilage tissue engineering applications. *Biofabrication* **2012,** *5* (1), 015001.

109. Liu, W.; Zhan, J.; Su, Y.; Wu, T.; Ramakrishna, S.; Liao, S.; Mo, X., Injectable hydrogel incorporating with nanoyarn for bone regeneration. *Journal of Biomaterials Science, Polymer Edition* **2014,** *25* (2), 168-180.

110. Kai, D.; Prabhakaran, M. P.; Stahl, B.; Eblenkamp, M.; Wintermantel, E.; Ramakrishna, S., Mechanical properties and in vitro behavior of nanofiber–hydrogel composites for tissue engineering applications. *Nanotechnology*

2012, *23* (9), 095705.

111. El-Sherbiny, I. M.; Yacoub, M. H., Hydrogel scaffolds for tissue engineering: Progress and challenges. *Global Cardiology Science and Practice* **2013**, 38.

112. Martens, P. J.; Bryant, S. J.; Anseth, K. S., Tailoring the degradation of hydrogels formed from multivinyl poly (ethylene glycol) and poly (vinyl alcohol) macromers for cartilage tissue engineering. *Biomacromolecules* **2003,** *4* (2), 283-292.

113. Asma, C.; Meriem, E.; Mahmoud, B.; Djaafer, B., Physicochemical characterization of gelatin-cmc composite edibles films from polyion-complex hydrogels. *Journal of the Chilean Chemical Society* **2014,** *59* (1), 2279-2283.

114. Neergaard-Petersen, S.; Ajjan, R.; Hvas, A.-M.; Hess, K.; Larsen, S. B.; Kristensen, S. D.; Grove, E. L., Fibrin clot structure and platelet aggregation in patients with aspirin treatment failure. *PloS one* **2013,** *8* (8), e71150.

115. Saghafi, H.; Palazzetti, R.; Zucchelli, A.; Minak, G., Impact response of glass/epoxy laminate interleaved with nanofibrous mats. *Engineering Solid Mechanics* **2013,** *1* (3), 85-90.

116. Garg, K.; Bowlin, G. L., Electrospinning jets and nanofibrous structures. *Biomicrofluidics* **2011,** *5* (1), 013403.

117. Yao, J.; Bastiaansen, C. W.; Peijs, T., High strength and high modulus electrospun nanofibers. *Fibers* **2014,** *2* (2), 158-186.

118. Stanishevsky, A.; Wetuski, J.; Walock, M.; Stanishevskaya, I.; Yockell-Lelièvre, H.; Košťáková, E.; Lukáš, D., Ribbon-like and spontaneously folded structures of tungsten oxide nanofibers fabricated via electrospinning. *RSC Advances* **2015,** *5* (85), 69534-69542.

119. Lin, T.; Wang, H.; Wang, H.; Wang, X., The charge effect of cationic surfactants on the elimination of fibre beads in the electrospinning of polystyrene. *Nanotechnology* **2004,** *15* (9), 1375.

120. Schuurman, W.; Khristov, V.; Pot, M. W.; van Weeren, P. R.; Dhert, W. J.; Malda, J., Bioprinting of hybrid tissue constructs with tailorable mechanical properties. *Biofabrication* **2011,** *3* (2), 021001.

121. Kim, T. G.; Lee, D. S.; Park, T. G., Controlled protein release from electrospun biodegradable fiber mesh composed of poly (ε-caprolactone)

and poly (ethylene oxide). *International journal of pharmaceutics* **2007,** *338* (1), 276-283.

122. Chen, M.; Dong, M.; Havelund, R.; Regina, V. R.; Meyer, R. L.; Besenbacher, F.; Kingshott, P., Thermo-responsive core− sheath electrospun nanofibers from poly (N-isopropylacrylamide)/polycaprolactone blends. *Chemistry of Materials* **2010,** *22* (14), 4214-4221.

CHAPTER 2. OPTIMIZED GELATION OF PEG-PNIPAAM HYDROGEL BY CONTROLLING REACTION CONCENTRATIONS

Abstract

Reverse thermo-sensitive hydrogels are unique physical hydrogels which appear as solutions at room temperature and then form a gel when the temperature is increased. Their ability to gel at physiological temperatures benefits protocols which seed cells 3-dimensionally at room temperature. Poly (ethylene glycol)-poly (N-isopropylacrylamide) (PEG-PNIPAAm) has been previously utilized as a cell culture substrate and as an *in vivo* injectable implant due to its ability to gel at temperatures above 32 °C. Crosslinking with PEG chains improves PNIPAAm's swelling ratio significantly, because of PEG's inherent hydrophilic properties. However, not much research has focused on the polymerization reaction rate of PEG-PNIPAAm, or the effect reaction rate has on its gelation properties. In this study, we looked at the effects changing polymerization reaction concentrations has on PEG-PNIPAAm's concentration-dependent gelation. Increasing the concentration of starting materials, lowered the minimum

concentration required for gelation in an aqueous solution, to a certain degree. Cell viability was also shown to be negatively affected as the concentration of our PEG-PNIPAAm, 3-dimensional (3D) scaffold increased. The synthesis conditions and scaffold concentration of PEG-PNIPAAm were optimized for 3D cell viability as a culture scaffold for human mesenchymal stem cells (hMSCs).

Keywords: Polyethylene glycol, Poly N-Isopropylacrylamide, PEG-PNIPAAm, free-radical polymerization, hydrogel synthesis, lower critical solution temperature

2.1. Introduction

Hydrogels are advantageous due to their ability to resemble the natural extra cellular matrix (ECM) found within the body. Hydrophilic polymer chains swell when dissolved in water based solutions, such as media, before curing into a gel and trapping the water within them. To prevent dissociation and improve structural stability hydrogel polymer chains must be crosslinked.

Hydrogel crosslinking can be accomplished by utilizing either chemically initiated or photo initiated[1-6] bifunctional molecules. Chemically crosslinked hydrogels utilize molecules that react with amine groups commonly found on many polymer chains. For example, hydrogels such as collagen, can use glutaraldehyde to chemically crosslink collagen peptide chains[7]. Glutaraldehyde can cause calcification of collagen and is potentially cytotoxic if not washed prior to cell introduction into the scaffold[8-9].

Crosslinking can also be photo initiated by application of ultra violet (UV) light. Hydrogels use free-radicals, generated by UV light, to crosslink the ends of polymer chains together[10]. Using this method, their crosslinking density is greatly increased, as every polymerized monomer can act as a crosslinking chain. Radicalized initiators cleave double bonded functional groups, transferring the radical to the polymer chain and propagating the reaction. Common photo initiators include peroxides, like benzoyl peroxide and Igracure compounds[11-12]. Most photo initiators can be used to cure hydrogels with dosages below toxic levels[13-15]. Studies have even used photocrosslinked hydrogels *in vivo* after being injected

into subdermal and cartilage tissue although their application is limited by the penetration of UV light into the hydrogel and the surrounding tissue[16-18].

With the potential of cytotoxic affects by chemical crosslinkers, and limitations of UV light penetration, environmental-initiated hydrogels prove to be an advantageous and reliable alternative. Unlike chemical or photo crosslinked hydrogels, the gelation of environmental hydrogels occurs during a physical change in the polymer's structure, resulting from changes in the surrounding environment[19]. Like other hydrogels, they originally swell in aqueous solutions as hydrophilic polymer chains. However, when their surrounding environment changes, they form ionic charges and become attracted to one another. This aggregates them together into a hydrophobic cluster, forcing the water between them outward, and forming a gel. Environmental alterations that can activate physical hydrogels, include changes in pH and temperature[20-21]. To date, hydrogels that respond to changes in pH have not been used for tissue scaffolds by themselves, as generating new tissue requires a relatively neutral pH (6.5-7.8) for the cell's survival[22].

Similar to pH-sensitive hydrogels, thermo-sensitive hydrogels can have direct (gel at lower temperatures) or inverse/reverse (gel at higher temperatures) sensitivity to environmental changes[23-24]. The most attractive physical hydrogels for tissue scaffolds are inverse thermo-sensitive hydrogels, which undergo gelation when the temperature rises toward/at physiological temperatures (> 37 °C). Like photo crosslinked and pH-sensitive hydrogels, reverse thermo-sensitive hydrogels

can also be injected into the body as a solution. They uniformly gel once exposed to the body's temperature, without the need for additional steps. Physical hydrogels can be made more hydrophilic by using free-radical polymerization to chemically crosslink them with hydrophilic polymer chains and reduce their loss in water content from gelation.

Unlike glutaraldehyde and other fixatives, free-radical polymerization chemically crosslinks the hydrogel as it is being polymerized. It can also utilize longer polymer chains with bifunctional acrylate groups[25-26]. Chemically crosslinking already formed polymer chains with molecules like glutaraldehyde can provide an organized arrangement in the crosslinking density, but this method is still limited by the following: the availability of reactive monomers, the resulting pore sizes between polymer chains and the necessity of subsequent washes to remove cytotoxic molecules. Crosslinking during hydrogel polymerization is advantageous when a 3-dimensional (3D) scaffold that allows for adequate pore size for cell infiltration is desired[27].

A variety of methods for free-radical polymerization are used for polymer fabrication. Polymerization with a thermal initiator is amongst the easiest to perform without requiring further equipment. Additionally, the method of introducing the initiator to the population of monomers can also differ. The most commonly used method with hydrogels is solution polymerization, in which the monomers and initiators are dissolved within a solvent and mixed together. Solvents used during polymerization must be unreactive to the reaction taking

place, and easily removed at its completion. The reaction can be affected by the concentration of the monomers and initiators, as well as the initiator's efficiency and the kinetic constants of dissociation, propagation and termination[28]. These factors determine both the rate and degree of polymerization[29]. Increasing the degree of polymerization can produce polymers with longer chain lengths, however longer chains also effect the viscosity of the reaction's solution. As the polymer chains become longer, their movement is restricted and the rate of chain termination decreases rapidly. At a certain point, the viscosity becomes too high and autoacceleration can occur, effectively ruining the hydrogel[30]. Therefore, careful control of the polymerization reaction is necessary to produce an advantageous thermo-sensitive hydrogel for tissue engineering applications.

Poly (ethylene glycol)-poly (N-isopropylacrylamide) (PEG-PNIPAAm) has been pursued as an attractive hydrogel for cell and tissue scaffolding. It is made of the reverse thermo-sensitive hydrogel PNIPAAm, which forms a gel above 32 °C, and is chemically crosslinked with the hydrophilic polymer chain PEG. PEG-PNIPAAm has recently been used as an injectable hydrogel for *in vivo* tissue repair, drug loading and as a cell culture substrate[24, 31-33]. Variations in PEG chain length and crosslinking densities have been investigated, but the effects of manipulating starting material concentrations during its free-radical polymerization have not been assessed[34-35]. In this study, we controlled the concentration of the starting materials within the synthesis reaction, effectively increasing the rate of polymerization and improving the hydrogels thermosensitive gelation properties.

2.2. Methods

2.2.1. PEG-PNIPAAm Synthesis

PEG-PNIPAAm was synthesized with N-isopropylacrylamide (NIPAAm) (Sigma Aldrich) and PEG-dimethylacrylate (PEG-DMA) (Fisher Scientific) monomers, by using a free-radical polymerization protocol, which we modified[24]. Briefly, NIPAAm and PEG-DMA were dissolved inside a three-necked round bottom flask under a nitrogen atmosphere. In this study, PEG-PNIPAAm samples were synthesized with varying reaction concentrations of NIPAAm and PEG-DMA, including 4.5 wt. % to 0.5 wt. % (5.0 total wt. %), 6.7 wt. % to 0.8 wt. % (7.5 total wt. %), 9.1 wt. % to 0.9 wt. % (10 total wt. %), 11.4 wt. % to 1.1 wt. % (12.5 total wt. %) and 13.6 wt. % to 1.4 wt. % (15.0 total wt. %), respectively. Azobisisobutyronitrile (AIBN) (Sigma Aldrich) was added to the solution as a free-radical initiator at a 1:130 molar ratio to the starting materials. The solution was heated inside a water bath to 65 °C, and refluxed for 48 hours, before evaporating methanol. The resulting solid polymer was washed to remove unreacted monomers with a surplus of n-hexane (Sigma Aldrich) at 45 °C for 12 hours. After grinding the product into a powder, it was vacuum filtered with n-hexane washes (x3).

2.2.2. Fourier Transform Infrared Spectroscopic characterization

Fourier transform infrared (FTIR) spectroscopy and proton nuclear

magnetic resonance (H NMR) spectroscopy were used to analyze the chemical structure of the synthesized PEG-PNIPAAm. A Nicolet 6700 FTIR Spectrometer (Thermo Fisher Scientific) was used for FTIR analysis with dry powder samples to produce infrared absorbance peaks of the hydrogel. The polymer was also dissolved in deuterated chloroform (Sigma Aldrich) at 20 wt. % before H NMR analysis with a Varian Inova 400 NMR machine (Varian, Inc.) and Mnova Analytical Chemistry Software (Mestrelab Research). Pure PEG-DMA and NIPAAm monomers were used as controls during both analyses. Peaks from PEG-PNIPAAm samples with different critical concentrations were characterized by FTIR analysis for their comparison.

2.2.3. Lower Critical Solution Temperature Characterization

PEG-PNIPAAm hydrogel samples were dissolved in Dulbecco's Modified Eagle Medium: nutrient mixture F-12 (DMEM/F12) (Fisher Scientific), overnight, at 4 °C. The product of each reaction was dissolved at varying concentrations (4-30 wt. %). The lower critical solution temperature (LCST) of the thermosensitive hydrogel was characterized with a standard inversion assay at varying temperatures. The temperature of the varying concentrations of PEG-PNIPAAm were gradually increased from room temperature (23 °C) to 49 °C. The dissolved hydrogel solutions were tilted 45° after every 2 °C temperature increase to test for gelation. The LCST of hydrogels with different critical concentrations were similarly quantified and compared. The lowest concentration that gelled for each synthesis

was characterized as the critical concentration (crit. conc.).

2.2.4. Three-Dimensional Cell Viability

The biocompatibility of PEG-PNIPAAm hydrogels was determined utilizing human mesenchymal stem cells (hMSCs). Dry hydrogel powder was gamma irradiated at 10 kGy, for sterilization, before dissolving them in sterile DMEM/F12, at 4 °C, overnight[36]. A cell seeding density of 12 x 10^6 cells/mL was inoculated into the optimized polymer solution (5 wt. % crit. conc.) at concentrations of 5, 7.5 and 10 wt. %. Cell/polymer solutions were plated in a 24-well plate and immediately incubated for 20 minutes at 37 °C. Additional DMEM/F12 solution was then added to the wells. Samples were cultured for 24 hours and then exposed to 2 μM Calcein-AM (Fisher Scientific) and 4 μM ethidium homodimer-1 (Fisher Scientific) in sterile phosphate buffer solution (PBS) (Fisher Scientific), for cell viability analysis with a live/dead cell assay[37-38]. The samples were incubated for 5 minutes at 37 °C after adding the staining solution. Excess stain was aspirated and the samples were washed with warm PBS. Cells were then fixed with 10% formaldehyde in PBS solution, for 30 minutes at 37 °C to maintain gelation. Samples were immediately imaged using a fluorescence microscope (Nikon Eclipse). Live (green) and dead (red) cells within each sample were analyzed and compared using Image J software.

2.2.5. Statistical analysis

All experiments were performed with at least three biologically independent samples, and represented as an average ± standard deviation (SD). The data was subjected to an ANOVA with a Tukey's post-hoc test using SPSS software (IBM) and statistical significance was determined by its p-value ($p < 0.05$).

2.3. Results

This study investigated ways to manipulate the LCST and critical concentration of PEG-PNIPAAm, previously synthesized for use as an injectable thermo-sensitive hydrogel for tissue engineering and cell culture scaffolds[31]. PEG-PNIPAAm gels were synthesized using a free-radical initiator, AIBN, to polymerize NIPAAm monomers with crosslinking PEG chains (**Fig. 2.1**). Multiple syntheses were performed with varying concentrations of starting materials. The molar ratio of NIPAAm monomers to crosslinking PEG chains was consistently maintained around 700:1, respectively (**Table 2.1**), in concurrence with the modified protocol taken from Comolli et al. The resulting mass ratio in each reaction was calculated to be roughly 9:1, NIPAAM:PEG-DMA. The total concentration of the starting materials was manipulated to improve the rate of PEG-PNIPAAm's polymerization[24]. PEG-PNIPAAm was first synthesized using a total concentration of 5 wt. % of its starting materials within methanol. The total concentration was increased incrementally to 7.5, 10, 12.5, and finally, 15 wt. %. Apart from reactions with 15 wt. % total concentrations, synthesis reactions produced yellow, crystalline

solids which were grinded into powders for quicker dissolution. Fifteen wt. % reactions produced non-reversible, swollen hydrogel structures after refluxing for one hour, and were ruled out of further experimentation. The resulting critical concentrations of the different PEG-PNIPAAM hydrogels produced were compared, along with their average values for starting materials, including mass, moles, ratios and concentrations (**Table 2.1**).

Resulting polymer samples were collected as finely ground powders and analyzed with FTIR and H NMR spectroscopy. Starting materials were also analyzed for characteristic peaks (**Fig. 2.2-3**). FTIR analysis of NIPAAm expressed peaks associated with amides at wavenumbers of 3300, 1650, and 1600 cm^{-1} (labeled as **1** in **Fig. 2.2a**). PEG-DMA samples demonstrated absorbance peaks associated with ethers at 1300 cm^{-1}, and those with esters at 1120 cm^{-1} (labeled as **2** and **3**, respectfully, in **Fig. 2.2b**). These characteristic peaks of NIPAAm and PEG-DMA were also observed among the peaks produced by FTIR analysis of PEG-PNIPAAm (labeled as **1**, **2** and **3**, respectfully, in **Fig. 2.2c**). Successful polymerization was validated by the comparison of peaks associated with C-H bond stretching (labeled as **4** in **Fig. 2.2a-c**). Absorbance peaks located just above 3000 cm^{-1} are characterized as hydrogen bonds attached to a carbon-carbon double bond. As unreacted monomers with acrylate functional groups, NIPAAm and PEG-DMA both have this peak. While NIPAAm expressed this peak predominately over similar C-H bonds, PEG-DMA's acrylate hydrogens are overshadowed by its overwhelming number of alkane hydrogens found along its

polymer chain at 2891 cm^{-1}. PEG-PNIPAAm carries over these peaks from the starting material, however the comparative ratio between the peak for acrylate and the peaks for hydrogens attached to alkanes is greatly decreased due to the polymerization of the alkene group.

Similar preservation of starting material resonance peaks was found following H NMR analysis (**Fig. 2.3a-c**). Prominent peaks included the 1-ethylene proton peak of NIPAAM at 1.1 ppm and its amide peak at 6.8 ppm (labeled as **1** in **Fig. 2.3a**). PEG-DMA expressed a large resonance peaks at 3.7 ppm associated with both esters and ethers (labeled as **2** in **Fig. 2.3b**). Characteristic NIPAAM and PEG-DMA peaks were carried over in PEG-PNIPAAm following polymerization (labeled as **1** and **2** in **Fig. 2.3c**). As seen with the FTIR analysis, there was a loss in resonance peaks resulting from the polymerization of the starting materials into PEG-PNIPAAM. Conjugated alkene functional groups with peaks at 5.5 ppm (labeled as **4** in **Fig. 2.3a-c**) were completely removed in samples of PEG-PNIPAAm.

PEG-PNIPAAm products from varying reaction concentrations were analyzed by FTIR spectroscopy for variations in chemical structure. The same characteristic peaks were identified as before: (1) amide, (2) ethers, (3) esters and (4) alkanes/allyls peaks. Separate powder samples were analyzed from synthesis reaction concentrations of 5 wt. % (**Fig. 2.4a**), 7.5 wt. % (**Fig. 2.4b**), 10 wt. % (**Fig. 2.4c**) and 12.5 wt. % (**Fig. 2.4d**). Apart from peaks associated with carbon dioxide (2325 cm^{-1}), no differences in absorbance peaks were evident (**Fig. 2.4a-d**).

The lower critical solution temperature was characterized for each hydrogel produced with different reaction conditions (total wt. %). Different weight percent solutions were dissolved in aqueous media and heated incrementally above room temperature. A standard inversion assay was used to determine the temperatures required for each sample to form a gel. At temperatures below the LCST, hydrogel solutions remained as fluids and moved when they were tilted (**Fig. 2.5a**). Above its LCST, a gel would form and the solution would no longer be able to move when tilted (**Fig. 2.5b**). Gelled solutions also experienced a color change at higher temperatures, where the phenol red of the media became pink and opaque.

The LCST curves of each condition followed similar trends of exponential decay (**Fig. 2.6a**). As the concentration of each hydrogel sample was increased the temperature required to illicit gelation was lowered. However, the critical concentrations changed between samples. The critical concentration of each sample was characterized as the lowest concentration that the hydrogel would form a gel, regardless of further temperature increases. Hydrogels made with a 12.5 total wt. % reaction concentration (green) formed gels at the lowest critical concentration of 5 wt. % in DMEM/F12, while gels made with a reaction concentration of 5 wt. % (blue) failed to gel below 19 wt. % in DMEM/F12. Samples with a crit. conc. at 5 wt. % did not gel at 4 wt. % even when the temperature was raised past 37 °C. The critical concentrations of the four reaction conditions decreased with increasing reaction concentrations (**Fig. 2.6b**).

The cytotoxicity was evaluated for the PEG-PNIPAAm with the lowest

critical concentration of 5 wt. %. Hydrogel powder was sterilized with gamma irradiation and then dissolved in sterile DMEM/F12 at 5, 7.5 and 10 wt. % concentrations. Cells were seeded 3-dimensionally within the hydrogel solutions before incubating them at 37 °C. After 24 hours of culture, they were fluorescently stained with a live/dead cell assay, fixed and imaged (**Fig. 2.7a-c**). Viability was quantified by the percentage of cells with green fluorescence. Cells incubated in 5 wt. % were uniformly distributed throughout the hydrogel and had approximately 90% cell viability (**Fig. 2.7a**). Increases in hydrogel concentration resulted in a negative effect on cell compatibility. At 7.5 wt. % PEG-PNIPAAm, the hydrogel decreased cell viability to 80%, and when the concentration was increased to 10 wt. %, the number of alive cells significantly decreased to 50%. Cells within higher weight percentages of PEG-PNIPAAm appeared clustered together within the gel.

2.4. Discussion

The synthetic polymer, PEG-PNIPAAm, was chosen for its thermo-sensitive gelation mechanics and its augmented hydrophilicity, swelling ratio and biocompatibility. PNIPAAm hydrogels, alone, transition into a gel at 32 °C, however the LCST can be increased closer to 37 °C by incorporating hydrophilic monomers or crosslinkers into the synthesized polymer chain[34-35, 39].

Vernengo et al. demonstrated the influence of varying lengths and number of crosslinking PEG chains on PNIPAAm hydrogels[34]. They showed that increasing the molecular weight, of PEG crosslinkers from 1000 g/mol to 8000

g/mol can increase the amount of water retained with in the gel during gelation from 35% to 71% of its wet mass. There was not a significant change in the water content when the crosslinking density was decreased from 1:700 to 1:1600 (per NIPAAm monomer), however a significant decrease was seen in the gel's compressive modulus. Higher PEG molecular weights also decreased the compressive modulus of PEG-PNIPAAm hydrogels. They reported that there was no change in the LCST of PEG-PNIPAAm as the PEG chain length and crosslinking density changed, contrary to similar studies of PEG-PNIPAAm's structure[24, 35, 40]. However, their differential scanning calorimetry data is absent from the article, preventing an objective analysis. It was noted that PEG-PNIPAAm hydrogels made with high and low crosslinking densities of PEG chains with molecular weights of 10,000 g/mol, and those made with 8,000 g/mol PEG chains with low crosslinking density, failed to form a gel. This is indicative of having a concentration too low to gel at physiological temperatures. It could be possible that 8,000 g/mol of PEG, and larger, require higher concentrations necessary for gelation, or by increasing the crosslinking density; effectively restricting the movement/swelling of PNIPAAm chains.

Other PEG-PNIPAAm hydrogels have found a correlation between the concentration of PEG (M_w= 575) and changes in their LCST. Increasing concentrations of PEG-DA monomers during polymerization, from 0 to 16 mM, showed an increase in its LCST from 32 °C to 38 °C, and a decrease in the rate of gelation[24, 35, 41]. While the gelation of pure PNIPAAm occurred between a

difference of 1 °C, PEG-PNIPAAm with a reaction concentration of 16 mM PEG, required a temperature change of 5.5 °C before the normalized absorbance equilibrated, indicating a solid gel. They also showed an increase in the swelling ratio when a lower concentration of PEG was used, due to less restrictions on the hydrogels swelling from increased crosslinking density.

In our study, we maintained a consistent ratio between PEG and PNIPAAm in every reaction and instead changed the total concentration of the starting materials within the reaction flask. The manipulation of PEG-PNIPAAm's LCST and the minimum (critical) concentration by changing the crosslinking ratios have been well researched, however little to no research was found on the manipulation of the reaction concentration within methanol. During initiation of our free-radical polymerization, our initiator, AIBN, was cleaved by thermal energy and two free-radicals form (**Fig. 2.1**). Once initiated, the reaction was propagated as long as there were free floating monomers nearby. Therefore, the concentration of a reactive species is contingent on the concentration of each monomer species and the initiator.

FTIR and H NMR analysis confirmed the structure produced after synthesis was PEG-PNIPAAm[24]. Characteristic amide, ester and ether peaks where preserved in PEG-PNIPAAm, while alkene group peaks decreased following polymerization (**Fig. 2.2a-c**). No changes were seen in the FTIR peaks from different synthesis concentrations (**Fig. 2.4a-d**). However, the LCST still changed with the reaction concentration, suggesting that a change in the rate or degree of

polymerization can influence the LCST similar to improving its hydrophilicity.

Solution polymerization, describes a reaction that takes place within a solution where the concentration of the reacting materials is diluted and provides the reaction with a solvent to absorb heat[42]. It was utilized during the polymerization of our hydrogel due to its ability to produce a polymer chain within a solution. The benefit of using a solvent is its ability to act as a heat sink. The efficiency of solution polymerization can be improved by increasing the concentration of monomers and initiators. However, the higher the concentration, the more viscous the solution becomes and the chance of autoacceleration increases.

During autoacceleration, polymer chains become closely packed and are unable to move freely, preventing them from binding with other free-radical polymer chains, and terminating their polymerization. Unreacted monomers continue to circulate unhindered, until they bind with one of the stationary polymer chains. Unable to terminate, the reaction continues to propagate until no more monomers remain. The products of autoacceleration have been found to exhibit undesirable characteristics[42]. Due to alterations in the chain length of the polymers, our products produced with reaction concentrations of 15 wt. % became overly viscous and swelled within the reaction flask. The physical change was irreversible and the resulting polymer proved to be hydrophobic; making it unfit for use as a reverse thermo-sensitive hydrogel.

The solution became overly viscous and swelled within the reaction flask.

The physical change was irreversible and the resulting polymer proved to be hydrophobic; making it unfit to be used as a hydrogel.

Higher concentrations of starting materials inside the reaction flask, likely improves the efficiency and rate of the reaction. The resulting increase in viscosity also improved the polymer's degree of polymerization and chain length. However, as a reverse thermos-sensitive hydrogel, PEG-PNIPAAm must be hydrophilic at lower temperatures. Therefore, the reaction concentration of 12.5 wt. %, resulting in a lower critical concentration of 5 wt. %, was determined to be optimal for improved gelation properties. At 15 wt. % autoacceleration of the polymerization reaction may have occurred, irreversibly impairing the hydrogel produced.

2.5. Conclusion

Our study aimed to modify an established method of free-radical polymerization and improve the gelation properties of the hydrogel it produced. PEG-PNIPAAm, synthesized with increasing concentrations of its starting materials, produced hydrogel products that did not change in chemical components, however did exhibit improved gelation properties, with lower critical concentrations and LCST curves. However, when the reaction concentration was increased to 15 wt. % an irreversible gel formed and was therefore unfit for a thermo-sensitive hydrogel. By improving our understanding of the reaction kinetics involved with hydrogels synthesis, superior and more specified scaffolds can be constructed for on-going tissue engineering research.

Acknowledgements

This study was supported by the UCR initial Complement Fund and submitted to ACS Applied Materials and Interfaces for publication.

Table 2.1. Table 2.2. Free-radical polymerization reaction values. Average masses, moles, molar ratios, and their concentrations were compared to their resulting critical concentrations.

Label	Total Rxn. Conc. (wt. %)	Molar Ratio (PNIPAAm:PEG)	Crit. Conc. (wt. %)
A	5.0 %	696:1	19 ± 1.0%
B	7.5 %	697:1	15 ± 1.0%
C	10.0 %	699:1	9 ± 1.0%
D	12.5 %	702:1	5 ± 2.0%
E	15.0 %	700:1	N/A

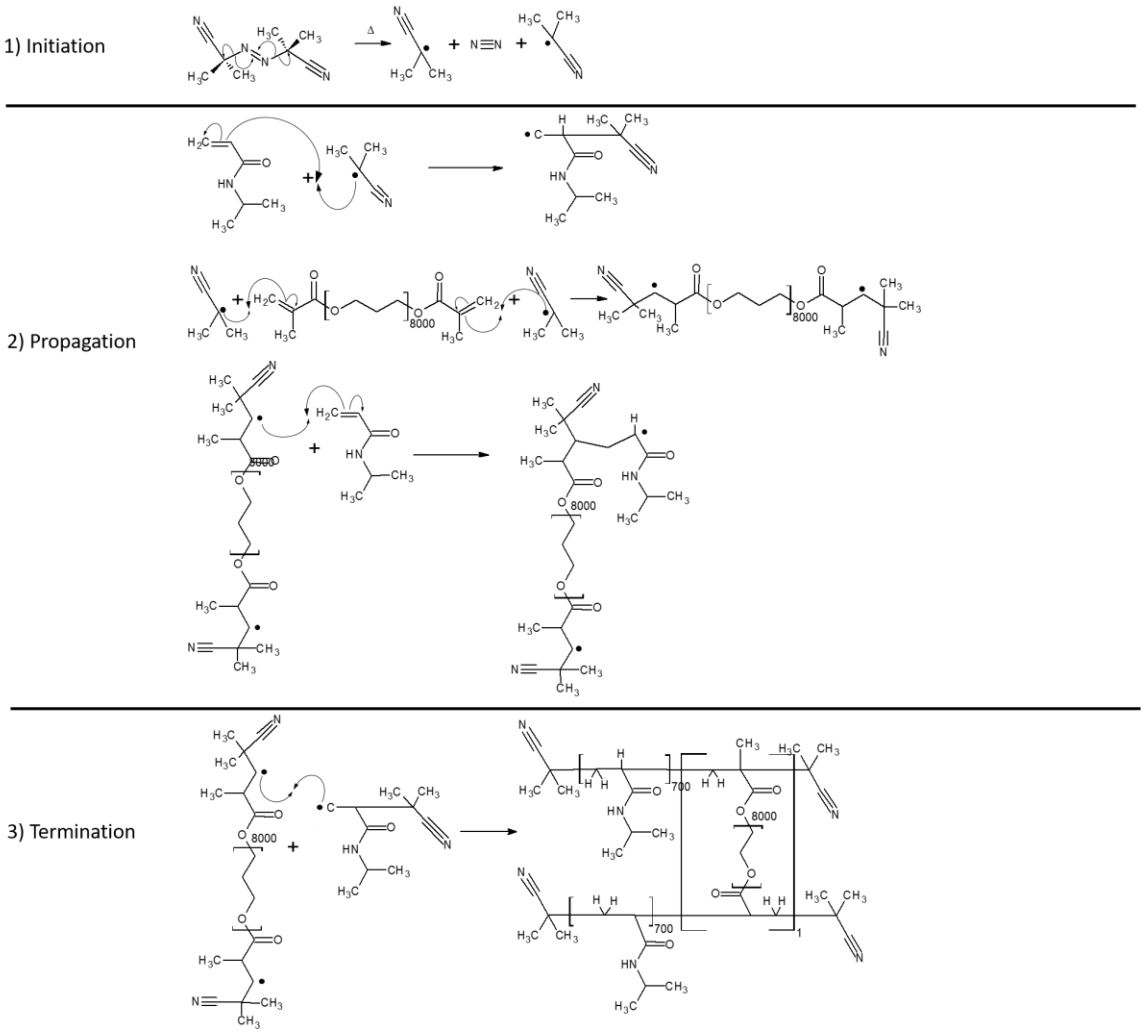

Figure 2.1. Synthesis Reaction Chemistry. (a) AIBN, forms two free-radical initiators due to increasing heat. (b) Radical initiators, propagate chain-growth free-radical polymerization by binding to and transferring free-radicals to NIPAAm and PEG-DMA monomers. Radical monomers form new bonds with unreacted monomers, transferring the free-radical and continuing the polymerization process. (c) Termination of free-radical polymerization occurs when two radicals react to form a bond.

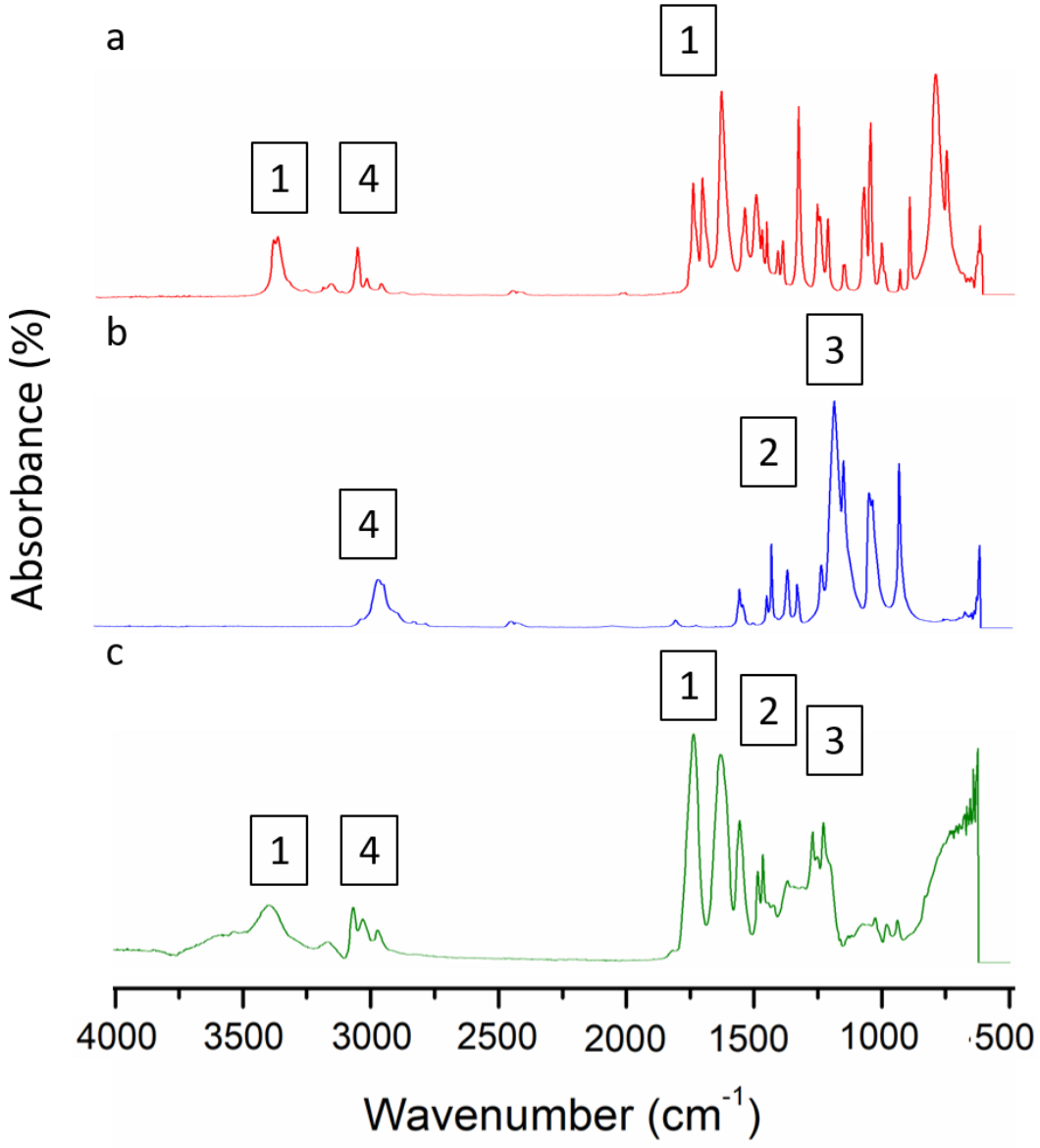

Figure 2.2. Fourier Transform Infrared Spectroscopy Characterization of PEG-PNIPAAm. FTIR peaks associated with (1) amide groups or (2) ether and (3) ester groups were carried over from (a) NIPAAm and (b) PEG-dimethylacrylate into (c) PEG-PNIPAAm. (4) Peaks associated with alkenes were replaced with peaks for alkanes.

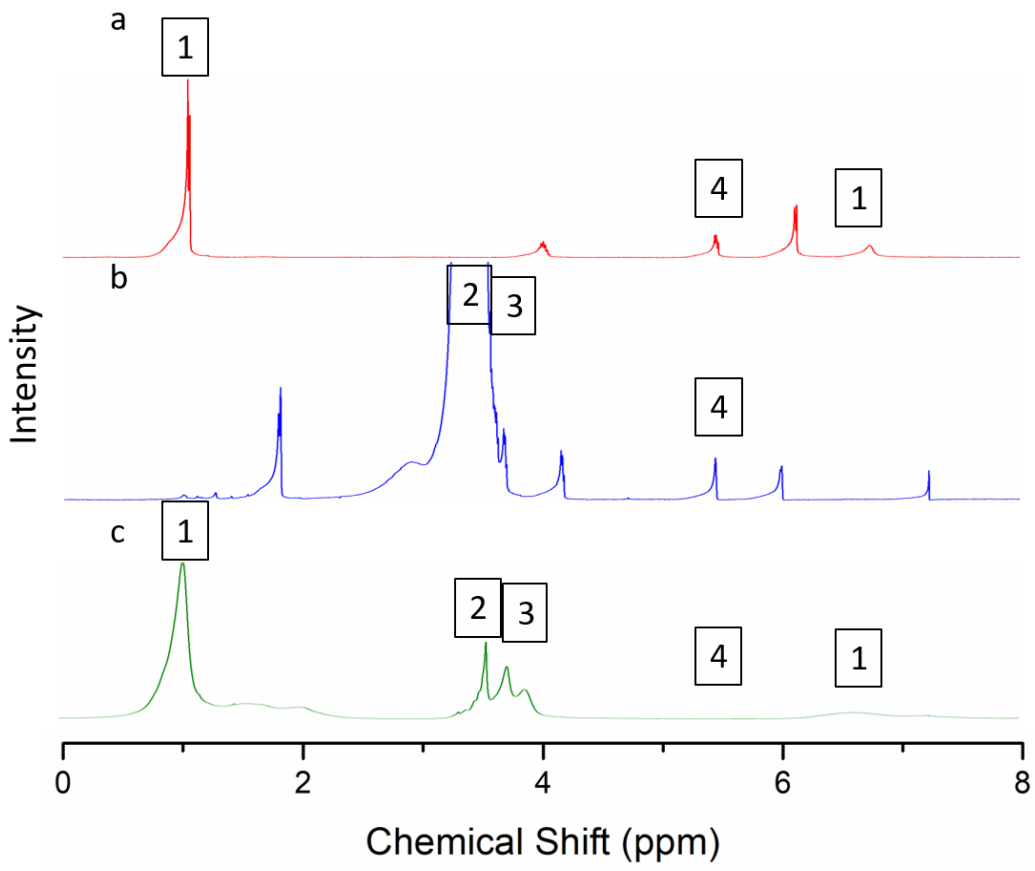

Figure 2.3. Proton Nuclear Magnetic Resonance Characterization of PEG-PNIPAAm. H NMR peaks associated with (1) amide groups or (2) ether and (3) ester groups were carried over from (a) NIPAAm and (b) PEG-dimethylacrylate, into (c) PEG-PNIPAAm. Peaks associated with conjugated (4) alkenes, were lost during polymerization.

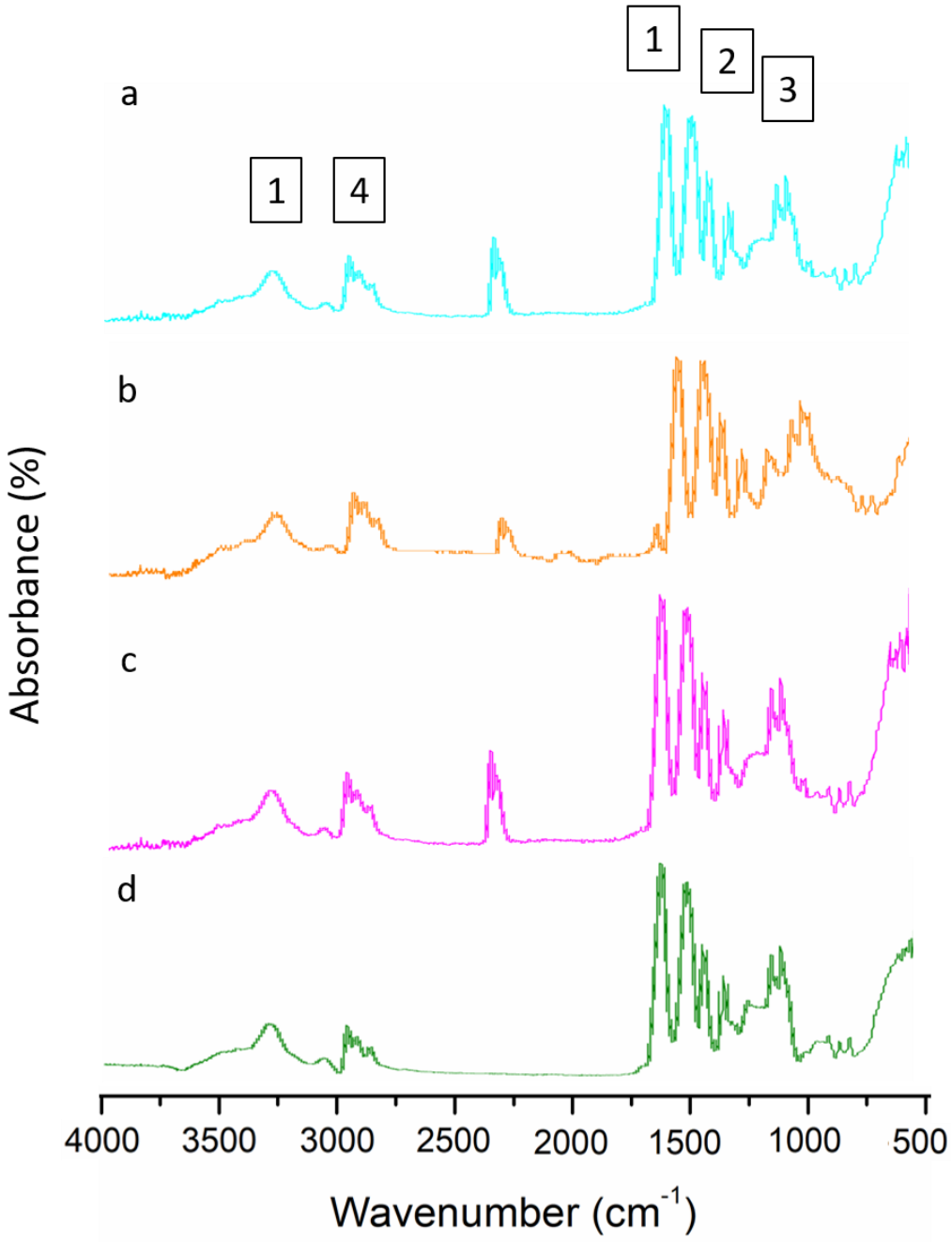

Figure 2.4. PEG-PNIPAAm Synthesis Comparison with FTIR Spectroscopy. FTIR peaks of PEG-PNIPAAm samples grouped by their reaction concentrations, (a) 5 wt. %, (b) 7.5 wt. %, (c) 10 wt. % and (d) 12.5 wt. %, were compared for differences in chemical composition. Characteristic peaks identified as (1) amide, (2) ethers, (3) esters and (4) alkanes/allyls groups.

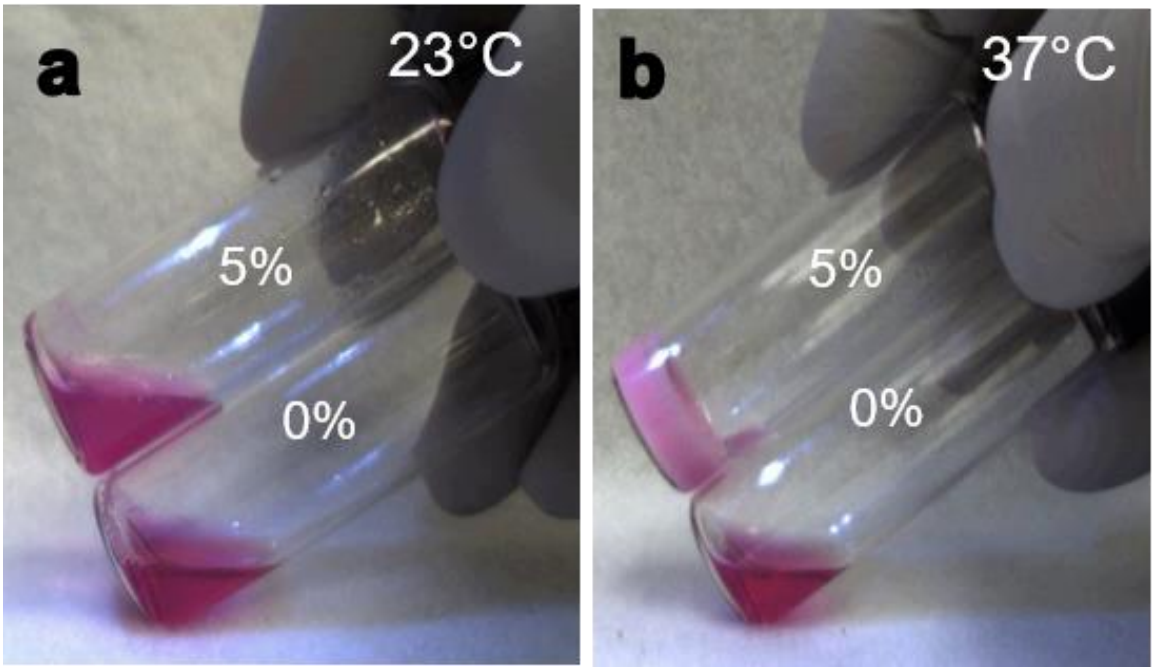

Figure 2.5. Gelation of PEG-PNIPAAm. Samples of dissolved hydrogel solutions with increasing concentrations (4-30 wt. %) were made for each synthesized reaction with different concentrations of starting materials. PEG-PNIPAAm's temperature-sensitive gelatin behavior at its critical concentration of 5 wt. % is compared to a 0 wt. % control at (a) room temperature (23 °C) and (b) 37 °C.

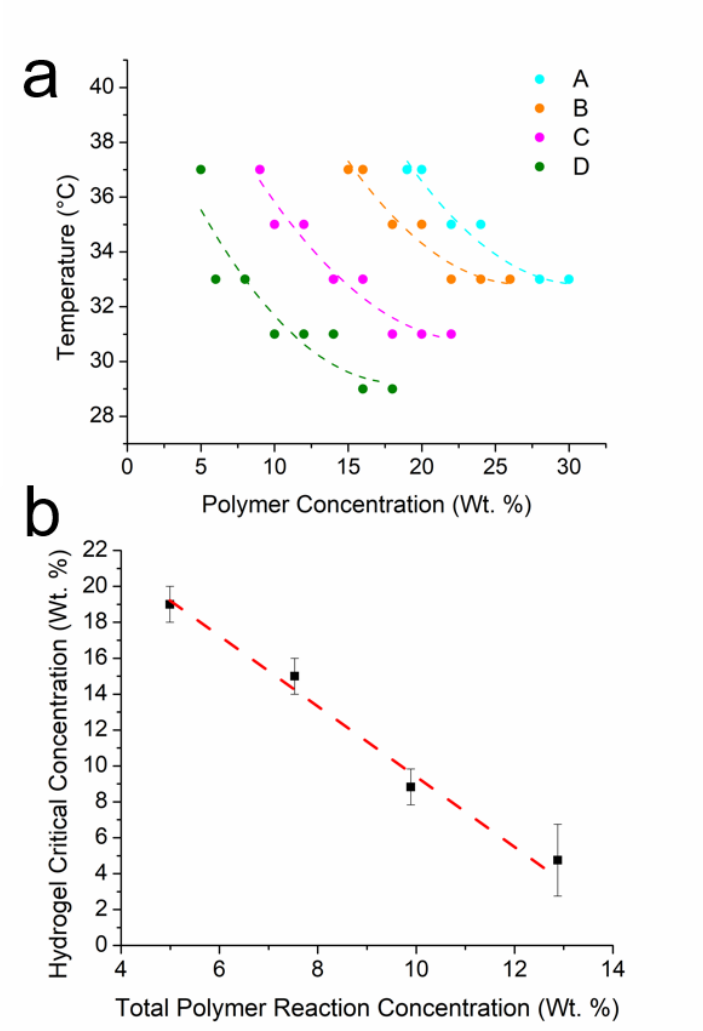

Figure 2.6. Lower Critical Solution Temperature Characterization. (a) The LCST curves of each PEG-PNIPAAm reaction concentration: (A) 5 wt. %, (B) 7.5 wt. %, (C) 10 wt. % and (D) 12.5 wt. % were characterized by determining at what temperature increasing concentrations of each sample formed a gel. (b) The lowest concentration to form a gel at any temperature (critical concentration) was inversely dependent on the reaction concentrations during synthesis.

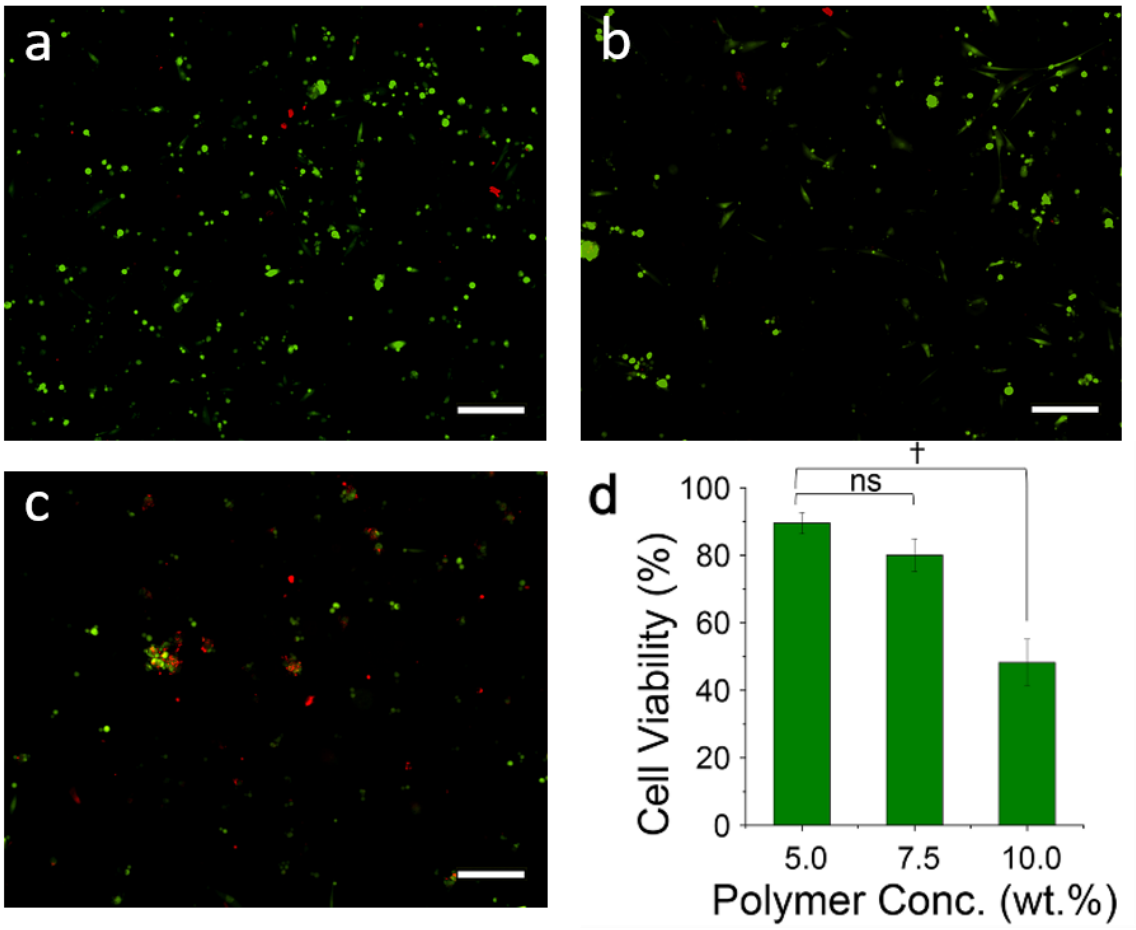

Figure 2.7. Concentration-dependent cell viability in PEG-PNIPAAm hydrogels. Human MSCs were cultured in PEG-PNIPAAm hydrogels with concentrations of (a) 5 wt. %, (b) 7.5 wt. % and (c) 10 wt. % for 24 hrs, and subjected to a live-dead cell assay showing alive (green) and dead (red) cells under fluorescent microscopy. (d) Cell viability was quantified from the fluorescent images. Scale bar = 100 μm. † denotes statistical significance of $p < 0.05$. ns denotes no statistical significance.

References

1. Bourke, S. L.; Al-Khalili, M.; Briggs, T.; Michniak, B. B.; Kohn, J.; Poole-Warren, L. A., A photo-crosslinked poly (vinyl alcohol) hydrogel growth factor release vehicle for wound healing applications. *The AAPS Journal* **2003,** *5* (4), 101-111.

2. Chou, A. I.; Akintoye, S. O.; Nicoll, S. B., Photo-crosslinked alginate hydrogels support enhanced matrix accumulation by nucleus pulposus cells in vivo. *Osteoarthritis and cartilage* **2009,** *17* (10), 1377-1384.

3. Yu, L.; Ding, J., Injectable hydrogels as unique biomedical materials. *Chemical Society Reviews* **2008,** *37* (8), 1473-1481.

4. Baier Leach, J.; Bivens, K. A.; Patrick Jr, C. W.; Schmidt, C. E., Photocrosslinked hyaluronic acid hydrogels: natural, biodegradable tissue engineering scaffolds. *Biotechnology and bioengineering* **2003,** *82* (5), 578-589.

5. Devine, D. M.; Higginbotham, C. L., Synthesis and characterisation of chemically crosslinked N-vinyl pyrrolidinone (NVP) based hydrogels. *European Polymer Journal* **2005,** *41* (6), 1272-1279.

6. Mansur, H. S.; Sadahira, C. M.; Souza, A. N.; Mansur, A. A., FTIR spectroscopy characterization of poly (vinyl alcohol) hydrogel with different hydrolysis degree and chemically crosslinked with glutaraldehyde. *Materials Science and Engineering: C* **2008,** *28* (4), 539-548.

7. Damink, L. O.; Dijkstra, P.; Van Luyn, M.; Van Wachem, P.; Nieuwenhuis, P.; Feijen, J., Glutaraldehyde as a crosslinking agent for collagen-based biomaterials. *Journal of materials science: materials in medicine* **1995,** *6* (8), 460-472.

8. Luyn, M.; Wachem, P.; Dijkstra, P.; Olde Damink, L.; Feijen, J., Calcification of subcutaneously implanted collagens in relation to cytotoxicity, cellular interactions and crosslinking. *Journal of materials science: materials in medicine* **1995,** *6* (5), 288-296.

9. Tomazic, B.; Brown, W.; Schoen, F., Physicochemical properties of calcific deposits isolated from porcine bioprosthetic heart valves removed from patients following 2–13 years function. *Journal of biomedical materials research* **1994,** *28* (1), 35-47.

10. Hoyle, C. E.; Kinstle, J. F., *Radiation curing of polymeric materials*. ACS

Publications: **1990**.

11. Ramanan, R. M. K.; Chellamuthu, P.; Tang, L.; Nguyen, K. T., Development of a temperature-sensitive composite hydrogel for drug delivery applications. *Biotechnology progress* **2006,** *22* (1), 118-125.

12. Fisher, J. P.; Dean, D.; Engel, P. S.; Mikos, A. G., Photoinitiated polymerization of biomaterials. *Annual review of materials research* **2001,** *31* (1), 171-181.

13. Sabnis, A.; Rahimi, M.; Chapman, C.; Nguyen, K. T., Cytocompatibility studies of an in situ photopolymerized thermoresponsive hydrogel nanoparticle system using human aortic smooth muscle cells. *Journal of Biomedical Materials Research Part A* **2009,** *91* (1), 52-59.

14. Bryant, S. J.; Nuttelman, C. R.; Anseth, K. S., Cytocompatibility of UV and visible light photoinitiating systems on cultured NIH/3T3 fibroblasts in vitro. *Journal of Biomaterials Science, Polymer Edition* **2000,** *11* (5), 439-457.

15. Fedorovich, N. E.; Oudshoorn, M. H.; van Geemen, D.; Hennink, W. E.; Alblas, J.; Dhert, W. J., The effect of photopolymerization on stem cells embedded in hydrogels. *Biomaterials* **2009,** *30* (3), 344-353.

16. Lee, J. H.; Prud'Homme, R. K.; Aksay, I. A., Cure depth in photopolymerization: experiments and theory. *Journal of Materials Research* **2001,** *16* (12), 3536-3544.

17. Elisseeff, J.; Anseth, K.; Sims, D.; McIntosh, W.; Randolph, M.; Langer, R., Transdermal photopolymerization for minimally invasive implantation. *Proceedings of the National Academy of Sciences* **1999,** *96* (6), 3104-3107.

18. Elisseeff, J.; McIntosh, W.; Anseth, K.; Riley, S.; Ragan, P.; Langer, R., Photoencapsulation of chondrocytes in poly (ethylene oxide)-based semi-interpenetrating networks. *Journal of biomedical materials research* **2000,** *51* (2), 164-171.

19. Omidian, H.; Park, K., Hydrogels. In *Fundamentals and applications of controlled release drug delivery*, Springer: **2012**, pp 75-105.

20. Qu, X.; Wirsen, A.; Albertsson, A.-C., Novel pH-sensitive chitosan hydrogels: swelling behavior and states of water. *Polymer* **2000,** *41* (12), 4589-4598.

21. Geever, L. M.; Devine, D. M.; Nugent, M. J.; Kennedy, J. E.; Lyons, J. G.; Hanley, A.; Higginbotham, C. L., Lower critical solution temperature control

and swelling behaviour of physically crosslinked thermosensitive copolymers based on N-isopropylacrylamide. *European Polymer Journal* **2006,** *42* (10), 2540-2548.

22. Khan, M. Z. I.; Prebeg, Ž.; Kurjaković, N., A pH-dependent colon targeted oral drug delivery system using methacrylic acid copolymers: I. Manipulation of drug release using Eudragit® L100-55 and Eudragit® S100 combinations. *Journal of Controlled Release* **1999,** *58* (2), 215-222.

23. Jeong, B.; Bae, Y. H.; Lee, D. S.; Kim, S. W., Biodegradable block copolymers as injectable drug-delivery systems. *Nature* **1997,** *388* (6645), 860-862.

24. Comolli, N.; Neuhuber, B.; Fischer, I.; Lowman, A., In vitro analysis of PNIPAAm–PEG, a novel, injectable scaffold for spinal cord repair. *Acta biomaterialia* **2009,** *5* (4), 1046-1055.

25. Haraguchi, K.; Li, H.-J.; Matsuda, K.; Takehisa, T.; Elliott, E., Mechanism of forming organic/inorganic network structures during in-situ free-radical polymerization in PNIPA− clay nanocomposite hydrogels. *Macromolecules* **2005,** *38* (8), 3482-3490.

26. Hennink, W.; Van Nostrum, C. F., Novel crosslinking methods to design hydrogels. *Advanced drug delivery reviews* **2012,** *64*, 223-236.

27. Kang, H.-W.; Tabata, Y.; Ikada, Y., Fabrication of porous gelatin scaffolds for tissue engineering. *Biomaterials* **1999,** *20* (14), 1339-1344.

28. Colombani, D., Chain-growth control in free radical polymerization. *Progress in polymer science* **1997,** *22* (8), 1649-1720.

29. Islamova, R.; Puzin, Y. I.; Fatykhov, A.; Monakov, Y. B., A ternary initiating system for free-radical polymerization of methyl methacrylate. *Polymer Science Series B* **2006,** *48* (3), 130-133.

30. Turner, D., Autoacceleration of free-radical polymerization. 1. The critical concentration. *Macromolecules* **1977,** *10* (2), 221-226.

31. Turturro, S. B.; Guthrie, M. J.; Appel, A. A.; Drapala, P. W.; Brey, E. M.; Pérez-Luna, V. H.; Mieler, W. F.; Kang-Mieler, J. J., The effects of cross-linked thermo-responsive PNIPAAm-based hydrogel injection on retinal function. *Biomaterials* **2011,** *32* (14), 3620-3626.

32. Jiang, B.; Larson, J. C.; Drapala, P. W.; Pérez-Luna, V. H.; Kang-Mieler, J. J.; Brey, E. M., Investigation of lysine acrylate containing poly (N-

isopropylacrylamide) hydrogels as wound dressings in normal and infected wounds. *Journal of Biomedical Materials Research Part B: Applied Biomaterials* **2012,** *100* (3), 668-676.

33. Schmaljohann, D.; Oswald, J.; Jørgensen, B.; Nitschke, M.; Beyerlein, D.; Werner, C., Thermo-responsive PNiPAAm-g-PEG films for controlled cell detachment. *Biomacromolecules* **2003,** *4* (6), 1733-1739.

34. Vernengo, J.; Fussell, G.; Smith, N.; Lowman, A., Evaluation of novel injectable hydrogels for nucleus pulposus replacement. *Journal of Biomedical Materials Research Part B: Applied Biomaterials* **2008,** *84* (1), 64-69.

35. Drapala, P. W.; Brey, E. M.; Mieler, W. F.; Venerus, D. C.; Kang Derwent, J. J.; Pérez-Luna, V. H., Role of thermo-responsiveness and poly (ethylene glycol) diacrylate cross-link density on protein release from poly (N-isopropylacrylamide) hydrogels. *Journal of Biomaterials Science, Polymer Edition* **2011,** *22* (1-3), 59-75.

36. Eljarrat-Binstock, E.; Bentolila, A.; Kumar, N.; Harel, H.; Domb, A. J., Preparation, characterization, and sterilization of hydrogel sponges for iontophoretic drug-delivery use. *Polymers for Advanced Technologies* **2007,** *18* (9), 720-730.

37. Probes, M., LIVE/DEAD® Viability/Cytotoxicity Kit* for mammalian cells*. MP: **2005**.

38. Wang, J.; Zhang, J.; Zhang, X.; Zhou, H., A protein-based hydrogel for in vitro expansion of mesenchymal stem cells. *PloS one* **2013,** *8* (9), e75727.

39. Bryant, S. J.; Chowdhury, T. T.; Lee, D. A.; Bader, D. L.; Anseth, K. S., Crosslinking density influences chondrocyte metabolism in dynamically loaded photocrosslinked poly (ethylene glycol) hydrogels. *Annals of biomedical engineering* **2004,** *32* (3), 407-417.

40. Qiu, Y.; Park, K., Environment-sensitive hydrogels for drug delivery. *Advanced drug delivery reviews* **2001,** *53* (3), 321-339.

41. Derwent, J. J. K.; Mieler, W. F., Thermoresponsive hydrogels as a new ocular drug delivery platform to the posterior segment of the eye. *Transactions of the American Ophthalmological Society* **2008,** *106*, 206.

42. Kiatkamjornwong, S., Superabsorbent polymers and superabsorbent polymer composites. *Science Asia* **2007,** *33* (S1), 39-43.

CHAPTER 3. MOLDLESS HYDROGEL SCAFFOLD FOR 3D CELL CULTURE

Abstract

Hydrogels have shown great potential for various tissue engineering applications due to their capability to encapsulate cells within biomimetic, 3-dimensional (3D) microenvironments. However, the multi-step synthesis process necessary to produce cell/scaffold constructs with defined dimensions, limits their off-the-shelf translational usage. In this study, we have developed a hybrid scaffolding system which combines a thermosensitive hydrogel, poly (ethylene glycol)-poly (N-isopropylacrylamide) (PEG-PNIPAAm), with a biodegradable polymer, poly (ε-caprolactone) (PCL), into a composite, electrospun microfibrous structure. A judicious optimization of material composition and electrospinning parameters produced a structurally self-supporting hybrid scaffold which requires only a simple inoculation of cell-containing media to encapsulate cells in a 3D hydrogel within a network of PCL microfibers. We demonstrated that the hybrid scaffold enhanced chondrogenic differentiation of human mesenchymal stem cells (hMSCs), a model system used in this study, resulting in superior mechanical properties of the cell/scaffold constructs as compared to those of the pure forms

of its constitutive components. The hybrid scaffold enables a facile, single-step cell seeding process to inoculate cells within a moldless 3D hydrogel with the potential for various tissue engineering applications.

Keywords: electrospun scaffold, thermosensitive hydrogel, polycaprolactone, poly (ethylene glycol)-poly (N-isopropylacrylamide), stem cell differentiation

3.1. Introduction

Senescence-related degenerative diseases, such as osteoarthritis, osteoporosis and various vascular disorders, have become prevalent due to the exponential growth of the aging population[1]. Tissue engineering approaches, especially those using stem cells, present a viable means to produce tissue replacements to overcome issues associated with allografts, such as shortage in donor organs and immuno-incompatibility. In addition to their potential for *in-vivo* implantation, engineered tissues also provide valuable *in-vitro* tissue models as platforms to develop therapeutic interventions including drug discovery/testing[2-4]. Depending on the complexity and dimensions of the assembly, two different approaches are typically utilized to create biomimetic *in-vitro* tissues. The first is a scaffold-less approach, utilizing individual cells or a patch of cells to assemble a structure resembling native tissue[5]. This process offers the ability to control each layer individually as they are added, enabling complex composition and spatial distribution of cells with various phenotypes. In contrast, a scaffold-based approach simplifies the tissue morphogenesis process by using a physical structure as a cell culture substrate, allowing for the generation of engineered tissues with relatively large dimensions. The consequence for its simplicity is the need for a well-designed scaffold to guide appropriate cellular behaviors such as stem cell self-renewal, differentiation and maturation.

Hydrogels are one of the most popular scaffolding systems due to their capability to encapsulate cells in a 3D physiological-like microenvironment[6-8].

Many different types of hydrogels have been developed through chemical modification and functionalization to direct stem cell behaviors for enhanced morphogenesis of various tissues, such as angiogenesis[9], neurogenesis/myogenesis[10], osteogenesis/adipogenesis[11], and dermal tissue formation[12]. Notably, several hydrogel systems have demonstrated an excellent ability to enhance chondrogenesis of stem cells due to their hydrated fibrous nanostructure providing a cellular environment similar to native cartilage[13-17]. However, a major drawback of using hydrogel scaffolds is the necessity for multi-step synthesis processes for cell/scaffold constructs with defined dimensions, limiting their off-the-shelf usage. The process generally requires dissolution of a hydrogel precursor polymer before mixing with cell-containing solution, followed by a gelation step via chemo-, photo- or thermo-sensitive crosslinking inside a mold to form cell-encapsulating hydrogels with a defined shape[18-19]. These multi-step processes would be eliminated with the development of a method to increase the surface area of a hydrogel precursor for faster dissolution in cell-containing culture media, while maintaining a proper shape without the need for a mold during gelation.

In this regard, electrospinning provides a means to produce a fibrous network exhibiting a very high surface area. The non-woven mesh of fibers can be produced with diameters ranging from a few nanometers to several micrometers, by electrically pulling a polymer solution with high electric potentials[20]. Any polymer solution with the appropriate viscosity, conductivity and surface tension can be

electrospun for a variety of applications. A few hydrogels, such as poly (ethylene glycol) (PEG)[21] and poly(N-isopropylacrylamide) (PNIPAAm)[22-23], have been electrospun to create fibrous scaffolds with high dissolution rates for cell culture applications. However, these electrospun hydrogel scaffolds do not maintain their structure upon cell seeding unless gelation or crosslinking occurs simultaneously during polymer dissolution.

In this study, we developed a novel electrospun hybrid scaffold which composites a thermosensitive hydrogel, PEG-PNIPAAm, with a biodegradable polymer, poly (ε-caprolactone) (PCL). We demonstrate that the thermosensitive hydrogel component of the hybrid scaffold quickly dissolves and fills the pores within the structure to encapsulate seeded cells, while PCL provides overall structural integrity, resulting in superior mechanical properties of cell/scaffold constructs as compared to scaffolds of the pure forms of its individual constitutive components (**Fig. 1**). The hybrid scaffold also enhanced chondrogenic differentiation of human mesenchymal stem cells (hMSCs), a model system used in this study. Our novel design provides a facile means to inoculate cells in 3D hydrogel with a mold-less, single step cell seeding process for various tissue engineering applications.

3.2. Methods

3.2.1. Thermosensitive hydrogel synthesis

N-isopropylacrylamide (NIPAAm) (Sigma Aldrich) monomer and PEG-

dimethylacrylate (PEG-DMA) (Fisher Scientific) were utilized to synthesize a thermosensitive hydrogel polymer, PEG-PNIPAAm, using a modified free-radical polymerization protocol[24]. Briefly, NIPAAm and PEG-DMA were dissolved together in methanol under nitrogen atmosphere at the concentrations of 9 wt. % and 1 wt. %, respectively. Azobisisobutyronitrile (AIBN) (Sigma Aldrich) was added to the solution as a free-radical initiator. The reaction flask was heated to 65 °C, and refluxed for 48 hours, followed by the evaporation of methanol. The resulting solid polymer was washed in n-hexane (Sigma Aldrich) at 45 °C for 12 hours to remove unreacted monomers. It was then grinded into a powder and vacuum filtered with three rinses of n-hexane.

3.2.2. Hydrogel characterization

Fourier transform infrared (FTIR) spectroscopy and proton nuclear magnetic resonance (H NMR) spectroscopy were used to analyze the chemical structure of the synthesized PEG-PNIPAAm. Dry powder samples were used for FTIR analysis with a Nicolet 6700 FTIR Spectrometer (Thermo Fisher Scientific) to produce infrared absorbance peaks of the PEG-PNIPAAm. Alternatively, the polymer was dissolved in deuterated chloroform (Sigma Aldrich) at 20 wt. % and subjected to H NMR spectroscopy using a Varian Inova 400 NMR machine (Varian, Inc.). The H NMR data was analyzed using Mnova Analytical Chemistry Software (Mestrelab Research). Pure PEG-DMA and NIPAAm monomers were used as controls.

The lower critical solution temperature (LCST) of the thermosensitive PEG-PNIPAAm hydrogel was characterized at various solution concentrations (4-18 wt. % dissolved in Dulbecco's Modified Eagle Medium: nutrient mixture F-12 (DMEM/F12) (Fisher Scientific) at 4 °C) using a standard inversion assay under various temperatures. The temperature of the polymer solution was gradually increased from room temperature (23 °C) to 41 °C, during which the vials containing the dissolved hydrogel solution were tilted 45° to test gelation after every 2 °C temperature increase.

3.2.3. Cell viability in hydrogel

Human MSCs were used to determine the biocompatibility of the PEG-PNIPAAm hydrogel. PEG-PNIPAAm powder was sterilized by an exposure to gamma irradiation at a dose of 10 kGy[25] before being dissolved in sterile DMEM/F12 overnight at 4 °C. The cells were inoculated into the polymer solution at 12 x 10^6 cells/mL with the final polymer solution concentrations of 5, 7.5 and 10 wt. %. The cell/polymer solutions were then plated in a 24-well plate and immediately incubated at 37 °C for 20 minutes to achieve gelation. An additional amount of warm DMEM/F12 solution was then added to the cell/hydrogel specimens. The samples were cultured for 24 hours before being subjected to a live/dead cell assay using 2 μM Calcein-AM (Fisher Scientific) and 4 μM ethidium homodimer-1 (Fisher Scientific) in sterile phosphate buffer solution (PBS) (Fisher Scientific)[26-27]. The samples were incubated in the staining solution for 5 minutes

at 37 °C. Unbound excess stain solution was aspirated and washed with warm PBS. 10% formaldehyde in PBS solution was used to fix the cells for 30 minutes while maintaining the gelled structure of the hydrogel at 37 °C. The fluorescently labeled samples were immediately imaged using a fluorescence microscope (Nikon Eclipse).

3.2.4. Hybrid scaffold fabrication

Different blending ratios of polymer solutions including but not limited to 25%, 50% and 65% PEG-PNIPAAm to PCL, were dissolved in chloroform at various overall polymer concentrations. Optimal electrospinning parameters, including overall polymer concentration (5 – 8 wt. %), solution feed rate (8 – 10 mL/hr), applied voltages (-9.5 to -13.0 kV), and spinneret-to-collector distance (25 – 55 cm), were experimentally determined by a design-of-experiment (DOE) approach for each blending ratio to achieve an appropriate average fiber diameter of 11 μm for uniform cell distribution upon cell seeding (**Fig. S1.1-S1.4**)[28-31]. Pure PCL scaffolds with similar morphology and fiber diameters were also electrospun as described previously and used as controls[31]. The electrospinning duration was adjusted to achieve a scaffold thickness of approximately 2.5 mm. The resulting fibrous mesh was then vacuum dried overnight at <30 mmHg to remove residual chloroform solvent[32]. Individual cylindrical scaffold samples were then cut from the mesh using a 6 mm medical biopsy punch (Miltex).

3.2.5. Hybrid scaffold characterization

Scaffold morphology and fiber diameters were evaluated using scanning electron microscopy (SEM) and ImageJ Software. Briefly, electrospun scaffold samples were sectioned into layers with a scalpel and sputter-coated with gold prior to being imaged with a Vega scanning electron microscope (Tescan). Individual scaffold dimensions were measured with digital calipers and weighed before further testing. Scaffold porosity was determined using a liquid displacement method similar to our previous work[33]. Gelation of the hybrid scaffolds was induced by injecting 65 µL of DMEM/F12 solution onto each scaffold and incubating them at 37 °C for 20 minutes. The gelled scaffolds were immediately snap frozen in liquid nitrogen and lyophilized for 2 days using a Freezone 1 lyophilizer (Labconco) before imaging by SEM. Alternatively, to visualize the PCL structure of the hybrid scaffolds, the hydrogel component was removed with a cold PBS wash overnight on a shaker plate, followed by SEM imaging.

3.2.6. Mechanical characterization

Mechanical characterization of the scaffolds was performed as previously described[31, 33]. Briefly, a custom-made compression system composed of a Soloist Motion servo controller and a Z-axis lift stage (Aerotech), was utilized to subject the scaffold to a sinusoidal compressive strain of 0.05 at 1 Hz while the force was recorded using a load cell (Honeywell). The characterization of dry scaffolds was

performed at room temperature, whereas the characterization of gelled scaffolds was performed after each scaffold was injected with 65 µL of warm DMEM/F12 media and incubated for 20 minutes at 37 °C. The compression setup was placed inside a cell culture incubator to maintain the temperature at 37 °C. Alternatively, the gelled scaffolds were cooled down to room temperature to examine the effect of the thermosensitive hydrogel on the overall mechanical properties of the hybrid scaffolds. Furthermore, the hybrid and pure PCL scaffolds after two weeks of cell culture were similarly subjected to mechanical characterization.

3.2.7. Scaffold cell culture

Scaffolds were sterilized by gamma irradiation at 10 kGy[25]. Approximately 12 x 10^6 hMSCs were suspended in 1 mL of DMEM/F12 media and 65 µL of the cell solution was seeded into each scaffold (**Fig. 3.1a and 1b**). The cell-seeded scaffolds were immediately incubated at 37 °C for 20 minutes before an additional 600 µL of media was supplemented into each well (**Fig. 3.1c**). Samples of cell/scaffold constructs were snap frozen in liquid nitrogen and cryosectioned to determine the cellular distribution throughout the thickness of the scaffolds upon seeding, as previously described (Horner, Ico et al. 2016). Alternatively, the cell/scaffold constructs were pre-cultured in DMEM/F12 media for three days before subjecting the cells to chondrogenic media (low glucose DMEM media with 0.1 µM Dexamethasone (Sigma Aldrich), 200 µM ascorbic acid (Sigma Aldrich), 10% fetal bovine serum (Fisher Scientific), 1% penicillin/streptomycin (Fisher

Scientific) and 10 ng/mL TGF-β3 (Peprotech Inc.) for 2 weeks. After the culture period, the cell/scaffold constructs were subjected to biomechanical analysis as described earlier, or biochemical and histological analyses as described below.

3.2.8. Gene expression

After 14 days of culture, mRNA was extracted from the samples using the Qiagen RNeasy MiniKit according to the manufacturer's protocol. The cDNA was synthesized by using the iScript cDNA Synthesis Kit (Bio Rad). The synthesized cDNA was subjected to real time-polymerase chain reaction (rt-PCR) using custom SYBR Green primers to determine chondrogenic gene expression. The primers used were collagen type II (*COL2A1; forward:* CAACACTGCCAACGTCCAGAT*, reverse:* CTGCTTCGTCCAGATAGGCAA), aggrecan (*ACAN; forward:* TGAAACCACCTCTGCATTCCA*, reverse:* GACGCCTCGCCTTCTTGAAAT), and *SOX9 (forward:* TGCTCAAAGGCTACGACTGGA*, reverse:* TTGACGTGCGGCTTGTTCT*)*. *GAPDH (forward:* ATGGGGAAGGTGAAGGTCG*, reverse:* TAAAAGCAGCCCTGGTGACC*)* was used as an endogenous control gene. The data were subjected to gene expression analysis by the comparative threshold method[34-35].

3.2.9. Histology

The cell/scaffold constructs were washed twice with warm PBS and then fixed in 10% buffered formalin at 37 °C for 30 minutes. The samples were snap

frozen in liquid nitrogen, embedded in OCT compound, and cryosectioned. The sectioned samples were quickly heated up to 37 °C to minimize the dissolution of hydrogel, and subjected to either Alcian Blue or Safranin-O staining as previously described[28, 30-31]. The stained samples were then imaged using a microscope in bright field mode.

3.2.10. Statistical analysis

All experiments were performed with at least three biologically independent samples, and represented as an average ± standard deviation (SD), except for gene expression in which the standard error of mean (SEM) was used. The data were subjected to ANOVA with Tukey's post-hoc test using the SPSS software (IBM) to determine statistical significance ($p < 0.05$).

3.3. Results

The aim of this study was to develop a hybrid scaffold that exploits the superior bioinductiveness of hydrogels and the mechanical stability of electrospun microfibers (**Fig. 3.1**). To minimize the number of steps required in traditional hydrogel processing techniques such as chemical or UV-irradiation crosslinking, a thermosensitive hydrogel, PEG-PNIPAAm, was utilized. First, the molecular structure of the synthesized PEG-PNIPAAm polymer was analyzed by FTIR and H NMR spectroscopy. The characteristic peaks of PEG-PNIPAAm in its FTIR spectrum were compared to those of the precursor components, NIPAAm and

PEG-DMA (**Fig. 3.2**). The peaks associated with NIPAAm's amide bonds were observed at wavenumbers of 3300, 1650, and 1600 cm^{-1} in PEG-NIPAAm (labeled as 1 in **Fig. 3.2a, c**)[24]. The major functional molecular groups observed in PEG-PNIPAAm which were derived from PEG-DMA include an ether peak at 1300 cm^{-1} and an ester peak at 1120 cm^{-1} (labeled as 2 and 3, respectively, in **Fig. 3.2b, c**). Peaks associated with CH bond stretching are seen in all three samples (labeled as 4 in **Fig. 3.2a-c**). CH_3 asymmetric stretching are seen at 2970 cm^{-1} with NIPAAm and PEG-PNIPAAm due to NIPAAm's branched isopropyl group and their other alkanes which were hydrolyzed from their alkene groups during polymerization. There is a significantly higher peak seen in NIPAAm above 3000, denoting the presence of the alkene group amongst the monomers. When compared to PEG-PNIPAAm, this peak is considerable less dominant compared to the newly formed alkanes. For PEG-DMA, a CH peak is seen at 2891 cm^{-1} representing the absorption of alkane found throughout its long ether chain. A similar validation of the molecular structure was performed with an H NMR analysis (**Fig. 3.3**). The most prominent peaks, NIPAAm's 1-ethylene proton peak at 1.1 ppm and amide peak at 6.8 ppm (labeled as 1 in **Fig. 3.3a**), as well as PEG-DMA's peak associated with PEG's ether groups, located at 4.3 ppm (labeled as 2 in **Fig. 3.3b**), were both present in PEG-PNIPAAm[24]. The intensity ratio of the peaks for 1-ethylene protons associated with NIPAAm and 1-ethylene protons associated with PEG-DMA were used to determine an approximate ratio of 650:1 between PNIPAAm and PEG crosslinking chains in the synthesized polymer. Conjugated

alkene peaks, located at 5.8 ppm, were cleaved during polymerization and more not carried over to PEG-PNIPAAm (labeled as 3 in **Fig. 3.3a-c**).

The gelation behavior of PEG-PNIPAAm was characterized by dissolving PEG-PNIPAAm in cell culture media (DMEM/F12) at various concentrations and subjecting them to an inversion assay at various temperatures (**Fig. 3.4**). The LCST of each solution dissolved at 4 °C was determined by incubation at increasing temperatures for five minutes until gelation was observed. The solution of pure DMEM/F12 (0 wt. %) was used as a control. The temperatures at which the thermosensitive hydrogel solidified were plotted with respect to solution concentration to determine the LCST (**Fig. 3.4**). The highest concentration tested (18 wt. %) formed a gel at 29 °C. As the concentration decreased, the temperature required to induce gelation gradually increased. A solution of 5 wt. % was the minimum concentration required to form a hydrogel at 37 °C.

Based on the determined LCST of PEG-PNIPAAm, cell viability was examined with hMSCs cultured in various hydrogel concentrations (5, 7.5 and 10 wt. %) using a Live/Dead cell assay (**Fig. 3.5**). Interestingly, greater cell clustering within the 3D constructs was observed as the hydrogel concentration increased. The quantification of live/dead cells by image analysis demonstrated that the hydrogel at 5 wt. % supported the highest cell viability at approximately 90%. Cells cultured in a 7.5 wt. % hydrogel were approximately 80% viable after 24 hours of culture, but was statistically insignificant from the 5 wt. % condition. In contrast, the cells cultured in a 10 wt. % hydrogel exhibited a significant decrease in cell viability

at approximately 50%.

After the chemical and biological characterization, the PEG-PNIPAAm hydrogel was composited into electrospun PCL to form hybrid scaffolds for 3D cell culture. Solutions with different blended mass ratios of PEG-PNIPAAm/PCL were synthesized to vary the scaffold characteristics (**Table 3.1, Fig. 3.6-3.9**). The optimization of electrospinning parameters was performed by a design-of-experiment (DOE) approach for each PEG-PNIPAAm/PCL ratio (**Table S1.1, Fig. S1.1-S1.4**). Solution properties, such as polymer concentration, and electrospinning parameters, such as solution feeding rate, applied voltages and collection distance, were optimized to synthesize fiber diameters of approximately 11 μm, with a scaffold porosity of approximately 90%, to promote complete cellular infiltration upon seeding without impacting the scaffolds' mechanical properties as previously shown (Horner, Ico et al. 2016). Solutions with a PEG-PNIPAAm concentration above 70% failed to produce fiber diameters greater than 8 μm, and were excluded from subsequent analyses. The individual electrospun fibers from all conditions exhibited a typical cylindrical morphology (**Fig. 3.6(a)-3.9(a)**). Various properties of the hybrid scaffolds having three representative PEG-PNIPAAm/PCL ratios including 25%, 50% and 65% (represented by PEG-PNIPAAm percentages) were examined as compared to pure PCL control scaffolds (0%) (**Table 3.1**). Based on the porosity of each scaffold condition, the appropriate volume of cell culture media was added to fill the pores, followed by incubation at 37 °C for 20 minutes. The media was maintained within the scaffold

during incubation, likely due to capillary force generated by the porous fibrous structure of the scaffold. The samples were subsequently lyophilized to reveal the structural changes of the scaffolds due to the gelation of PEG-PNIPAAm (**Fig. 3.6(b)-3.9(b)**). As expected, the hydration of pure PCL control did not change the scaffold structure. In contrast, the hydration of the hybrid scaffolds resulted in the dissolution and gelation of PEG-PNIPAAm as evident from the structural change, i.e., formation of nanostructured hydrogel within the micro pores of the scaffolds. The structural integrity of the scaffolds after hydrogel formation was determined by subsequent washes with room temperature PBS to de-gelate and remove PEG-PNIPAAm from the scaffold (**Fig. 3.10**). Although there were pit formations on the surface of the electrospun fibers after washing, the overall structure of the scaffold was maintained. From these morphological observations, it was determined that the 65% PEG-PNIPAAm scaffold provided the optimal concentration of PEG-PNIPAAm to form a hydrogel that completely filled the pores of the scaffold. The 65% PEG-PNIPAAm scaffold had minimal dimensional changes upon hydration with an approximately 10% reduction in height from its original thickness (**Fig. 3.11)**.

Mechanical testing of the hybrid scaffolds was performed to determine the effects of gelation of the hydrogel on the overall mechanical properties of the scaffolds. The scaffolds were subjected to a dynamic compressive strain of 0.05 at 1 Hz to determine the compressive moduli, which were further decomposed to the elastic and viscoelastic moduli as previously shown (**Fig. 3.12 and Fig. S1.5**)[31,

[36]. As-synthesized samples (Dry 23 °C) of pure PCL, and 25%, 50% and 65% PEG-PNIPAAm hybrid scaffolds exhibited similar compressive moduli of approximately 35–40 kPa. However, hydration and incubation of the scaffolds at 37 °C (Wet 37 °C) resulted in a significant increase in the compressive modulus of the 65% hybrid scaffold due to the gelation of PEG-PNIPAAm. Specifically, the compressive modulus of the 65% hybrid scaffolds, 62.1 ± 6.7 kPa, increased by close to 2-fold from its dry modulus of 29.8 ± 4.6 kPa, significantly higher than both pure PCL and PEG-PNIPAAm scaffolds in the same condition. Meanwhile, the 25% scaffold remained at 30.1 ± 7.4 kPa, relatively similar to its dry compressive modulus, likely due to the PEG-PNIPAAm concentration being below the 5 wt. % minimum concentration, and failing to form a hydrogel within the scaffolds. The 50% hybrid scaffold exhibited a slight increase to 42.6 ± 4.5 kPa upon hydration. In comparison, pure PEG-PNIPAAm hydrogel constructs exhibited a significantly lower compressive modulus of 19.3 ± 4.2 kPa, as compared to the scaffolds containing electrospun PCL fibers. The compressive modulus of the 65% hybrid scaffolds significantly decreased to approximately 25 kPa, when the temperature was returned to 23 °C (Wet 23 °C), slightly below its as-synthesized dry compressive modulus. In contrast, the pure PCL scaffold maintained around 40 kPa at both 37 and 23 °C under the hydration conditions. The elastic (G', **Fig. 3.12b**) and viscoelastic (G", **Fig. 3.12c**) moduli were also derived from the mechanical data. As expected, the pure PCL samples retained their elastic and viscoelastic properties throughout all conditions. In contrast, both elastic and

viscoelastic moduli of the hybrid scaffolds were changed upon hydration. Only the 65% hybrid scaffold exhibited a statistically significant increase in viscoelasticity, indicating more efficient gelation within the scaffolds as demonstrated from the morphological observation (**Fig. 3.6-3.9**).

Another important characteristic of an optimal scaffold is its ability to allow uniform cellular infiltration within the structure[28]. To examine such uniform cell seeding, hMSCs were seeded in the hybrid scaffolds having various blend ratios. Cellular localization was determined by fluorescence imaging of the vertical cross-sections of the cell/scaffold constructs using DAPI nuclear staining (**Fig. 3.13**). Cells seeded in both the 25% and 50% hybrid scaffolds showed sedimentation of the seeded cells near the bottom of the scaffolds. In contrast, cells seeded in the 65% hybrid scaffold penetrated the entire thickness and uniformly distributed throughout the thickness of the scaffold.

Based on the results from the scaffold characterizations, the 65% hybrid scaffolds were utilized to test their performance in tissue morphogenesis. Approximately 8 x 10^5 hMSCs were seeded in either pure PCL (0%) or 65% hybrid scaffolds with a similar thickness of 2.5 mm, and the hMSC/scaffold constructs were subjected to chondrogenic conditions. After a two-week culture period, chondrogenic gene expression including collagen type II (*COL2a1*), aggrecan (*ACAN*) and *SOX9* was significantly upregulated in the cells cultured in the 65% hybrid scaffolds as compared to those in pure PCL controls (0%) (**Fig. 3.14**). At the protein level, the deposition of chondrogenic ECM was enhanced in the 65%

hybrid scaffolds as evident from greater intensities of Safranin-O and Alcian blue stains for glycosaminoglycan (**Fig. 3.15**). As expected from the gene and protein expression results, the culture of hMSCs in the 65% hybrid scaffold resulted in greater compressive moduli, and significantly greater viscoelasticity as compared to that of the cell-cultured pure PCL, indicating greater chondrogenic maturation (**Fig. 3.16**).

3.4. Discussion

In conjunction with biochemical factors, the physical environment of the cells in engineered tissues, such as scaffold stiffness, pore size and its spatial arrangement, significantly affects tissue morphogenesis. The dimensionality of the scaffolds, which governs the availability of adhesion sites in 3D, has especially been shown to alter intracellular signaling cascades as compared to those in 2D[37-39]. In fact, stem cell behaviors including self-renewal, migration, and more importantly differentiation, are partly regulated by 3D distribution of adhesion sites[40]. Chondrogenesis of MSCs has been particularly shown to be enhanced by 3D encapsulation of the cells as compared to a monolayer culture, likely due to a similar cellular arrangement found in the native environment. The 3D encapsulation of MSCs maintains a spherical cell structure which is believed to disrupt stress actin fiber formation within the cell, activating various signaling pathways including the p38 MAPK pathway, and inhibiting the ERK and Rho kinase pathways[41-45]. Such activation/inhibition of the signaling cascades

collectively upregulates the activity of *SOX9*, the major chondrogenic transcription factor for ECM associated genes: *COL2A1* and *ACAN*. For this reason, various types of hydrogels have been utilized for cartilage tissue engineering applications[14-15, 17].

Several different approaches for the gelation of hydrogels have been developed for specific applications while chemical and UV crosslinking strategies are popular choices for cell encapsulation. However, their dependency on diffusion kinetics of the chemical crosslinkers or the penetration depth of UV light, limits the size of cell/hydrogel constructs that can be manufactured having uniform cellular infiltration and material properties[46-47]. In this regard, thermosensitive hydrogels offer an alternative strategy for uniform cellular encapsulation due to the relatively fast and thickness-independent thermal transfer in aqueous conditions. Among many thermosensitive hydrogels considered, PEG-PNIPAAm was employed in this study because of its biocompatibility, chemical modifiability, solvent miscibility for electrospinning, and its reverse thermo-sensitivity. PEG-PNIPAAm utilizes the thermosensitive gelation properties of PNIPAAm and the hydrophilicity of PEG for improved water retention. Both of the individual components, PEG and PNIPAAm, as well as their conjugated form, are biocompatible with a limited immune response from the body[24, 48-50]. Through a cell viability assay, we also demonstrated the minimal cytotoxicity of PEG-PNIPAAm. Although there was a noticeable decrease in cell viability at a high hydrogel concentration, this is likely due to hydrogel syneresis causing dehydration within the gel[51]. Nevertheless, our results

demonstrated the capability of PEG-PNIPAAm to uniformly encapsulate seeded cells in 3D and support their viability. However, it presents limited potential for applications in load-bearing tissue applications due its inferior structural stability.

One approach to address the relatively weak mechanical properties of hydrogels utilizes alloying the hydrogel with supporting materials, including electrospun fibers[52]. Slow biodegradable polymers including PCL and its conjugates have been used in the form of either a mesh or cut segments to reinforce various hydrogels[53]. The inclusion of electrospun fibers, typically nanofibers, has been shown to increase the mechanical modulus of the hydrogel constructs, as compared to their pure forms[52]. Recently, a few studies have electrospun a blend of a hydrogel precursor and a supporting polymer to synthesize a monolithic scaffold. Although this strategy enhanced the mechanical properties of the scaffolds upon hydration, while minimizing the processing steps (i.e., no separate electrospinning step for the supporting material), the inherently small pore sizes of the nanofibrous structure typically prevented cellular infiltration, negatively impacting 3D tissue morphogenesis. In this regard, our previous studies have demonstrated the utility of electrospun microfibrous scaffolds for uniform cellular distribution, upon seeding via capillary action of the porous structure[28-31, 33]. In the present study, a careful screening of electrospinable hydrogel polymers and solvent compatibility with supporting polymers, enabled the synthesis of the hybrid scaffolds.

As expected, the incorporation of PCL into PEG-PNIPAAm enhanced the

mechanical properties of the hybrid scaffolds. The compressive modulus of the 65% hybrid scaffold was almost 3-fold greater than that of pure hydrogel. Moduli, especially the viscoelastic modulus, were considerably enhanced as compared to that of the pure PCL scaffolds, likely due to the hydrogel filling the pores of the microfibrous PCL backbone. In addition to the enhancement in mechanical properties, the hybrid scaffold judiciously optimized for blending composition and fiber diameter, enabled the uniform encapsulation of cells upon seeding throughout the thickness of the constructs. Notably, the process does not require any additional steps for cell seeding, unlike typical hydrogel systems, where the use of a mold is necessary to maintain the scaffold shape. Encapsulation of cells within the hydrogel of the hybrid scaffold further enhanced the chondrogenic differentiation of hMSCs, as evident by the gene expression analysis and histology, demonstrating superior bioinductivity over pure PCL scaffolds.

Overall, the developed hybrid scaffold offers advantages over pure hydrogel or pure PCL electrospun fibrous scaffolds for enhanced processability and improved stem cell behaviors. Unlike other hydrogel systems, the hybrid scaffold contains a non-fragmented supporting structure of electrospun microfibers that provides mechanical stability. Furthermore, such structural integrity simplifies the processing steps for 3D cell encapsulation in the hydrogel, by removing the necessity of using molds during gelation to shape the construct. It also accommodates uniform cell seeding throughout the scaffold while providing a nanofibrous hydrogel network to mimic native ECM. The hybrid scaffold developed

in this study potentially offers a platform for tailored tissue scaffolding with easy modification of the hydrogel chemistry for functional enhancement, such as ligand incorporation for cell type-specific adhesion and crosslinking density for mechanical property modulation. At the same time, it mediates the inherent shortcomings of other hydrogel systems, i.e., mechanical instability and a multi-step fabrication process. Although MSC-derived chondrogenesis was investigated in this study to demonstrate the functionality of the developed hybrid scaffold, it is possible to expand the customization of either the hydrogel or the polymer backbone to optimize the scaffold for different applications and desired tissue types.

3.5. Conclusion

In this study, we have developed a hybrid scaffold system that combines the superior bioinductivity of a hydrogel with the mechanical stability of electrospun fibers. The combination of thermosensitive PEG-PNIPAAm and PCL microfibers in a monolithic form enabled 3D cell encapsulation within the hydrogel by a simple cell seeding process. The hybrid scaffold improved the mechanical properties of cell/scaffold constructs while enhancing chondrogenic differentiation of hMSCs. Therefore, this novel scaffolding strategy may provide an opportunity to develop off-the-shelf, easy-to-use tissue scaffolding systems for various engineered tissues that benefit from 3D cell encapsulation within hydrogels.

Acknowledgements

This study was supported by the UCR initial Complement Fund and submitted to ACS Applied Materials and Interfaces for publication.

Supporting Information

Appendix 1. Table of design-of-experiment (DOE) conditions, Morphological analysis of electrospun hybrid scaffolds, Stress-Strain data for hybrid scaffolds

Table 3.1. Characterization of PEG-PNIPAA/PCL Hybrid Scaffolds. Morphological, compositional and mechanical characterization of PEG-PNIPAAm/PCL scaffolds with various blending ratios.

Ratio of PEG-PNIPAAm	Avg. Fiber Dimeter (μm)	Avg. Scaffold Porosity (%)	Avg. Wt. % of PEG-PNIPAAm (%)	Avg. Loss in Scaffold Height (%)	Avg. Room Temp. Compressive Modulus (kPa)	Avg. 37 °C Compressive Modulus (kPa)
0%	11.6 ± 1.0	92.7 ± 0.2	N/A	0.1 ± 0.1	40.7 ± 2.9	41.4 ± 3.1
25%	11.1 ± 0.5	94.9 ± 4.9	2.9 ± 0.2	1.0 ± 0.2	27.2 ± 11.5	30.1 ± 7.4
50%	11.2 ± 0.6	92.8 ± 3.8	6.5 ± 1.1	8.5 ± 0.5	28.0 ± 5.3	42.6 ± 4.5
65%	11.2 ± 0.8	89.7 ± 5.2	6.2 ± 0.4	10.0 ± 0.6	23.8 ± 9.1	62.1 ± 6.7

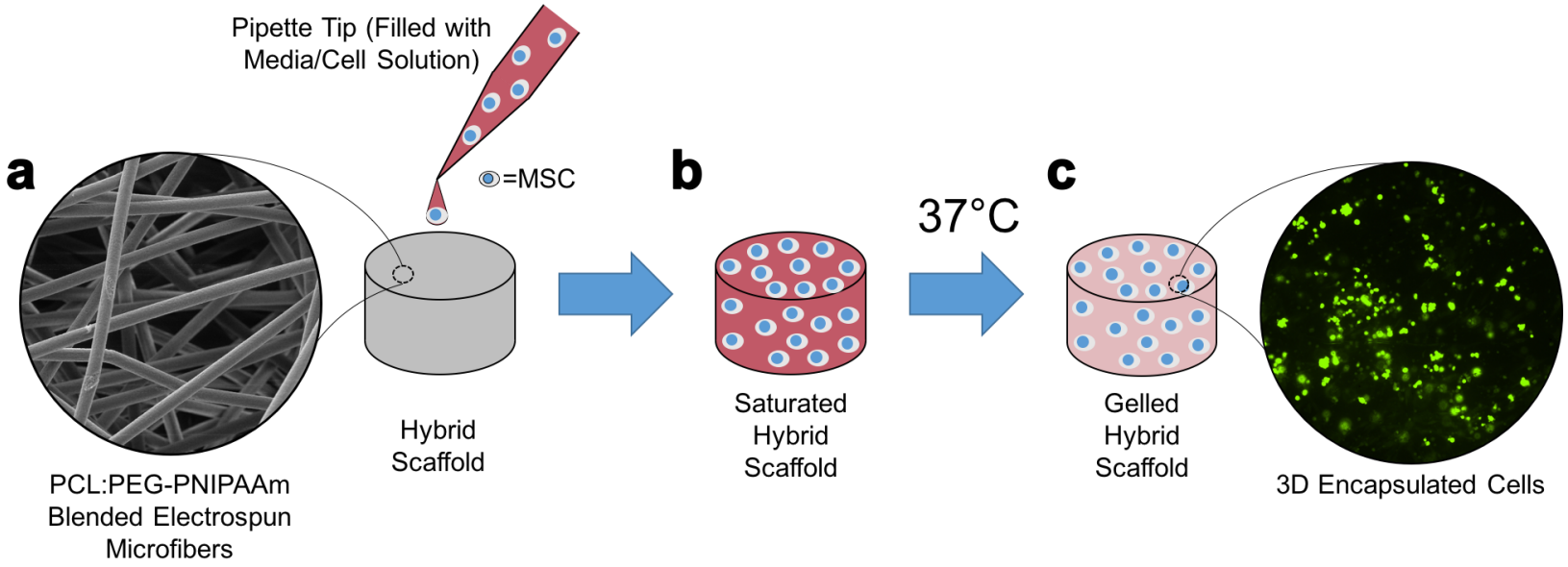

Figure 3.1. Schematic of electrospun hybrid scaffolds for moldless 3D cell encapsulation in hydrogel. (a) Thermosensitive PEG-PNIPAAm composited with PCL was electrospun to produce thick (~ 2.5 mm) hybrid scaffolds composed of micro-sized fibers. (b) Large pores allow uniform cell infiltration upon seeding throughout the thickness of the scaffolds at room temperature. (c) Subsequent increase in temperature to 37 °C induces the gelation of PEG-PNIPAAm to encapsulate the seeded cells in 3D.

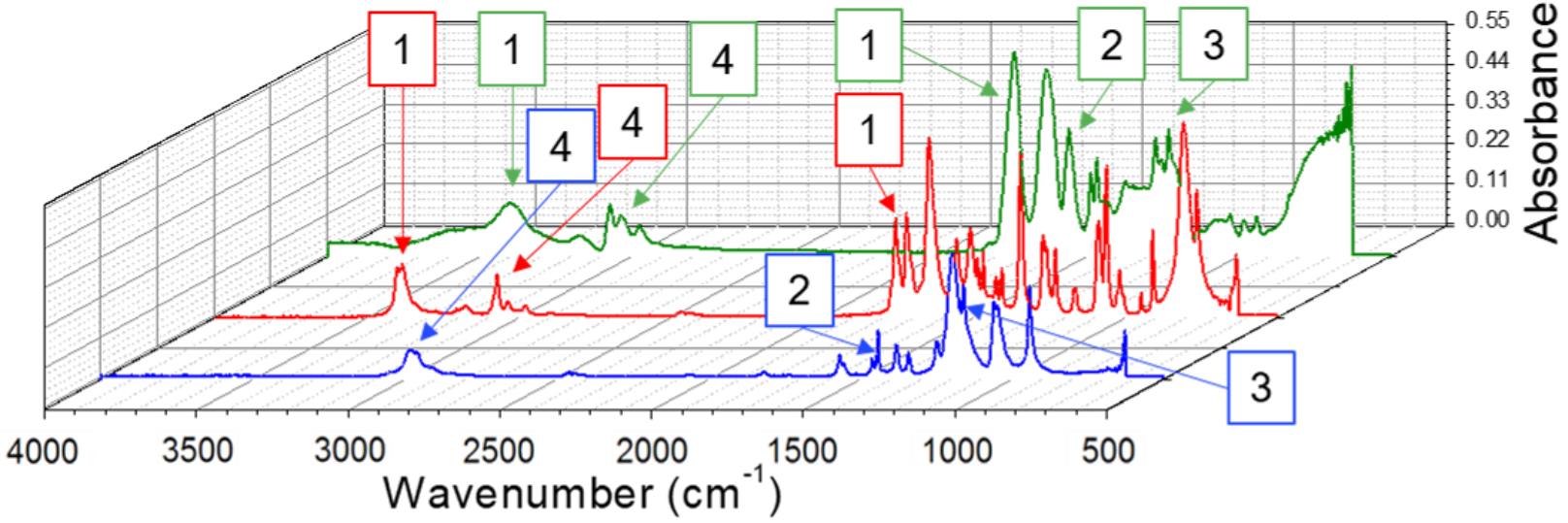

Figure 3.2. FTIR characterization of PEG-PNIPAAm hydrogel. The chemical structure of the synthesized PEG-PNIPAAm was characterized by FTIR. Peaks of PEG-DMA (blue) and NIPAAm (red) monomers were compared to those of the synthesized PEG-PNIPAAm (green) hydrogel, showing the retention of characteristic (1) acrylamide peaks of NIPAAm and the (2) ether and (3) ester peaks of PEG-DMA within the PEG-PNIPAAm hydrogel. (4) Alkene C-H bond peaks are reduced from NIPAAm and PEG-DMA, while alkane C-H bond peaks are increased in PEG-PNIPAAm.

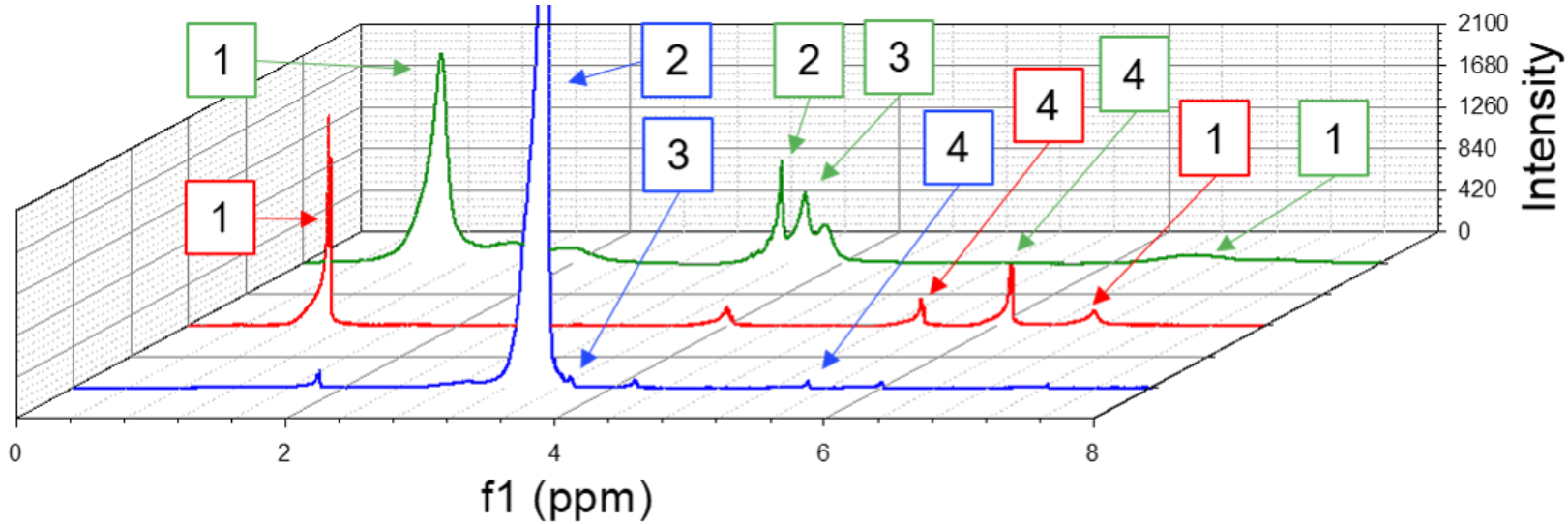

Figure 3.3. H NMR characterization of PEG-PNIPAAm hydrogel. The chemical structure of the synthesized PEG-PNIPAAm was characterized by H NMR. Peaks of PEG-DMA (blue) and NIPAAm (red) monomers were compared to those of the synthesized PEG-PNIPAAm (green) hydrogel, showing the retention of characteristic (1) acrylamide peaks of NIPAAm and the (2) ether and (3) ester peaks of PEG-DMA, present within the PEG-PNIPAAm hydrogel. (4) Conjugated alkene resonance peaks are lost in PEG-PNIPAAm following polymerization.

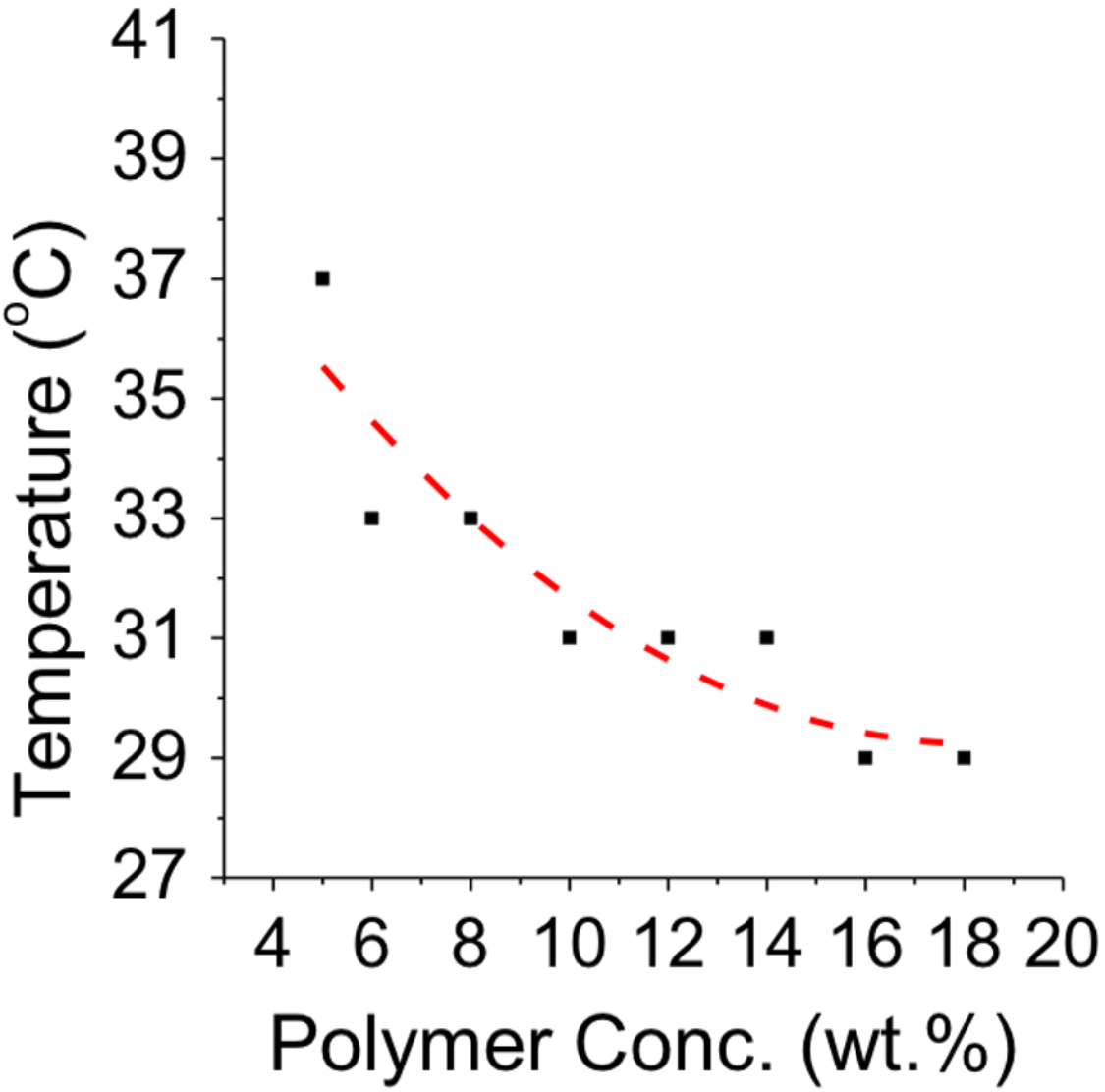

Figure 3.4. Lower critical solution temperature characterization. LCST was determined by subjecting different concentrations of PEG-PNIPAAm to a temperature sweep. Critical Concentration was determined to be the lowest concentration the hydrogel could gel (5 wt. %).

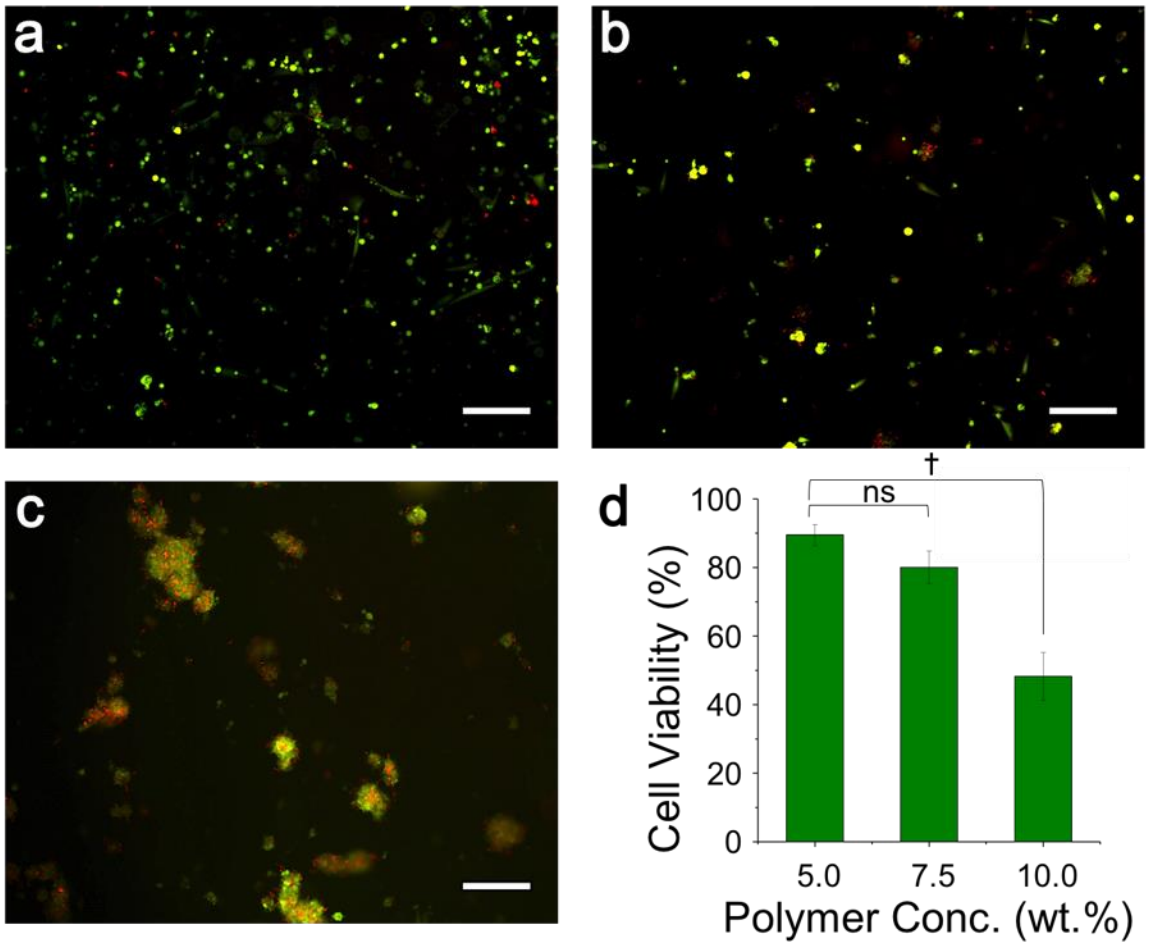

Figure 3.5. Concentration-dependent cell viability in PEG-PNIPAAm hydrogels. Human MSCs cultured in PEG-PNIPAAm with concentrations of (a) 5 wt.%, (b) 7.5 wt.% and (c) 10 wt.% for 24 hours, alive (green) and dead (red) cells under fluorescent microscopy. (d) Cell viability was quantified from the fluorescent images. Scale bar = 100 μm. † denotes statistical significance of $p < 0.05$. ns denotes no statistical significance.

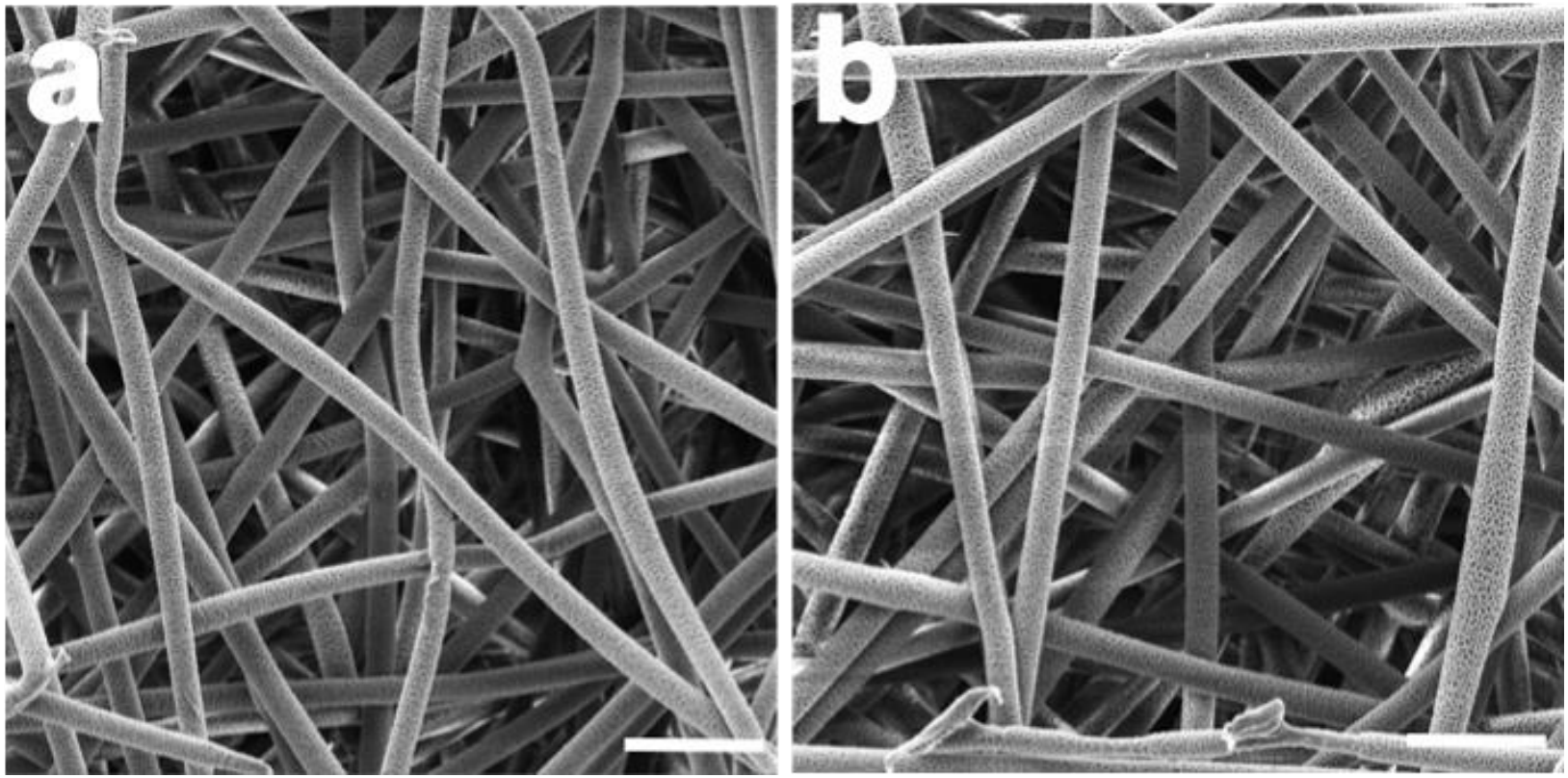

Figure 3.6. Morphology of PCL electrospun scaffolds. Microstructure of pure PCL examined by SEM (a) before and (b) after hydration followed by lyophilization. Scale bar = 50 µm.

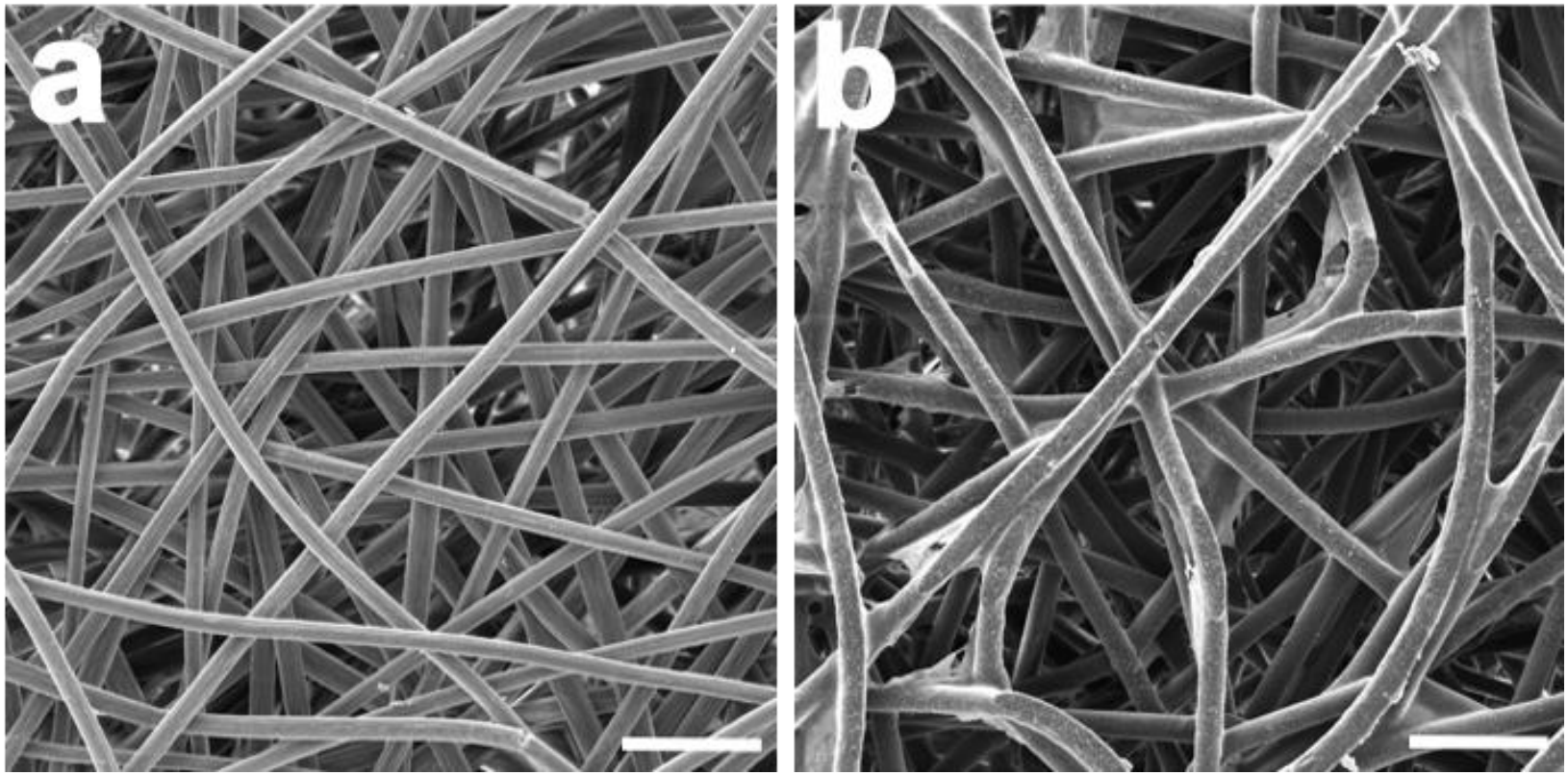

Figure 3.7. Morphology of 25% PEG-PNIPAAm/PCL hybrid electrospun scaffolds. Microstructure of 25% PEG-PNIPAAm/PCL blends examined by SEM (a) before and (b) after hydration followed by lyophilization. Scale bar = 50 µm.

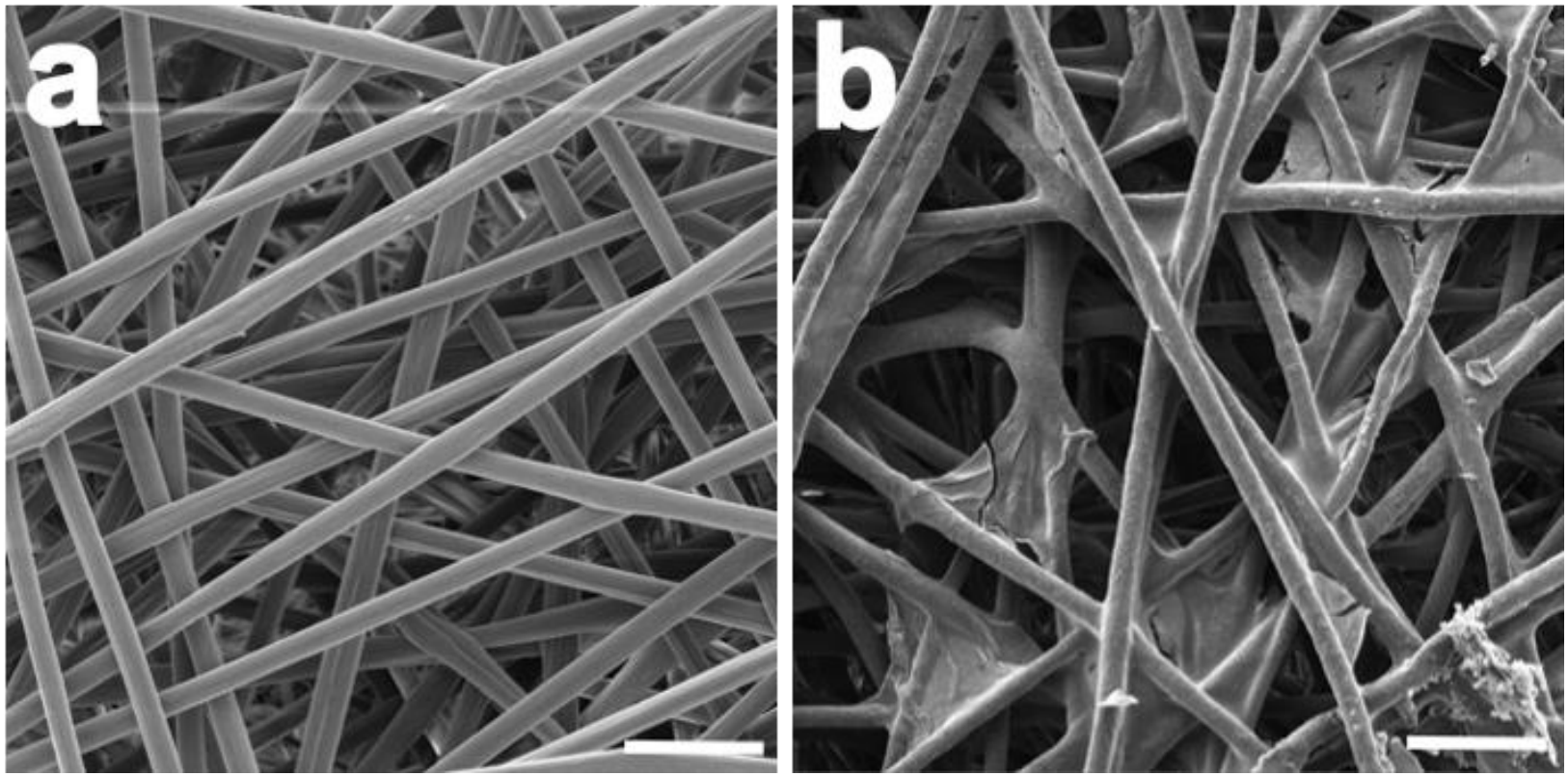

Figure 3.8. Morphology of 50% PEG-PNIPAAm/PCL hybrid electrospun scaffolds. Microstructure of 50% PEG-PNIPAAm/PCL blends examined by SEM (a) before and (b) after hydration followed by lyophilization. Scale bar = 50 µm.

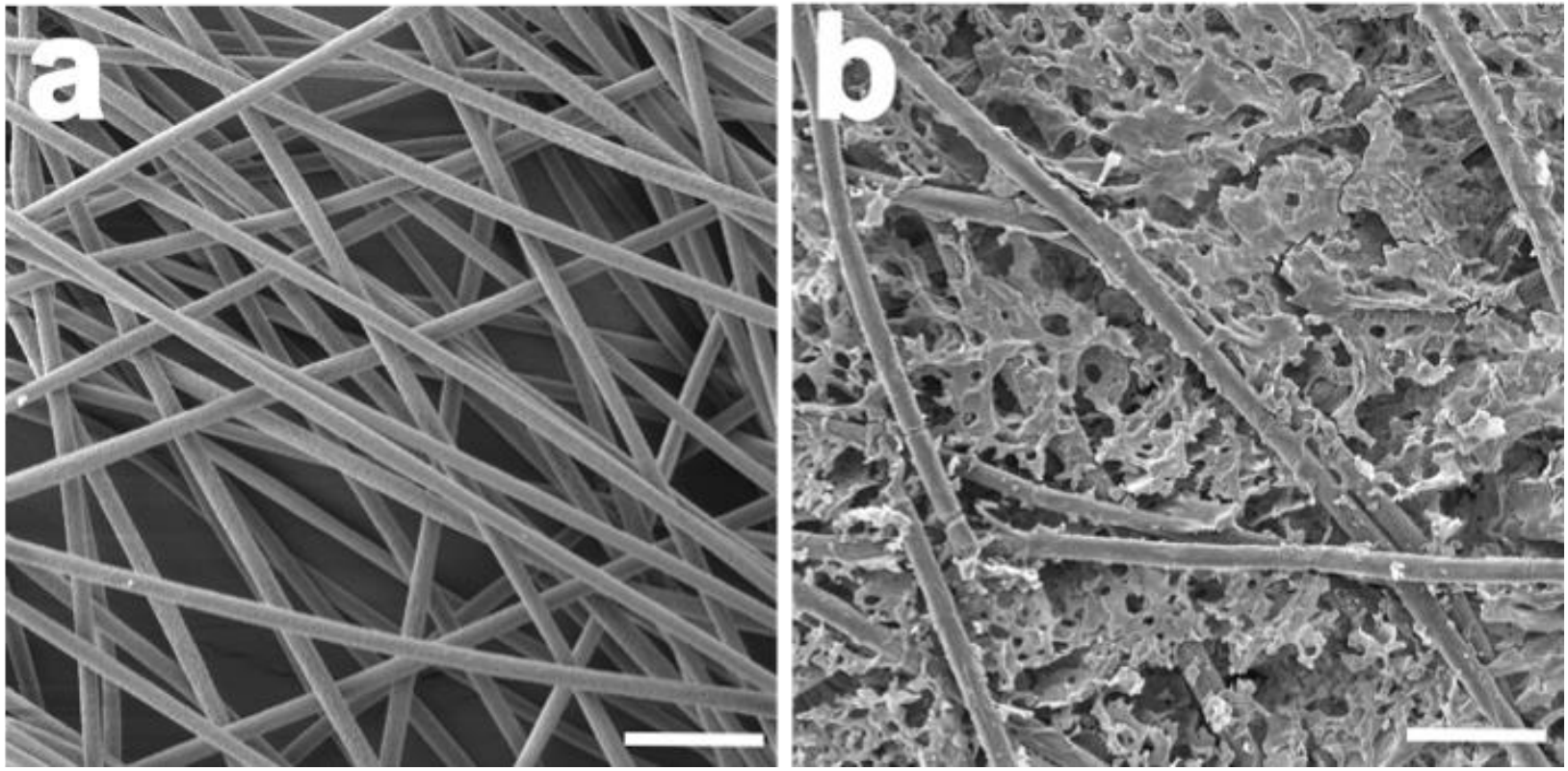

Figure 3.9. Morphology of 65% PEG-PNIPAAm/PCL hybrid electrospun scaffolds. Microstructure of 65% PEG-PNIPAAm/PCL blends examined by SEM (a) before and (b) after hydration followed by lyophilization. Scale bar = 50 µm.

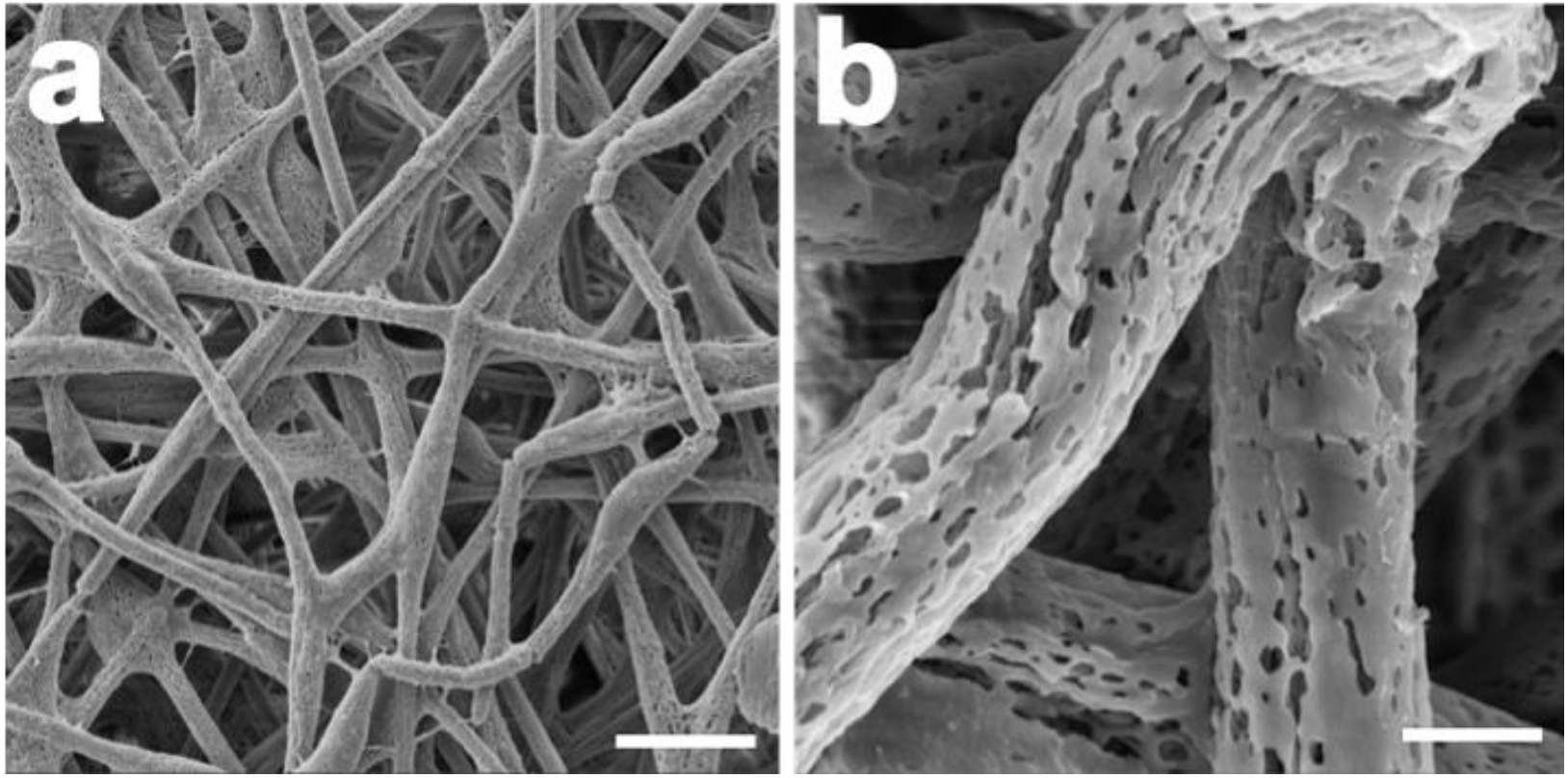

Figure 3.10. Morphology of washed PEG-PNIPAAm/PCL hybrid electrospun scaffolds. Microstructure of 65% PEG-PNIPAAm scaffold (a) washed with PBS overnight at 23 °C to remove the hydrogel component, showing (b) the dissolution and removal of PEG-PNIPAAm and the resulting generation of pits in the PCL fibers. (a) Scale bar = 50 µm. (b) Scale bar = 5 µm.

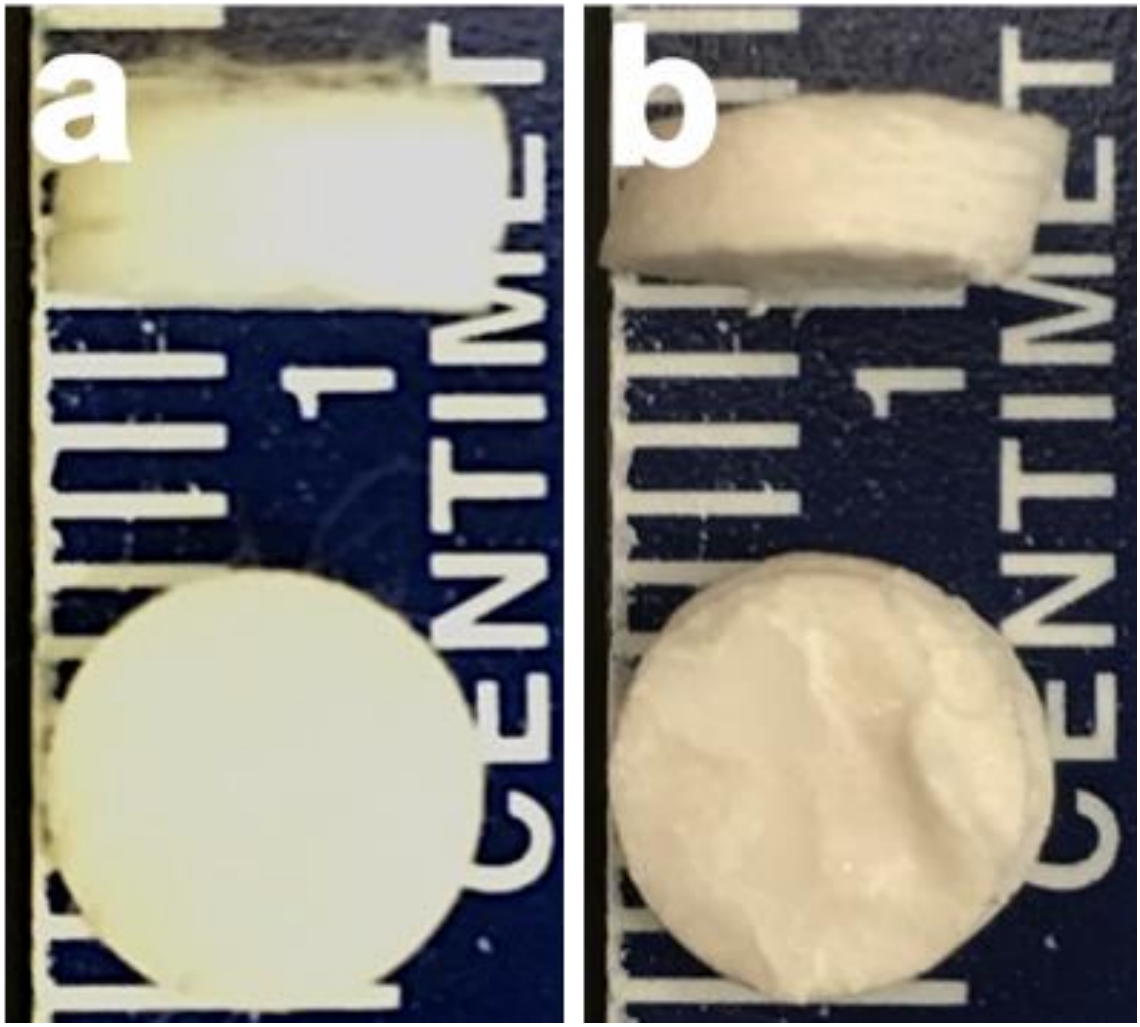

Figure 3.11. Macroscale characterization of PEG-PNIPAAm/PCL hybrid electrospun scaffolds. A macroscale image of 65% PEG-PNIPAAm/PCL scaffolds (a) before and (b) after hydration and lyophilization showed approximately 10% shrinkage in thickness.

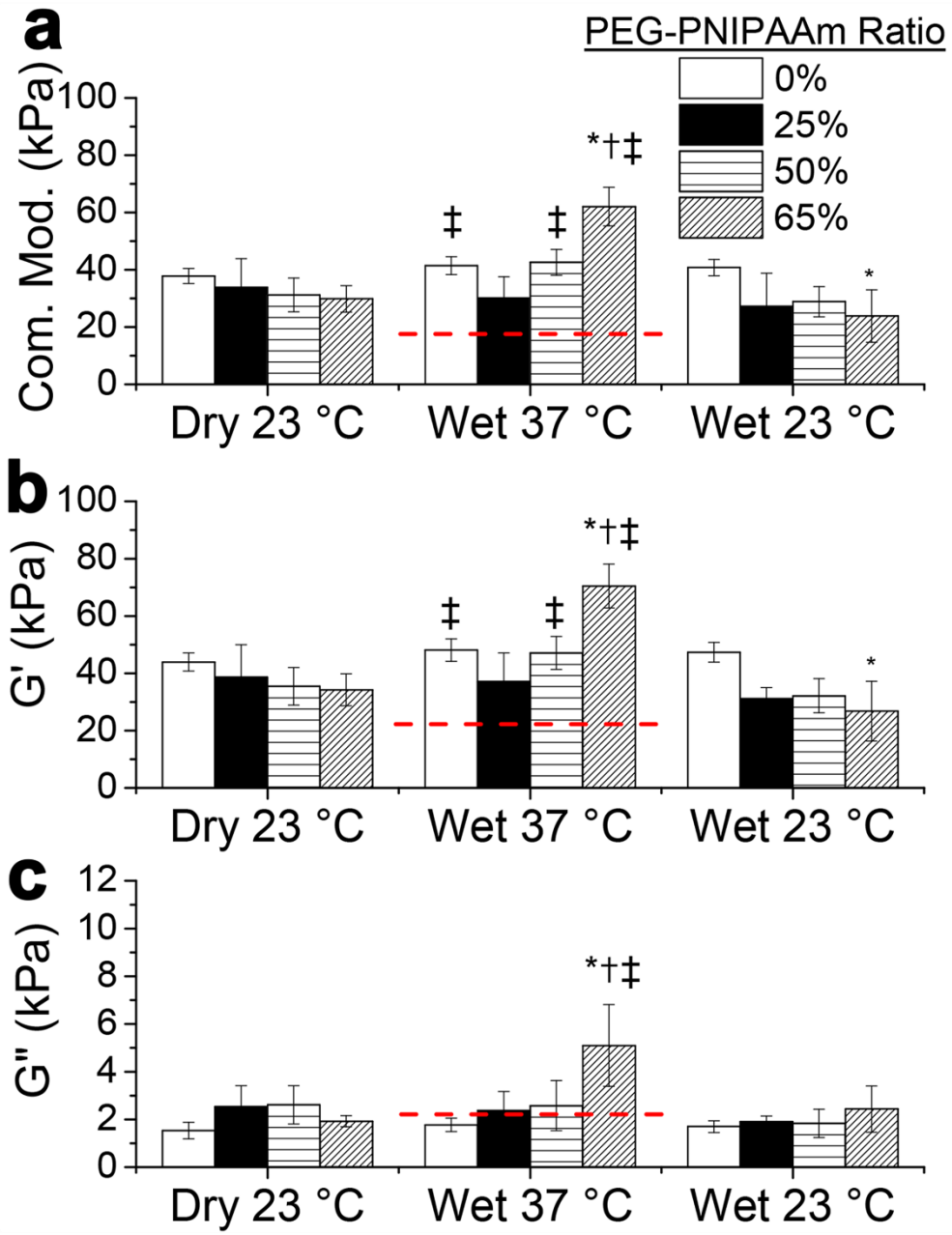

Figure 3.12. Mechanical characterization of PEG-PNIPAAm/PCL hybrid scaffolds. PEG-PNIPAAm/PCL scaffolds were subjected to mechanical testing as-synthesized (Dry 23 °C), after gelation (Wet 37 °C), and cooled down (Wet 23 °C). (a) The dynamic compressive moduli were decomposed to (b) elastic and (c) viscoelastic moduli at the different hydration and temperature conditions. Pure PCL scaffolds (0%) and pure PEG-PNIPAAm at 37 °C (--) were used as controls. *, †and ‡ denote statistical significance ($p<0.05$) with respect to control scaffolds in the same environmental condition, the same scaffold in the low temperature environmental condition and pure PEG-PNIPAAm hydrogel at 37 °C, respectively.

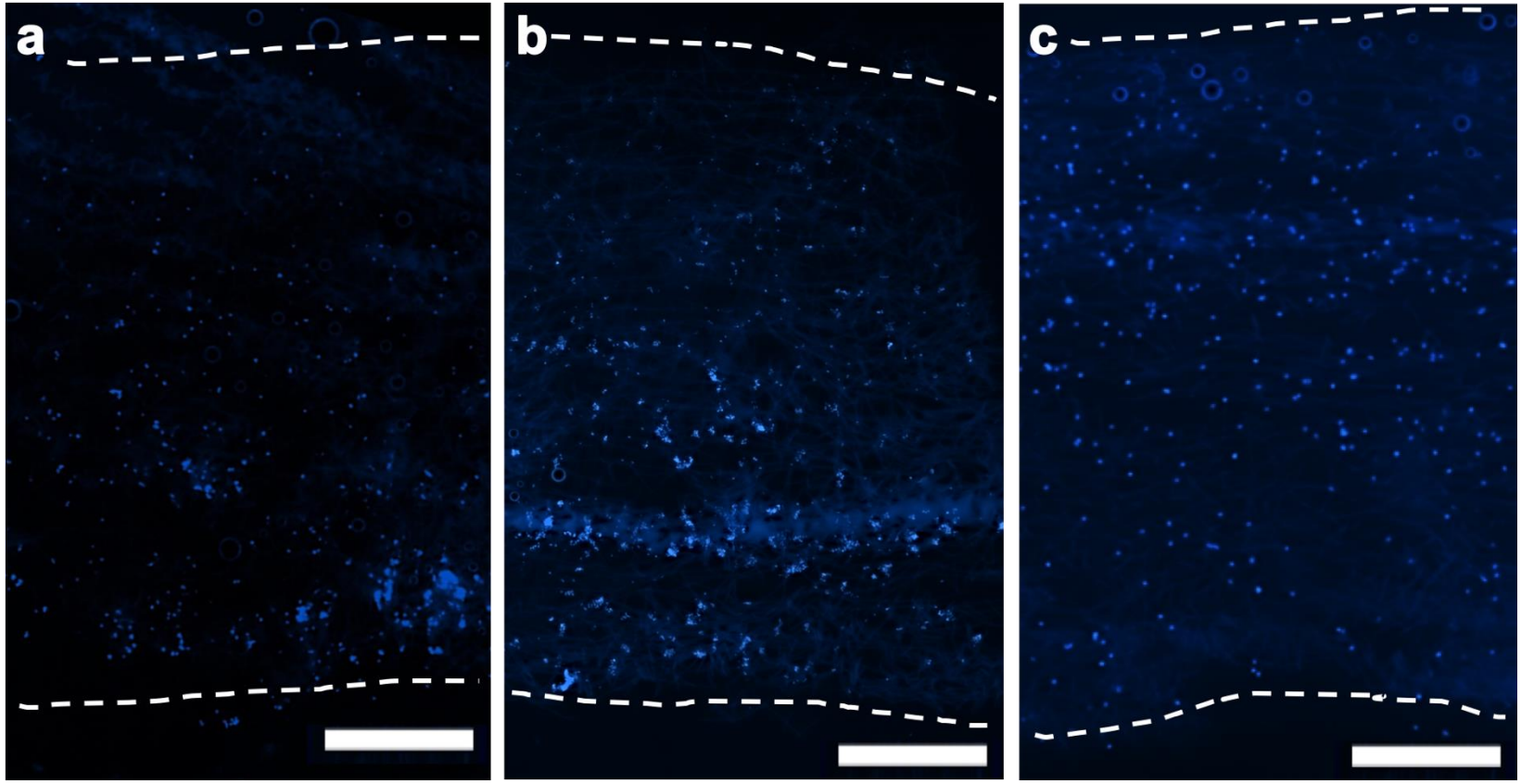

Figure 3.13. Localization of the inoculated cells in PEG-PNIPAAm/PCL hybrid scaffolds. Human MSCs were seeded into (a) 25%, (b) 50% and (c) 65% PEG-PNIPAAm hybrid scaffolds (approximately 2.5 mm thick). Cross-sectional images show cells seeded in the 65% scaffolds evenly distributed throughout while cells in the 25% and 50% scaffolds exhibited sedimentation. Dashed lines outline the top and bottom of the scaffolds. Cells visualized by DAPI nuclear staining. Scale Bar = 500 μm.

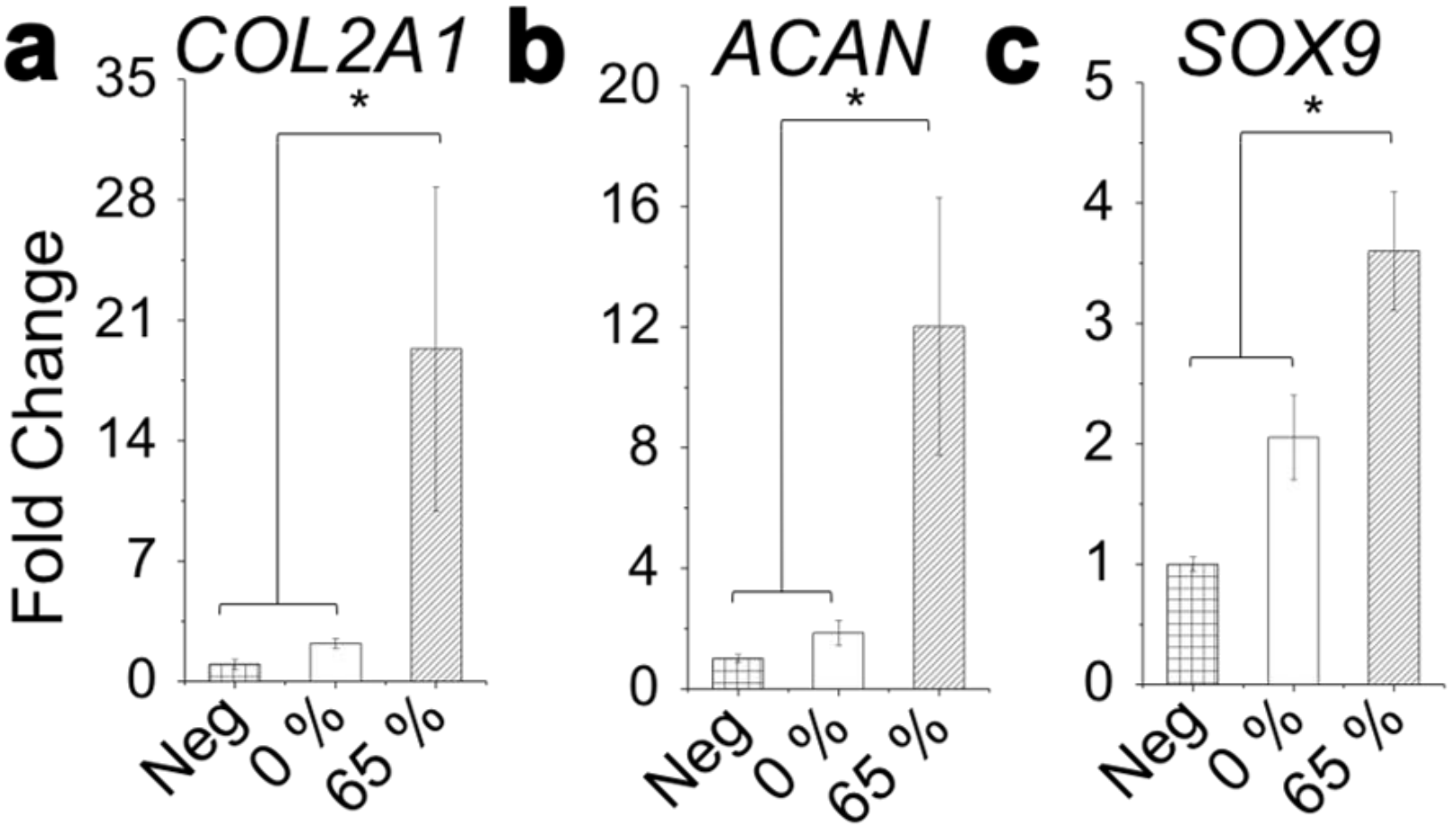

Figure 3.14. Enhanced chondrogenic differentiation of human MSCs cultured in the PEG-PNIPAAm/PCL hybrid scaffolds. Chondrogenic gene expression of (a) COL2A1, (b) ACAN, and (c) SOX9 was upregulated in the cells cultured in the 65% PEG-PNIPAAm hybrid scaffolds (65%) for two weeks compared to that of the cells cultured on the tissue culture polystyrene as a negative control (Neg) and in the pure PCL scaffolds (0%).

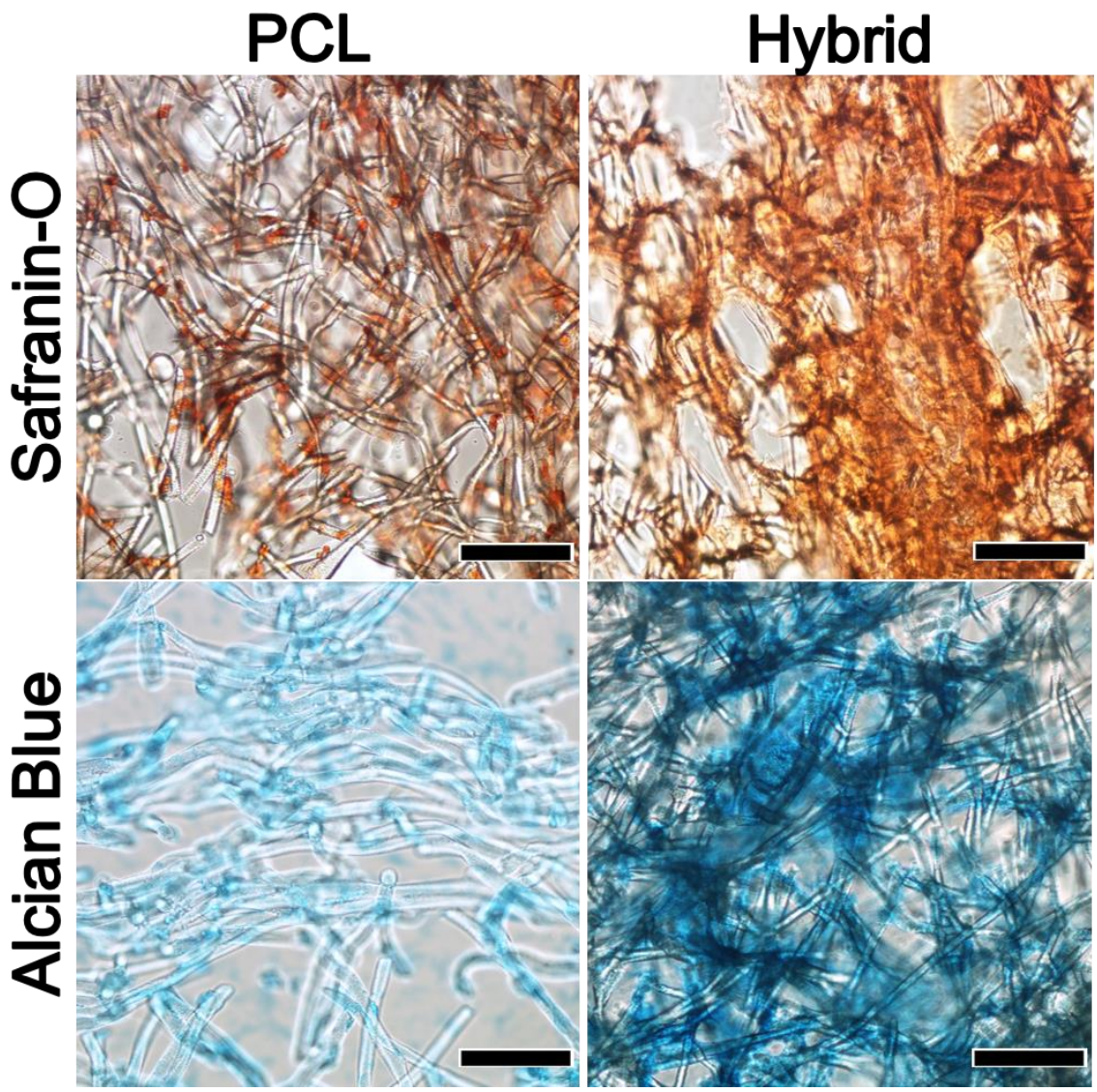

Figure 3.15. Enhanced chondrogenic differentiation of human MSCs cultured in the PEG-PNIPAAm/PCL hybrid scaffolds. Histochemical staining with Safranin-O and Alcian blue shows enhanced deposition of chondrogenic ECM in the hybrid scaffolds as compared to pure PCL. Scale bar = 100 μm.

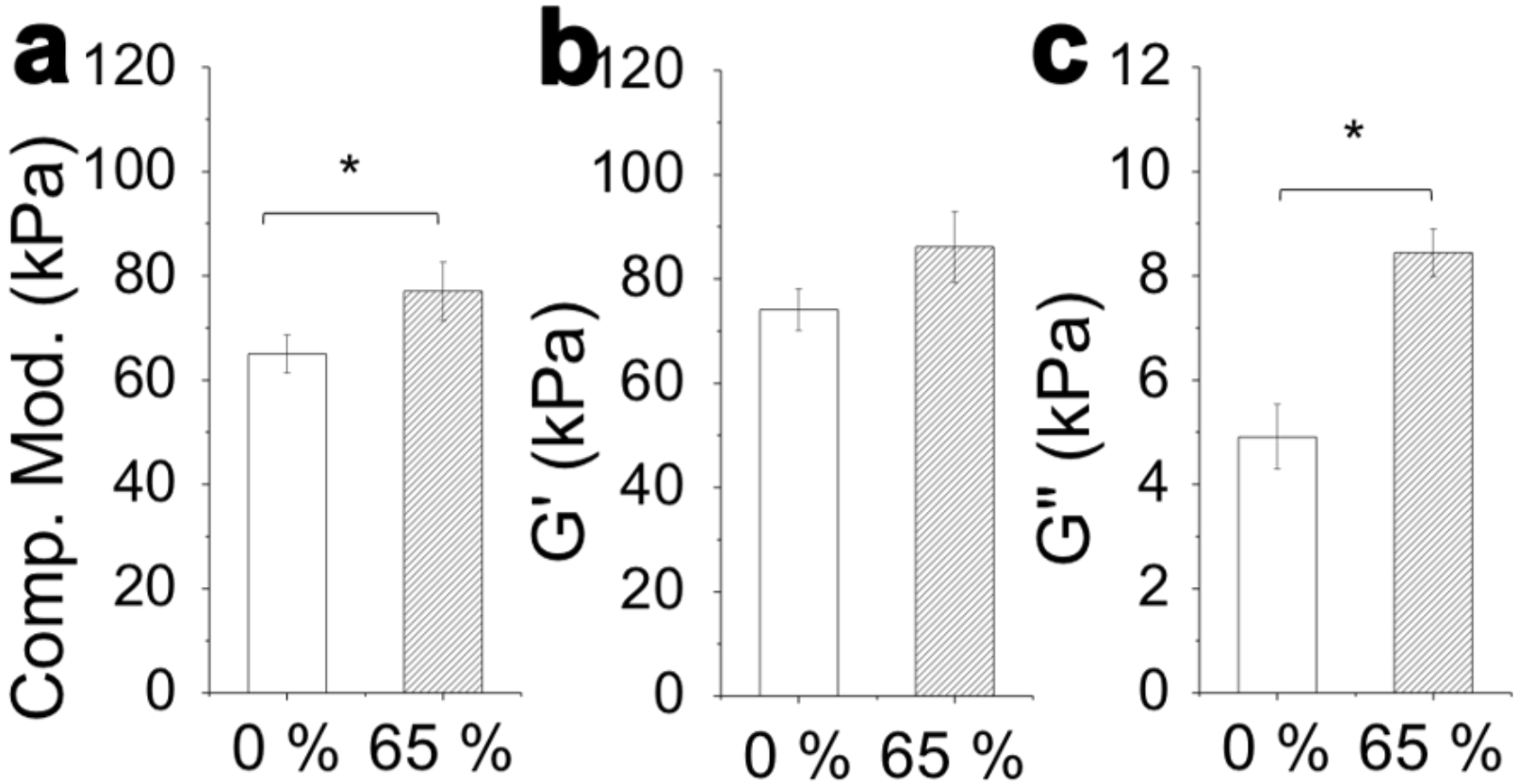

Figure 3.16. Enhanced chondrogenic differentiation of human MSCs cultured in the PEG-PNIPAAm/PCL hybrid scaffolds. Mechanical characterization of cell/scaffold constructs after two-week culture showed a greater (e) dynamic compressive, (f) elastic and (g) viscoelastic modulus in the hybrid scaffold over the pure PCL control. * denotes significant differences of $p<0.05$ between different scaffold types.

References

1. Jin, K.; Simpkins, J. W.; Ji, X.; Leis, M.; Stambler, I., The critical need to promote research of aging and aging-related diseases to improve health and longevity of the elderly population. *Aging and disease* **2015,** *6* (1), 1.

2. Bianco, P.; Robey, P. G., Stem cells in tissue engineering. *Nature* **2001,** *414* (6859), 118-121.

3. Kang, X.; Xie, Y.; Powell, H. M.; Lee, L. J.; Belury, M. A.; Lannutti, J. J.; Kniss, D. A., Adipogenesis of murine embryonic stem cells in a three-dimensional culture system using electrospun polymer scaffolds. *Biomaterials* **2007,** *28* (3), 450-458.

4. Villasante, A.; Vunjak-Novakovic, G., Tissue-engineered models of human tumors for cancer research. *Expert opinion on drug discovery* **2015,** *10* (3), 257-268.

5. Nichol, J. W.; Khademhosseini, A., Modular tissue engineering: engineering biological tissues from the bottom up. *Soft matter* **2009,** *5* (7), 1312-1319.

6. Lee, K. Y.; Mooney, D. J., Hydrogels for tissue engineering. *Chemical reviews* **2001,** *101* (7), 1869-1880.

7. Tan, H.; Marra, K. G., Injectable, biodegradable hydrogels for tissue engineering applications. *Materials* **2010,** *3* (3), 1746-1767.

8. Alexander, A.; Khan, J.; Saraf, S.; Saraf, S., Polyethylene glycol (PEG)–Poly (N-isopropylacrylamide)(PNIPAAm) based thermosensitive injectable hydrogels for biomedical applications. *European Journal of Pharmaceutics and Biopharmaceutics* **2014,** *88* (3), 575-585.

9. Bakshi, A.; Fisher, O.; Dagci, T.; Himes, B. T.; Fischer, I.; Lowman, A., Mechanically engineered hydrogel scaffolds for axonal growth and angiogenesis after transplantation in spinal cord injury. *Journal of Neurosurgery: Spine* **2004,** *1* (3), 322-329.

10. Wang, L. S.; Boulaire, J.; Chan, P. P.; Chung, J. E.; Kurisawa, M., The role of stiffness of gelatin-hydroxyphenylpropionic acid hydrogels formed by enzyme-mediated crosslinking on the differentiation of human mesenchymal stem cell. *Biomaterials* **2010,** *31* (33), 8608-16.

11. Benoit, D. S.; Schwartz, M. P.; Durney, A. R.; Anseth, K. S., Small functional groups for controlled differentiation of hydrogel-encapsulated human mesenchymal stem cells. *Nature materials* **2008,** *7* (10), 816-823.

12. Zhao, X.; Sun, X.; Yildirimer, L.; Lang, Q.; Lin, Z. Y. W.; Zheng, R.; Zhang, Y.; Cui, W.; Annabi, N.; Khademhosseini, A., Cell infiltrative hydrogel fibrous scaffolds for accelerated wound healing. *Acta biomaterialia* **2017,** *49*, 66-77.

13. Wakitani, S.; Goto, T.; Pineda, S. J.; Young, R. G.; Mansour, J. M.; Caplan, A. I.; Goldberg, V. M., Mesenchymal cell-based repair of large, full-thickness defects of articular cartilage. *J Bone Joint Surg Am* **1994,** *76* (4), 579-592.

14. Bosnakovski, D.; Mizuno, M.; Kim, G.; Takagi, S.; Okumura, M.; Fujinaga, T., Chondrogenic differentiation of bovine bone marrow mesenchymal stem cells (MSCs) in different hydrogels: influence of collagen type II extracellular matrix on MSC chondrogenesis. *Biotechnology and bioengineering* **2006,** *93* (6), 1152-1163.

15. Hwang, N. S.; Varghese, S.; Zhang, Z.; Elisseeff, J., Chondrogenic differentiation of human embryonic stem cell–derived cells in arginine-glycine-aspartate–modified hydrogels. *Tissue engineering* **2006,** *12* (9), 2695-2706.

16. Park, H.; Temenoff, J. S.; Tabata, Y.; Caplan, A. I.; Mikos, A. G., Injectable biodegradable hydrogel composites for rabbit marrow mesenchymal stem cell and growth factor delivery for cartilage tissue engineering. *Biomaterials* **2007,** *28* (21), 3217-3227.

17. Toh, W. S.; Lee, E. H.; Guo, X.-M.; Chan, J. K.; Yeow, C. H.; Choo, A. B.; Cao, T., Cartilage repair using hyaluronan hydrogel-encapsulated human embryonic stem cell-derived chondrogenic cells. *Biomaterials* **2010,** *31* (27), 6968-6980.

18. Lu, Z.; Doulabi, B. Z.; Huang, C.; Bank, R. A.; Helder, M. N., Collagen type II enhances chondrogenesis in adipose tissue–derived stem cells by affecting cell shape. *Tissue Engineering Part A* **2009,** *16* (1), 81-90.

19. Jeong, B.; Kim, S. W.; Bae, Y. H., Thermosensitive sol–gel reversible hydrogels. *Advanced drug delivery reviews* **2012,** *64*, 154-162.

20. Teo, W. E.; He, W.; Ramakrishna, S., Electrospun scaffold tailored for tissue-specific extracellular matrix. *Biotechnology journal* **2006,** *1* (9), 918-929.

21. Son, W. K.; Youk, J. H.; Lee, T. S.; Park, W. H., The effects of solution properties and polyelectrolyte on electrospinning of ultrafine poly (ethylene oxide) fibers. *Polymer* **2004,** *45* (9), 2959-2966.

22. Rockwood, D. N.; Chase, D. B.; Akins, R. E.; Rabolt, J. F., Characterization of electrospun poly (N-isopropyl acrylamide) fibers. *Polymer* **2008,** *49* (18), 4025-4032.

23. Okuzaki, H.; Kobayashi, K.; Yan, H., Non-woven fabric of poly (N-isopropylacrylamide) nanofibers fabricated by electrospinning. *Synthetic metals* **2009,** *159* (21), 2273-2276.

24. Comolli, N.; Neuhuber, B.; Fischer, I.; Lowman, A., In vitro analysis of PNIPAAm-PEG, a novel, injectable scaffold for spinal cord repair. *Acta Biomater* **2009,** *5* (4), 1046-55.

25. Eljarrat-Binstock, E.; Bentolila, A.; Kumar, N.; Harel, H.; Domb, A. J., Preparation, characterization, and sterilization of hydrogel sponges for iontophoretic drug-delivery use. *Polymers for Advanced Technologies* **2007,** *18* (9), 720-730.

26. Probes, M., LIVE/DEAD® Viability/Cytotoxicity Kit* for mammalian cells*. MP: **2005**.

27. Wang, J.; Zhang, J.; Zhang, X.; Zhou, H., A protein-based hydrogel for in vitro expansion of mesenchymal stem cells. *PloS one* **2013,** *8* (9), e75727.

28. Nam, J.; Huang, Y.; Agarwal, S.; Lannutti, J., Improved cellular infiltration in electrospun fiber via engineered porosity. *Tissue engineering* **2007,** *13* (9), 2249-2257.

29. Nam, J.; Rath, B.; Knobloch, T. J.; Lannutti, J. J.; Agarwal, S., Novel electrospun scaffolds for the molecular analysis of chondrocytes under dynamic compression. *Tissue Engineering Part A* **2008,** *15* (3), 513-523.

30. Nam, J.; Perera, P.; Rath, B.; Agarwal, S., Dynamic regulation of bone morphogenetic proteins in engineered osteochondral constructs by biomechanical stimulation. *Tissue engineering. Part A* **2013,** *19* (5-6), 783-92.

31. Horner, C. B.; Hirota, K.; Liu, J.; Maldonado, M.; Park, B. H.; Nam, J., Magnitude-Dependent and Inversely-related Osteogenic/Chondrogenic Differentiation of Human Mesenchymal Stem Cells Under Dynamic Compressive Strain. *Journal of Tissue Engineering and Regenerative Medicine* **2016**.

32. Nam, J.; Huang, Y.; Agarwal, S.; Lannutti, J., Materials selection and residual solvent retention in biodegradable electrospun fibers. *Journal of Applied Polymer Science* **2008,** *107* (3), 1547-1554.

33. Horner, C. B.; Ico, G.; Johnson, J.; Zhao, Y.; Nam, J., Microstructure-dependent mechanical properties of electrospun core–shell scaffolds at multi-scale levels. *journal of the mechanical behavior of biomedical materials* **2016,** *59*, 207-219.

34. Livak, K. J.; Schmittgen, T. D., Analysis of relative gene expression data using real-time quantitative PCR and the 2(-Delta Delta C(T)) Method. *Methods* **2001,** *25* (4), 402-8.

35. Schmittgen, T. D.; Livak, K. J., Analyzing real-time PCR data by the comparative CT method. *Nature protocols* **2008,** *3* (6), 1101-1108.

36. Nam, J.; Johnson, J.; Lannutti, J. J.; Agarwal, S., Modulation of embryonic mesenchymal progenitor cell differentiation via control over pure mechanical modulus in electrospun nanofibers. *Acta Biomater* **2011,** *7* (4), 1516-1524.

37. Cukierman, E.; Pankov, R.; Stevens, D. R.; Yamada, K. M., Taking cell-matrix adhesions to the third dimension. *Science* **2001,** *294* (5547), 1708-1712.

38. Grayson, W. L.; Ma, T.; Bunnell, B., Human mesenchymal stem cells tissue development in 3D PET matrices. *Biotechnology progress* **2004,** *20* (3), 905-912.

39. Berrier, A. L.; Yamada, K. M., Cell–matrix adhesion. *Journal of cellular physiology* **2007,** *213* (3), 565-573.

40. Huebsch, N.; Arany, P. R.; Mao, A. S.; Shvartsman, D.; Ali, O. A.; Bencherif, S. A.; Rivera-Feliciano, J.; Mooney, D. J., Harnessing traction-mediated manipulation of the cell/matrix interface to control stem-cell fate. *Nature materials* **2010,** *9* (6), 518-526.

41. Solursh, M.; Linsenmayer, T. F.; Jensen, K. L., Chondrogenesis from single limb mesenchyme cells. *Developmental biology* **1982,** *94* (1), 259-264.

42. Zanetti, N. C.; Solursh, M., Induction of chondrogenesis in limb mesenchymal cultures by disruption of the actin cytoskeleton. *The Journal of cell biology* **1984,** *99* (1), 115-123.

43. Lim, Y. B.; Kang, S. S.; An, W. G.; Lee, Y. S.; Chun, J. S.; Sonn, J. K., Chondrogenesis induced by actin cytoskeleton disruption is regulated via protein kinase C-dependent p38 mitogen-activated protein kinase signaling. *Journal of cellular biochemistry* **2003,** *88* (4), 713-718.

44. Woods, A.; Wang, G.; Beier, F., RhoA/ROCK signaling regulates Sox9 expression and actin organization during chondrogenesis. *Journal of Biological Chemistry* **2005,** *280* (12), 11626-11634.

45. Haudenschild, D. R.; Chen, J.; Pang, N.; Lotz, M. K.; D'Lima, D. D., Rho kinase–dependent activation of SOX9 in chondrocytes. *Arthritis & Rheumatology* **2010,** *62* (1), 191-200.

46. Anseth, K. S.; Wang, C. M.; Bowman, C. N., Kinetic evidence of reaction diffusion during the polymerization of multi (meth) acrylate monomers. *Macromolecules* **1994,** *27* (3), 650-655.

47. Lee, J. H.; Prud'Homme, R. K.; Aksay, I. A., Cure depth in photopolymerization: experiments and theory. *Journal of Materials Research* **2001,** *16* (12), 3536-3544.

48. Liu, X. Y.; Nothias, J.-M.; Scavone, A.; Garfinkel, M.; Millis, J. M., Biocompatibility investigation of polyethylene glycol and alginate-poly-L-lysine for islet encapsulation. *ASAIO journal* **2010,** *56* (3), 241-245.

49. Conova, L.; Vernengo, J.; Jin, Y.; Himes, B. T.; Neuhuber, B.; Fischer, I.; Lowman, A., A pilot study of poly (N-isopropylacrylamide)-g-polyethylene glycol and poly (N-isopropylacrylamide)-g-methylcellulose branched copolymers as injectable scaffolds for local delivery of neurotrophins and cellular transplants into the injured spinal cord: Laboratory investigation. *Journal of Neurosurgery: Spine* **2011,** *15* (6), 594-604.

50. Cooperstein, M. A.; Canavan, H. E., Assessment of cytotoxicity of (N-isopropyl acrylamide) and Poly (N-isopropyl acrylamide)-coated surfaces. *Biointerphases* **2013,** *8* (1), 19.

51. Cha, C.; Jeong, J. H.; Shim, J.; Kong, H., Tuning the dependency between stiffness and permeability of a cell encapsulating hydrogel with hydrophilic pendant chains. *Acta biomaterialia* **2011,** *7* (10), 3719-3728.

52. Liu, W.; Zhan, J.; Su, Y.; Wu, T.; Ramakrishna, S.; Liao, S.; Mo, X., Injectable hydrogel incorporating with nanoyarn for bone regeneration. *Journal of Biomaterials Science, Polymer Edition* **2014,** *25* (2), 168-180.

53. Kai, D.; Prabhakaran, M. P.; Stahl, B.; Eblenkamp, M.; Wintermantel, E.; Ramakrishna, S., Mechanical properties and in vitro behavior of nanofiber–hydrogel composites for tissue engineering applications. *Nanotechnology* **2012,** *23* (9), 095705.

CHAPTER 4. CONCLUSIONS

The study of biomaterials for their applications in tissue engineering has improved many properties necessary for tissue morphogenesis. Biodegradable polymers provide tissue engineers with a versatile scaffold substrate that can be tailored to function and resemble many types of natural tissue. Customization of the polymers and the fabrication methods used, continues to advance the field and provide valuable information toward comprehensive regeneration of every tissue type. Their inherent molecular structure provides cells with a scaffold reminiscent of natural ECM, further exemplified by incorporating hydrophilic polymers that swell within aqueous solutions to form nano-sized fiber networks. In this study, combining a hydrophilic hydrogel, PEG-PNIPAAm, with a structural polymer, PCL, was shown to enhance the mechanical properties of the hydrogel, improve the functionality of the structural polymer and differentiate stem cells toward a chondrogenic phenotype. These results demonstrate the practicality of our hybrid scaffold design, with the potential to be modified further for other specified differentiations and their necessary mechanical properties.

The experiments covered here-in have provided the field of tissue engineering with a novel method for fabricating a hybrid scaffold using electrospun

fibers with a structural polymer, PCL, blended with the temperature-sensitive hydrogel, PEG-PNIPAAm. We presented procedures that optimized the proposed scaffold by controlling the free-radical synthesis reaction to produce a hydrogel with improved thermal induced hydrogelation and its appropriate concentration for cell culturing with optimized viability. The scaffold's mechanical properties were augmented for its design as a load-bearing tissue implant and enhanced the chondrogenic differentiation of mesenchymal stem cells. Suggested investigations for hybrid scaffolds manufactured with our method are discussed below.

Recommendations:

- Core-Shell Electrospinning: Another fabrication method for electrospun scaffolds is core-shell, or coaxial, electrospinning. It allows the researcher to electrospin two polymers into a layered fiber for various applications. This could be advantageous for the scaffold's mechanical properties as the structure of PCL would not be affected by the dissolution of PEG-PNIPAAm, and remain as an intact fiber. Coaxial electrospinning will require additional optimization for the scaffolds fiber structure. The shell layer is believed to be the most influential over the fiber morphology and would likely be made of the hydrogel material, as it would require direct contact with the media to form an encapsulating gel, and fill the pores. Re-optimization of its electrospun structure would have to be performed with special attention on the hydrogel's ability to fill the pore volume during gelation.
- Alternative Tissue Morphogenesis: To date, many attempts to replace

cartilage tissue have been made with considerable success using stem cells. We have shown that our purposed scaffold can also direct cartilage development *in vitro*, but the potential for alternative tissue morphogenesis exists. Further experimentation, utilizing variations in cell differential media and modification to PEG-PNIPAAm's structure, can provide the opportunity for the directed development of tissue such as bone, nervous, muscle, skin and other soft tissue.

- *In vivo* Assessment: The scaffold has been evaluated for two weeks within *in vitro* conditions, however an *in vivo* assessment is necessary for advancement toward a viable option for artificial tissue implants. Implantation within a living organism would provide the opportunity to observe the longevity, biocompatibility and functionality of the hybrid scaffold. The regeneration of damaged or diseased tissue will take longer than the two week culture already performed, and with the dynamic conditions within the body, the degradation of the scaffold can be effected by many variables commonly overlooked or difficult to replicate within a cell culture dish. An acceptable immunogenic response must also be confirmed as well. Though PEG-PNIPAAm improves the mechanical properties of an electrospun PCL scaffold, it must be evaluated when exposed to the repetitive strain experienced within the body, by cartilage and other tissue.
- Hydrogel Drug-loading: Other uses of PEG-PNIPAAM include drug-loading for delayed drug release. The aggregation of its hydrophobic regions

encapsulates drugs, providing a barrier for delayed diffusion release. By loading a drug within PEG-PNIPAAm prior to electrospinning, it could be used for a delayed drug release of tissue growth factors or beneficial small molecules. The effects of loading a drug within PEG-PNIPAAm should be evaluated, as it may result in changes to its electrospinning behavior. However, utilizing a drug-loaded hydrogel with a scaffold could provide improved cell differentiation and tissue morphogenesis as they facilitate desired effects from cells through molecular signaling pathways.

- Crosslinking Modifications: As a chemically crosslinked hydrogel, PEG-PNIPAAm's characteristics can be modified by changing the structure, length and density of its crosslinker. Shorting the PEG chains used during synthesis can provide a stiffer hydrogel, further strengthening the hybrid scaffold. The same result would likely occur by increasing the density of crosslinking chains. Modifying the scaffold in this way would likely produce a scaffold better suited for osteogenic differentiation. Modifications to PEG-PNIPAAm's structure may cause changes to its electrospinning behavior and should be evaluated.
- Hydrogel Functionalization: The addition of peptide-based attachment complexes, such as RGD, could help enhance cell viability and proliferation by improving cell attachment and motility throughout the scaffold. PEG is commonly used to reduce the immune response from an implant by coating the surface with a bio-inert polymer. Other researchers have developed

methods to attach peptide complexes to PEG when it is used as a tissue scaffold. This process would be performed after the scaffolds fabrication and would therefore not affect its electrospinning. However, it could have an effect on the gelation of the hydrogel and the porosity of the scaffold.

- Hydrogel Substitution: Alternative hydrogels could be used as substitutes for PEG-PNIPAAm with the hybrid scaffold. For similar uses and properties, other reverse thermo-sensitive hydrogels, such as PEG-chitosan, would have the most similar properties and applications to PEG-PNIPAAm.

APPENDIX 1. SUPPORTING INFORMATION

Table S1.4.1. Design of experiment (DOE). Electrospun fiber diameter optimization of different PEG-PNIPAAm/PCL ratios. Overall polymer concentration and collector distance were used as variables. Values shown are average fiber diameter in μm.

25% PEG-PNIPAAm Blended Fiber Diameters				
Distance (cm)		35	45	55
Poly. Conc. (wt. %)	5	7.8 ± 1.0		7.4 ± 0.8
	6		8.2 ± 1.2	
	8	11.1 ± 0.5		10.2 ± 0.6
50% PEG-PNIPAAm Blended Fiber Diameters				
Distance (cm)		35	45	55
Poly. Conc. (wt. %)	5	8.4 ± 2.3		7.7 ± 1.9
	6		9.1 ± 0.8	
	8	13.6 ± 3.0	11.2 ± 0.6	10.0 ± 3.0
65% PEG-PNIPAAm Blended Fiber Diameters				
Distance (cm)		35	45	55
Poly. Conc. (wt. %)	5	8.3 ± 1.3		6.6 ± 0.8
	6		8.7 ± 0.6	
	8	12.3 ± 1.0		11.1 ± 1.0
75% PEG-PNIPAAm Blended Fiber Diameters				
Distance (cm)		25	35	45
Poly. Conc. (wt. %)	5	6.5 ± 1.9		6.0 ± 1.4
	5.5		6.6 ± 0.8	
	6	7.9 ± 0.9		6.0 ± 1.6

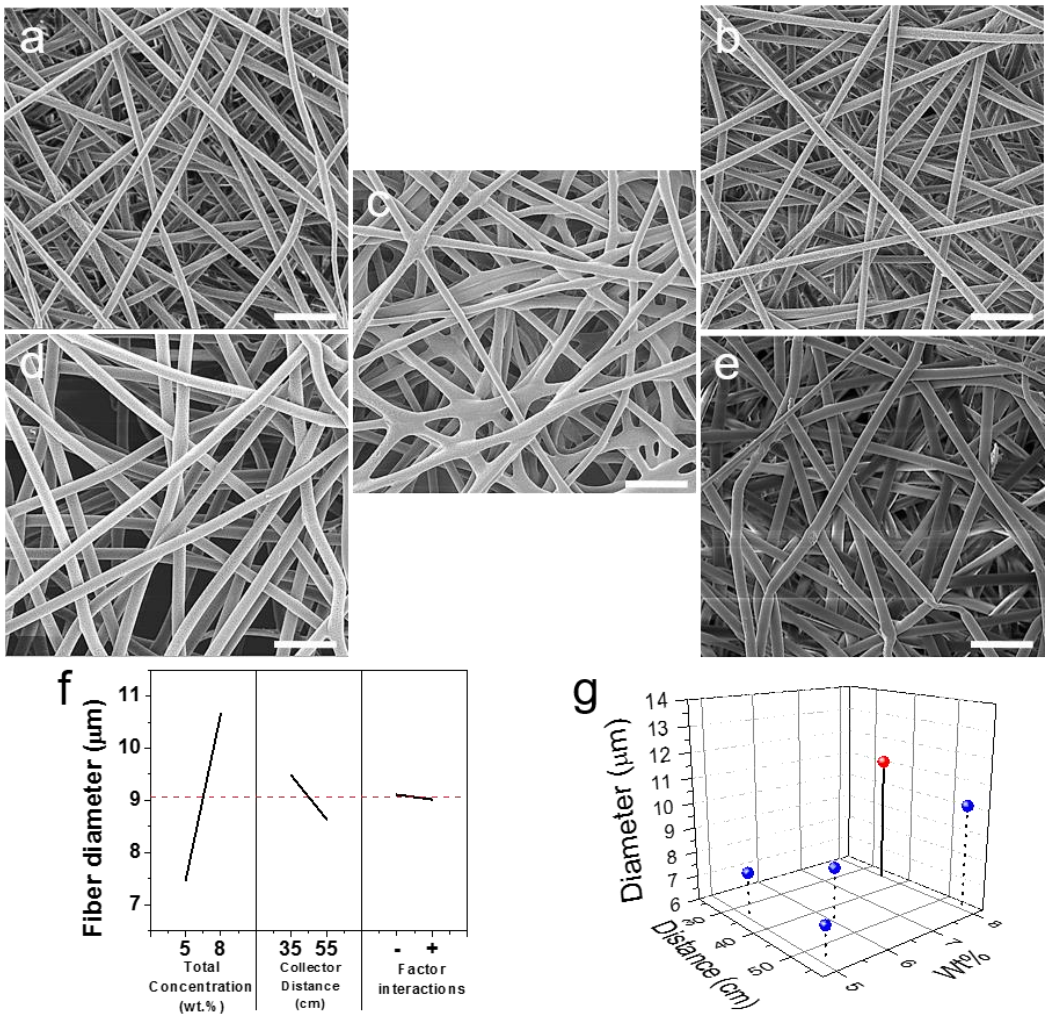

Figure S1.4.1. 25% PEG-PNIPAAm Hybrid Electrospun Fiber Optimization. Based on the DOE in Table S1, the electrospinning parameters, overall polymer concentration and collector distance, were optimized to produce microfibers having an average fiber diameter of approximately 11 µm with a typical cylindrical morphology. First, maximum (+) and minimum (-) electrospinning conditions at which cylindrical fibers were achievable, were determined for both weight percentage (wt. %) and distance (D). Within these limits, five conditions were electrospun: SEM images of (a) - wt. %, - D; (b) - wt. %, + D; (c) median (mid) wt. %, mid D; (d) + wt. %, - D; (e) + wt. %, + D (Scale bar = 50 µm). Average fiber diameters were digitally measured using ImageJ software (n = 100). (f) Using the DOE, the magnitude and direction of the effect of the electrospinning variables on fiber diameter were determined. (g) Three-dimensional plot of polymer solution concentration vs. collector distance vs. electrospun fiber diameter showing optimized (red) and non-optimized (blue) electrospinning conditions.

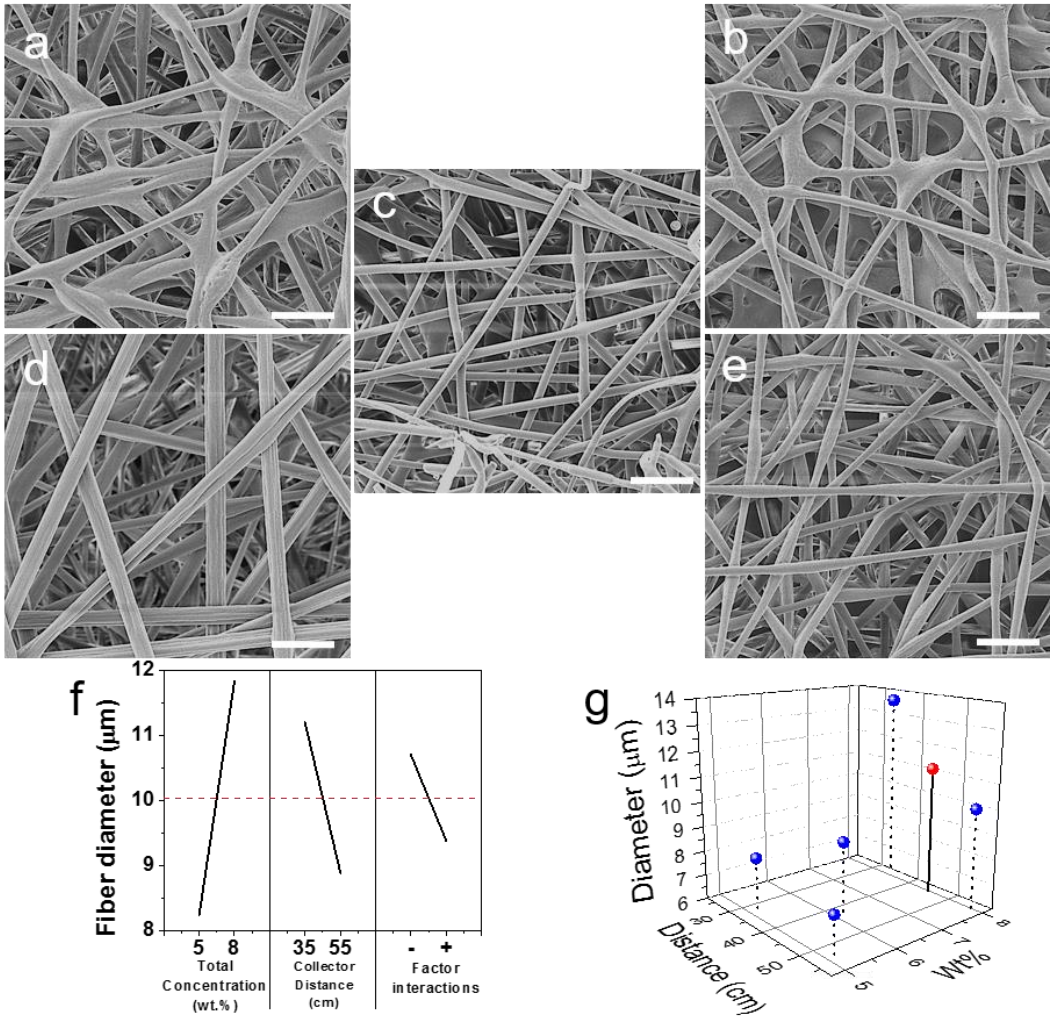

Figure S1.4.2. 50% PEG-PNIPAAm Hybrid Electrospun Fiber Optimization. Based on the DOE in Table S1 and electrospinning limits to produce a typical cylindrical fiber morphology, five conditions were electrospun: SEM images of (a) - wt. %, - D; (b) - wt. %, + D; (c) median (mid) wt. %, mid D; (d) + wt. %, - D; (e) + wt. %, + D (Scale bar = 50 µm). Average fiber diameters were digitally measured using Image J software (n=100). (f) Using the DOE, the magnitude and direction of the effect of the electrospinning variables on fiber diameter were determined. (g) Three-dimensional plot of polymer solution concentration vs. collector distance vs. electrospun fiber diameter showing optimized (red) and non-optimized (blue) electrospinning conditions.

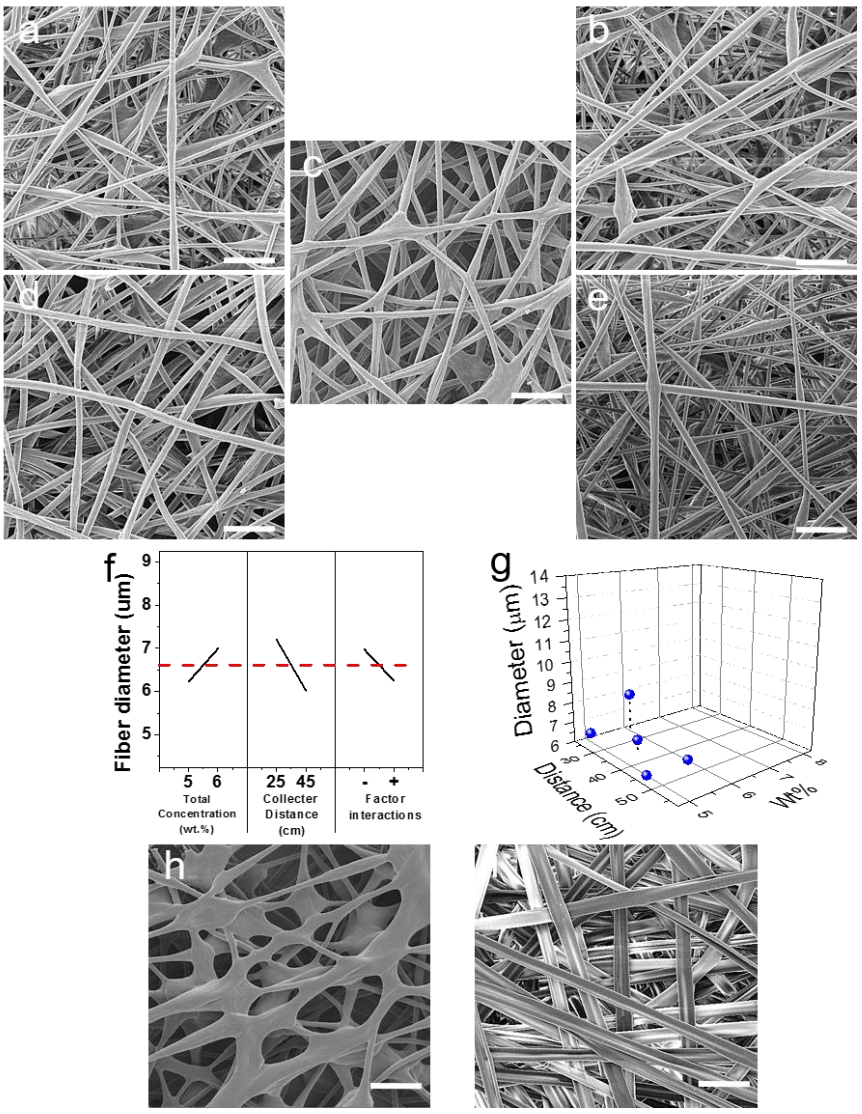

Figure S1.4.3. 75% PEG-PNIPAAm Hybrid Electrospun Fiber Optimization. Based on the DOE in Table S1 and electrospinning limits to produce a typical cylindrical fiber morphology, five conditions were electrospun: SEM images of (a) - wt. %, - D; (b) - wt. %, + D; (c) median (mid) wt. %, mid D; (d) + wt. %, - D; (e) + wt. %, + D (Scale bar = 50 µm). Average fiber diameters were digitally measured using Image J software (n=100). (f) Using the DOE, the magnitude and direction of the effect of the electrospinning variables on fiber diameter were determined. (g) Three-dimensional plot of polymer solution concentration vs. collector distance vs. electrospun fiber diameter showing the electrospinning conditions tested. All conditions produced non-optimized (blue) fiber diameters. (h) When distance was decreased further than the minimum, fiber mats became fused. (i) When wt. % was increased from the maximum, fiber morphologies became flat and limited the pore diameter of the scaffolds.

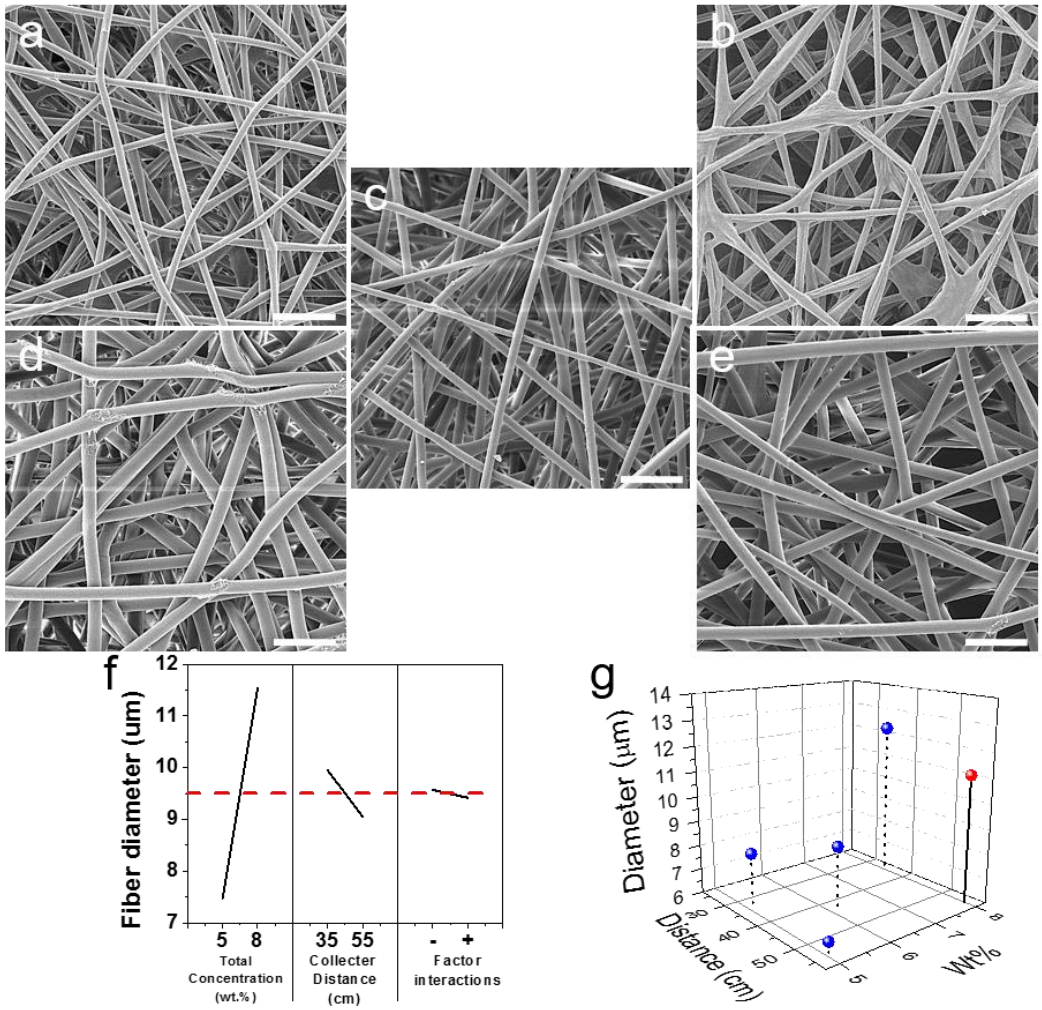

Figure S1.4.4. 65% PEG-PNIPAAm Hybrid Electrospun Fiber Optimization. To replace the 75% condition, 65% PEG-PNIPAAm scaffolds were electrospun under a similar five conditions to 25% and 50% PEG-PNIPAAm fibers: SEM images of (a) - wt. %, - D; (b) - wt. %, + D; (c) median (mid) wt. %, mid D; (d) + wt. %, - D; (e) + wt. %, + D (Scale bar = 50 μm). Average fiber diameters were digitally measured using Image J software (n=100). (f) Using the DOE, the magnitude and direction of the effect of the electrospinning variables on fiber diameter were determined. (g) Three-dimensional plot of polymer solution concentration vs. collector distance vs. electrospun fiber diameter showing optimized (red) and non-optimized (blue) electrospinning conditions.

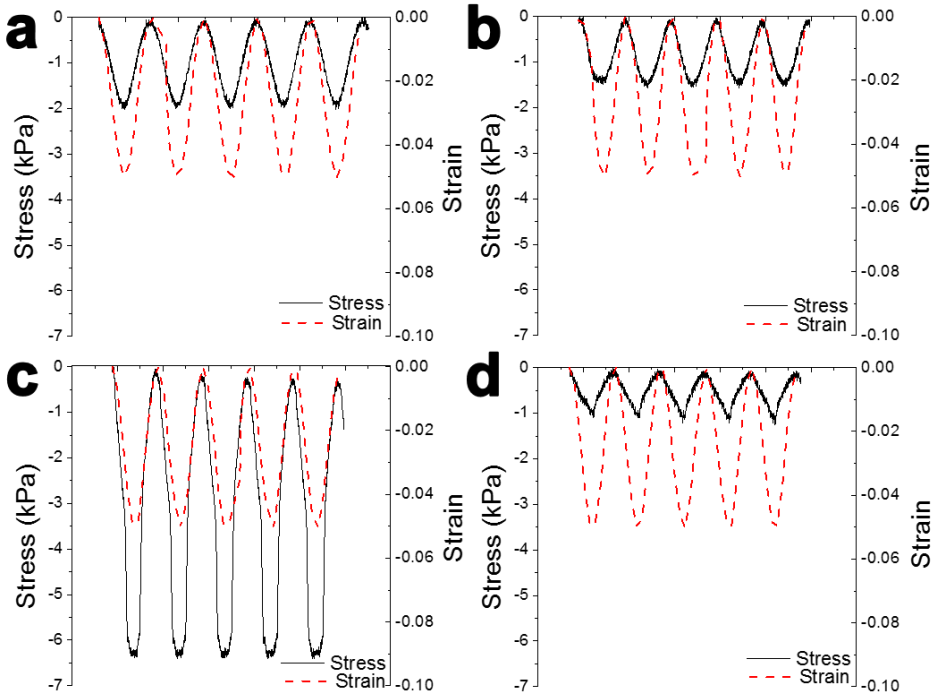

Figure S1.4.5. Representative stress-strain curves of various scaffolds under dynamic compressive forces. (a) A representative stress (solid black)-strain (dashed red) curve of the pure PCL scaffold at 23 °C. Hybrid scaffolds of 65% PEG-PNIPAAm blend were subjected to mechanical testing (b) as-synthesized at 23 °C, (c) after gelled at 37 °C and (d) after cooled to 23 °C.

APPENDIX 2. CONTROLLING APPLIED STRAIN FOR DIRECTING OSTEOGENIC DIFFERENTIATION WITH A MECHANICAL STAGE

Abstract

Scaffold stiffness has been found to direct the differentiation of stem cells. Many researchers have begun to investigate applying tensile and compressive forces upon cell structures to facilitate differentiation. Some companies have begun manufacturing devices which would allow researchers to apply tensile forces on to cell scaffolds and help direct stem cell differentiation. In this study, we have designed and built our own device that applies tensile forces to a specially designed 6-well plate with an electrospun, nanofibrous, poly (ε-caprolacetone) (PCL) scaffold. Unlike other devices on the market, our stage is designed to apply the designated amount of tensile strain by increasing the height of 6 indenters operated by an Arduino board to control six individual motors. This allows users to change the tension of the scaffolds in each well independently, and maintain it even when disconnected from the controlling computer. Using our mechanical stage during a model system test, we showed that by dynamically changing the

tensile strain of the scaffolds over the course of a two-week culture, human mesenchymal stem cells (hMSCs) can be directed to differentiate toward osteogenic gene expression by dynamically increasing or decreasing the tensile forces.

S2.1. Introduction

The use of stem cells in tissue engineering applications has been a popular choice due to their pluripotent and proliferative abilities. Utilizing them allows bioengineers to generate desired phenotypic tissue within scaffolds for tissue regeneration. Their differentiation can be initiated in a number of ways including: chemical and physical environmental cues. While the use of growth factors and small molecules can elicit a desired phenotype, they can also be initiated by inherent physical cues of their substrate[1].

By seeding cells on to a substrate, the inherent mechanical properties of the structure effect the activation and inhibition of cell signaling pathways[2-7]. Studies with stem cells have shown that a significant inherent property of the substrate is its stiffness. When mesenchymal stem cells (MSCs) are seeded on stiff substrates (>100 kPa), showed expression of osteogenic genes and their cell colony morphology appears spread out and flat[8-9]. Meanwhile, softer scaffolds produce rounder cell colony morphologies and express chondrogenic genes.

External forces can also be used to direct differentiation[10-11]. By applying a compressive or stretching/tensile force, cell substrates become stiffer and can be used to change inherently softer scaffolds, such as poly (ε-caprolactone) (PCL). With this in mind, we designed a device and scaffold combination for controlling the differentiation of stem cells. It utilizes an electrospun scaffold on a bendable PDMS mat and external forces are applied to the bottom to cause stretching. By stretching the scaffolds, the scaffold stiffness should increase and the cells

differentiation should be effected. To study its affect we produced a device of our own design to push up on the scaffold bottoms, and applied either a static force or dynamic increased or decreased the force over the course of the cell culture. Human MSCs were used as a model. We expect that by increasing the stiffness of the scaffold, we will see an increase in the osteogenic gene expression.

S2.2. Methods

S2.2.1. Electrospun Scaffold Fabrication

PCL (Sigma Aldrich) was dissolved in deionized, nano-pure water and 2,2,2-trifluoroethanol (TFE), with a v/v ratio of 1:5 and a PCL weight percent (wt.%) of 8%. Once dissolved, the PCL solution was electrospun, with a traditional vertical electrospinning setup, using previously optimized parameters for 500 nm fiber diameters, as previously described[9, 12]. Briefly, solution was pumped from a negatively charged syringe needle tip at a flow rate of 0.3 mL/hr, and was collected on a positively charged collector plate (17x12 cm), wrapped in aluminum foil, 26 cm directly below the needle tip. Scaffolds were electrospun to a thickness of around 15 μm thick, before being dried under a vacuum overnight. PCL fiber samples were examined under a Vega Scattering Electron Microscope (SEM) (Tescan) for an average fiber diameter of 500 nm.

Polydimethylsiloxane (PDMS) (Ellsworth Adhesives) was cured in a tissue culture plate lid to form a PDMS mat with a uniform thickness of 2.3 mm. Electrospun scaffolds, with a thickness of 15 μm, were transferred from the

collector plate to the cured PDMS mat while keeping the scaffold flat and relaxed. A bottomless 6-well plate was adhered to the electrospun scaffold and PDMS mat using non-sterile silicone medical adhesive (Factor II, Inc.). Thick mm thick PDMS rings were cured using a 6-well tissue culture plate and a 3D printed mold, made in-house, using a 3D Printer. Uncured PDMS was lightly applied to the underside of the PDMS rings and placed inside the wells of the bottomless 6-well plate and cured at 40 °C for 4 hours.

A two-level stage was designed and 3D printed, in house, to hold 6 individual NEMA 14 motors below the 6-well plate. Six individual indenters were 3D printed and adhered to bolts using silicon sealant. NEMA 14 motors were to allow for the adjustable movement of the indenter bolts by the motors. The motors were controlled using an Arduino code written to adjust the height of the indenters by inputting the number of steps to reach the new height (**Fig. S2.1a-b**).

S2.2.2. Scaffold Characterization

Biaxial strain of our PCL scaffolds on top of the PDMS mat was measured using a vertical displacement technique. Briefly, 12 dots were made on our scaffolds using black ink in the shape of an “X”. Pictures were taken as the scaffold was stretched, and subsequently relaxed, at different displacement heights (0 mm to 4 mm). Strain was calculated by the distance change between the dots at the different displacements. PCL scaffolds were screened for plastic deformation by comparing pictures of the scaffolds after allowing them to relax from being

stretched.

Atomic force microscopy was used to measure the reduced Young's Modulus of the PCL scaffolds using an atomic force microscope. Scaffolds were submerged in non-sterile Phosphate Buffer Solution without Mg^{2+} and Ca^{2+} (PBS) (Fisher Scientific). Tension values of the scaffolds were taken at different displacements (0 mm to 4 mm) and again after relaxation.

Scaffolds were also screened for leaks before using them to culture cells. By adding 2 mLs of Dulbecco's Modified Eagle Medium: nutrient mixture F-12 (DMEM/F12) (Fisher Scientific) and incubating them at 37 °C for three days at various heights (0 mm to 4 mm), scaffolds demonstrated an ability to withstand increasing strain under culture conditions.

S2.2.3. Cell Culture on Mechanostage

Once 6-well plate scaffolds were constructed, they were plasma treated at 30 W for 5 minutes using a Plasma Etcher. They were immediately soaked in a 100 mM N-hydroxysuccinimide/N-(3-dimethylaminopropyl)-N'-ethylcarbodiimide hydrochloride solution for PCL functionalization. Scaffolds were then crosslinked with fetal bovine collagen type I[13]. They were then sterilized with 70% ethanol and immediately washed 3x with sterile PBS. After solution was aspirated, scaffolds were dried under a fume hood blower for 12 hours before being treated for 6 hours with ultraviolet (UV) light. The stages were also sprayed with 70% ethanol and wiped clean before being treated with UV for 6 hours.

Fetal human bone marrow derived mesenchymal stem cells (MSCs) were expanded in t25 flasks with DMEM/F12 media till confluent before being seeded on to the sterilized PCL scaffolds, with a density of 6.0 x 10^5 cells/cm^2. Negative control cells were seeded on polystyrene tissue culture plates. The cells were cultured normally for three days with DMEM/F12 media. On the third day of culture, each stage was given a tensile strain condition (static at 0 mm, static at 4 mm, dynamic from 0-4 mm, and dynamic from 4-0 mm). Three wells were filled with chondrogenic media and three with osteogenic media. Cells were cultured with these media solutions for two weeks. Meanwhile the scaffold displacement of the dynamic stages was adjusted by 0.143 mm, every 12 hours. Osteogenic media was made with low glucose DMEM media with 0.1 μM Dexamethasone (Sigma Aldrich), 200 μM ascorbic acid (Sigma Aldrich), 10% fetal bovine serum (Fisher Scientific), 1% penicillin/streptomycin (Fisher Scientific) and 10 ng/mL BMP (Peprotech Inc.).

S2.2.4. Gene Expression

After a 14-day cell culture, scaffolds were washed 3x with warm and sterile PBS before the scaffolds were cut free from the PDMS mat with a scalpel and placed into cell lysis buffer (Qaigen). Using a Qaigen RNeasy MiniKit, RNA was extracted by following the manufacturer's protocol. cDNA was synthesized with the iScript cDNA Synthesis Kit (Bio-Rad) and exposed to real time-polymerase chain reaction (rt-PCR) with custom primers with SYBR Green fluorescent dye. The

following osteogenic primers were utilized: collagen type I (*COL1A1*) (forward: 5′-CAACCTGGATGCCATCAAAG-3′; reverse: 5′-TGCTGATGTACCAGTTCTTCTGG-3′), osteoclacien (*OC*) (forward: 5′-AGGCGCTACCTGTATCAATGGC-3′; reverse: 5’-TCCTGAAAGCCGATGTGGT-3’), runt-related transcription factor 2 (*RUNX2*) (forward: 5′-GAATGCACTATCCAGCCACCTT-3′; reverse: 5′-TAGTGAGTGGTGGCGGACATAC-3′), osteopontin (*OP*) (forward: 5’-TTCACTCCAGTTGTCCCCACA-3’; reverse: 5’-TGGATGTCAGGTCTGCGAAAC-3’), alkaline phosphatase (*ALP*) (forward: 5’-CCATTCCCACGTCTTCACATTT-3’; reverse: 5’-GCTTCTTGTCTGTGTCACTCAGCA-3’), and osteonectin (*ON*) (forward: 5′-TGGACTCTGAGCTGACCGAATT-3′; reverse: 5′-AGAAGGTTGTTGTCCTCATCCC-3′). GAPDH (forward: 5′-GCAAATTCCATGGCACCGT-3′; reverse: 5′-TCGCCCCACTTGATTTTGG-3′) was used as an endogenous control gene to analyze the comparative threshold of each gene expressed[14-15].

S2.2.5. Immunohistochemistry

Scaffold samples were removed after two weeks of culture and washed 3x with PBS before submerging them in 10% formaldehyde overnight. Osteogenic samples were similarly preserved and stained with Alizarin Red and Von Kossa stain for collagen type I and calcium salts, respectfully[10, 13, 16-17]. Briefly, 2% (wt/v) aqueous solution of Alizarin Red (Sigma Aldrich) was made and filtered with a 0.22

μm filter (Millipore). The solution's pH was adjusted with sodium hydroxide to 4.1-4.3 pH. Samples were soaked on glass slides for 15 minutes and rinsed with distilled water. Stained scaffolds were cover slipped with mounting media.

S2.2.6. Statistical Analysis

Three biologically independent samples were used in all experiments and were represented as an average ± their standard deviation (SD), except for gene expressions which were represented as standard error of mean (SEM). Analytical data was subjected to ANOVA and Tukey's post-hoc test using SPSS software (IBM) to determine statistical significance ($p < 0.05$).

S2.3. Results

The scaffolds fabricated were made using a PDMS mat, 2.3 mm thick and an electrospun PCL scaffold, 15 μm thick. The scaffolds were placed on top of the PDMS mats and both were adhered to a bottomless 6-well plate using medical grade adhesive. Each well was given a PDMS O-ring to improve the seal between the scaffold and the well plate. After construction of the mechanical stage and the scaffold was completed, the strain of displaced scaffold was measured. Black dots were made on the scaffolds and images were taken at different displacement height. The change in position was measured and the overall strain of the scaffold was analyzed (**Fig. S2.2**). The strain each displacement caused was evaluated, as was the strain on the scaffold as it was slowly returned to 0 mm. The maximum

displacement studied was 6 mm.

AFM testing was also done to ascertain the reduced Young's Modulus of the scaffold during stretching. Measurements were taken across random points of the scaffolds and compared as an average (**Fig. S2.3**). As the displacement increased, so did the stiffness of the scaffold. At 5 mm the reduced Young's Modulus was around 350 kPa.

For cell culture experiments, 4 mm displacements were chosen as the high in order to increase the scaffold stiffness to 200 kPa. The strain was also around 5%. hMSCs were cultured on to the scaffolds and were allowed to culture for two-weeks in osteogenic differentiation media. During the two-weeks, the dynamic scaffolds had their stiffnesses adjusted every 3 hours, continuously during the days. At night the scaffolds remained unchanged until the morning. After the cell culture period, RNA was collected from the samples and rt-PCR was run to analyze osteogenic gene expression. Cells cultured on polystyrene cell culture plates were used as the control and GAPDH was used as a comparative control gene. Cells cultured on the dynamically changing scaffolds showed many increased osteogenic genes. The static scaffold at 0 mm had no noticeable increase over the negative control samples. Scaffolds that started at a high displacement and were slowly lowered, had increased expression of collagen type I and *RUNX2*. The scaffolds that started low and increased in displacement, showed increased expression of osteopontin, osteocalcin and alkaline phosphatase. However, no changes were significantly different between the two and both had about the same

level of osteonectin expression. Histology also showed similar deposition of collagen type I in both dynamic samples. Alzarin red stain was used on samples that were collected after cell culture. The presence was much higher in the dynamic samples than in the static at 0 mm sample.

S2.4. Discussion

Our group designed a scaffold that placed a bottomless 6-well plate on top of an electrospun PCL scaffold with nanometer wide fiber diameters and a PDMS map. The PCL scaffold supplies the cells with an ECM-like substrate while the PDMS mat provides a bendable surface. The scaffold and plate was sealed with medical adhesive and PDMS O-rings and placed on a mechanical stage of our own design with six individual indenters attached to motors. Using the design of ECM as a guide, electrospun fibers have been designed to create porous, fibrous scaffolds. Seeding cells within an electrospun scaffold provides the cells with a porous environment and with polymer fibers that resemble the natural polymer matrices in the body.

The motors moved the indenters and displaced the scaffolds to the desired tension values. Cells seeded on the scaffolds expressed osteogenic gene expression when the motors were changed dynamically over the course of a two-week culture period. The design of our device allows for each well to experience its own stiffness values which is maintained even when disconnected from the controlling computer. Devices such as the FlexCell FX-5000T can also create a

radial, biaxial strain on to a cell culture substrate using pressurized gas[18]. However, their setup requires a complicated setup and must be constantly monitored and maintained by a computer during use. They also require specialized plates for their use while our design allows for the user to purchase more readily available parts and customize the scaffold with their desired electrospun scaffold.

With MSCs, high stiffness (>100 kPa) have resulted in osteogenic differentiation[8]. The reduced Young's modulus of the PCL scaffolds was analyzed with an AFM microscope. In this study we displaced our scaffolds to 4 mm to achieve 200 kPa, well above the desired stiffness for osteogenic differentiation and 10x the stiffness of the average for our control PCL scaffolds. We were also able to dynamically change the stiffness of the scaffold over the period of two weeks. By adjusting the height of the indenters every few hours, the scaffolds changed the stiffness slightly as time went on. Two separate conditions were used for dynamic testing: high to low (4-0 mm) and low to high (0-4 mm). The cells cultured on these dynamic scaffolds expressed higher osteogenic gene expression than those cultured on un-stretched PCL. Histological staining of the scaffolds showed increased deposition of collagen type I, a common ECM found with osteogenic tissue. No plastic deformation of the scaffolds was observed during testing.

These changes in phenotype and ECM deposition are due to the increased stiffness. However, further assessment of the cell scaffolds is required with an additional condition. These scaffolds should also be compared with ones maintained at 4 mm high displacement. The rate of differentiation should also be

assessed. Using a von Kossa stain it would be possible to see the calcification of the scaffolds. The longer a group of cells have been producing osteogenic ECM, the more calcified the scaffold would become. This might give us some insight into which condition produces osteogenic cells at a faster rate. The same analysis could also be done with a time-dependent study, where samples are evaluated at different time points.

S2.5. Conclusion

Our device has the potential for many applications for directing the development of stem cell differentiation. Applying individual tension to each well, increased the stiffness of the scaffold accordingly. The motor also allowed for dynamic increases or decreases in the scaffold stiffness. Changing the stiffness effected the phenotypic response of the seeded cells and increased expression of osteogenic genes. Further study on the effects of tension forces and the stiffness of the scaffolds will reveal the optimal conditions for different desired cell differentiations and using more pluripotent cells.

Acknowledgments

This study was supported by the UCR initial Complement Fund and submitted to ACS Applied Materials and Interfaces for publication. This project was studied with the help of Andrew Nguyen, Rebeccah Luu, Vinh Nguyen, Vincent Mah, Balmeet Singh and Angela Barron.

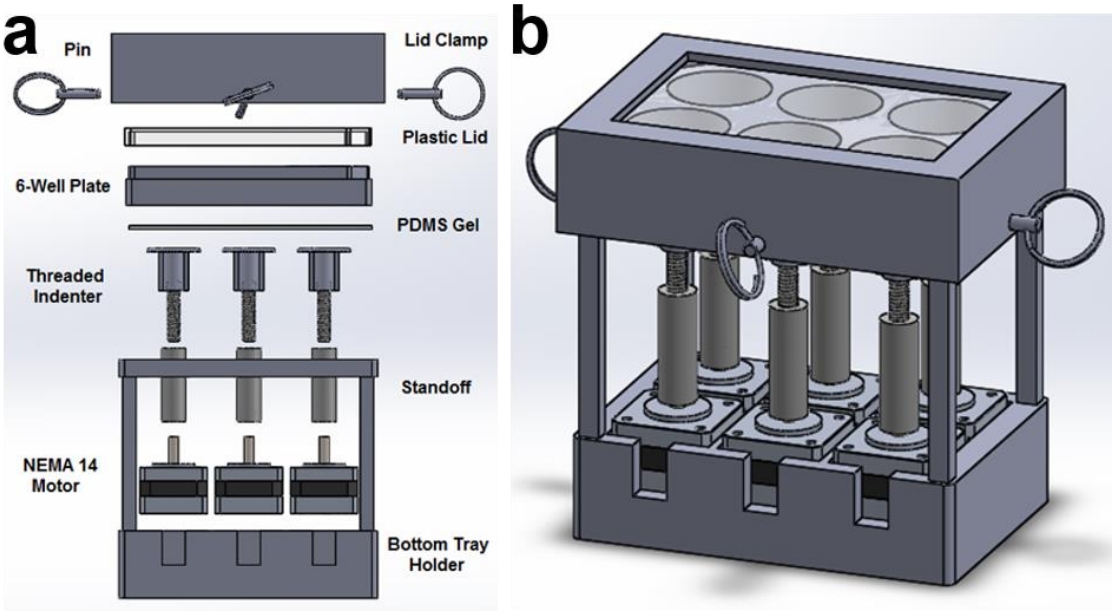

Figure S2.1. Schematic of mechanical stage device with electrospun scaffold for 2D stem cell seeding and directed hMSC differentiation. (a) An exploded view of the mechanical stage device. 2D electrospun PCL scaffolds were transferred on to a PDMS gel and adhered with medical-grade silicone adhesive to a bottomless 6-well plate. The plate is placed on the mechanical stage platform over an arrangement of six indenters and held down by lid clamp and 4 metal pins. An Arduino script is used to elevate/de-elevate threaded indenters against PDMS gel, using individual NEMA 14 motors, located on the bottom tray holder. (b) An assembled view of the mechanical stage device.

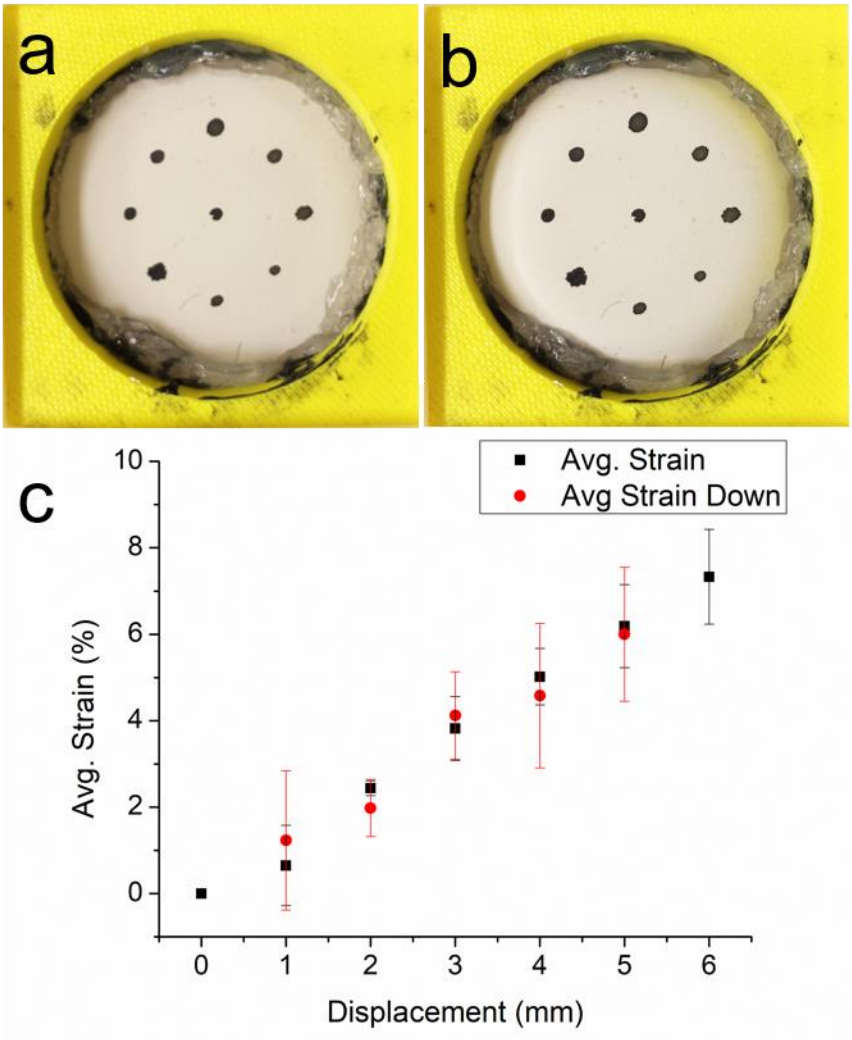

Figure S2.2. Mechanical characterization of applied scaffold displacement by mechanical stage device. Representative images of scaffolds at (a) o mm displacement and (b) 4 mm displacement. (c) The strain experienced by the PDMS and PCL scaffolds was quantified and analyzed against the displacement exerted by the threaded indenters on the scaffolds.

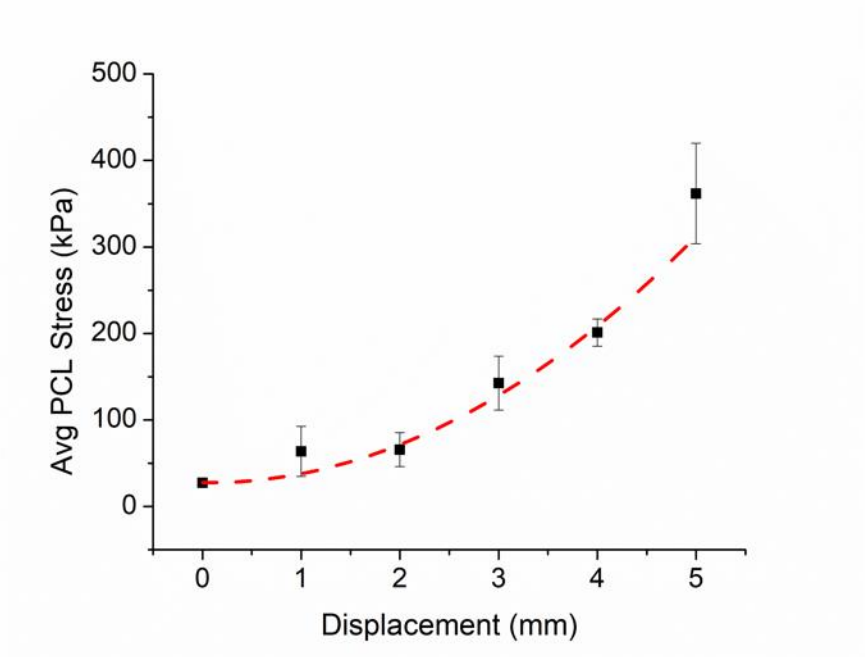

Figure S2.3. AFM measurements. Scaffolds were analyzed to determine the reduced Young's Modulus for scaffolds at various displacements.

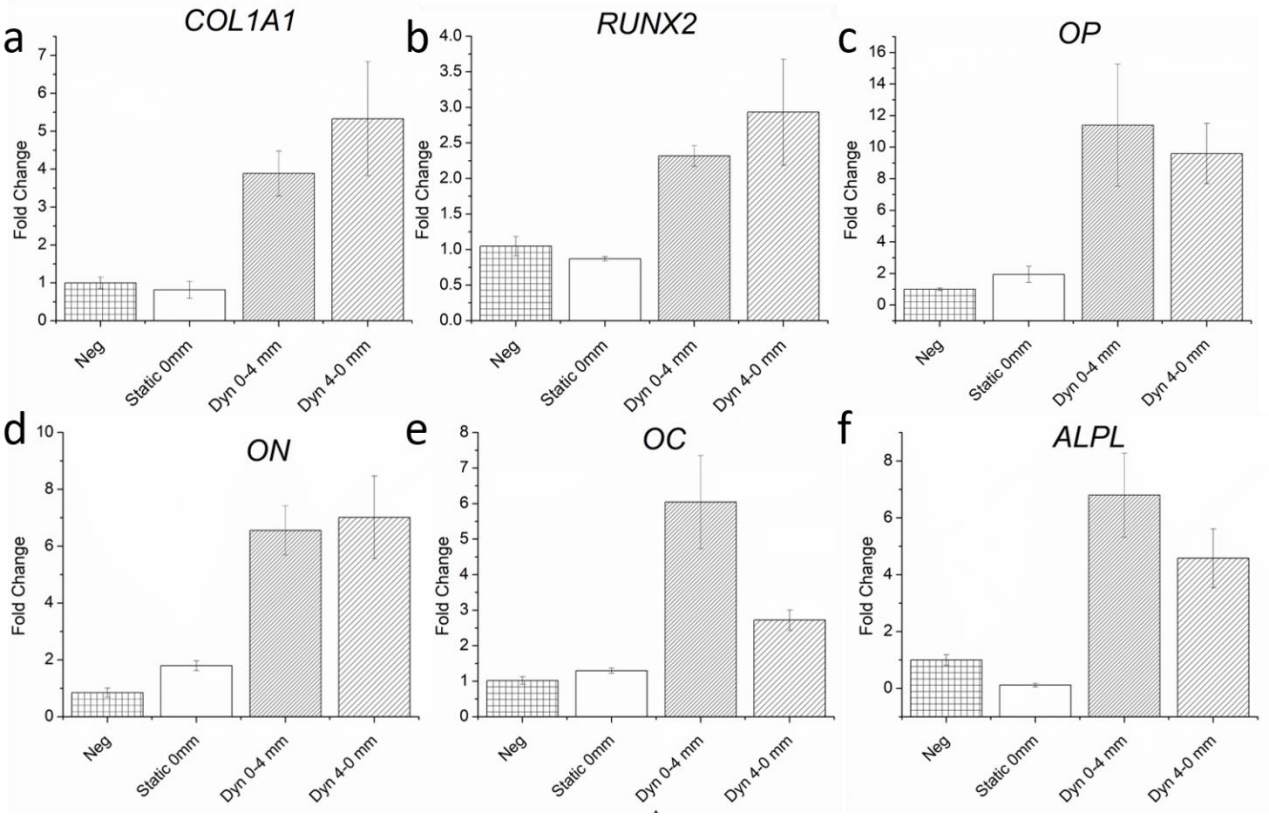

Figure S2.4. Osteogenic gene expression of human MSCs cultured on electrospun PCL scaffolds with various applied scaffold displacements. (a) Collagen type I (COL1A1), (b) RUNX2, (c) osteopontin (OP), (d) osteonectin (ON), (e) osteocalcin (OC) and (f) alkaline phosphatase (ALPL) genes were expressed higher in the cells cultured with dynamic strain for two weeks, compared to cells cultured on the Neg. control and on staic conditions at 0 mm.

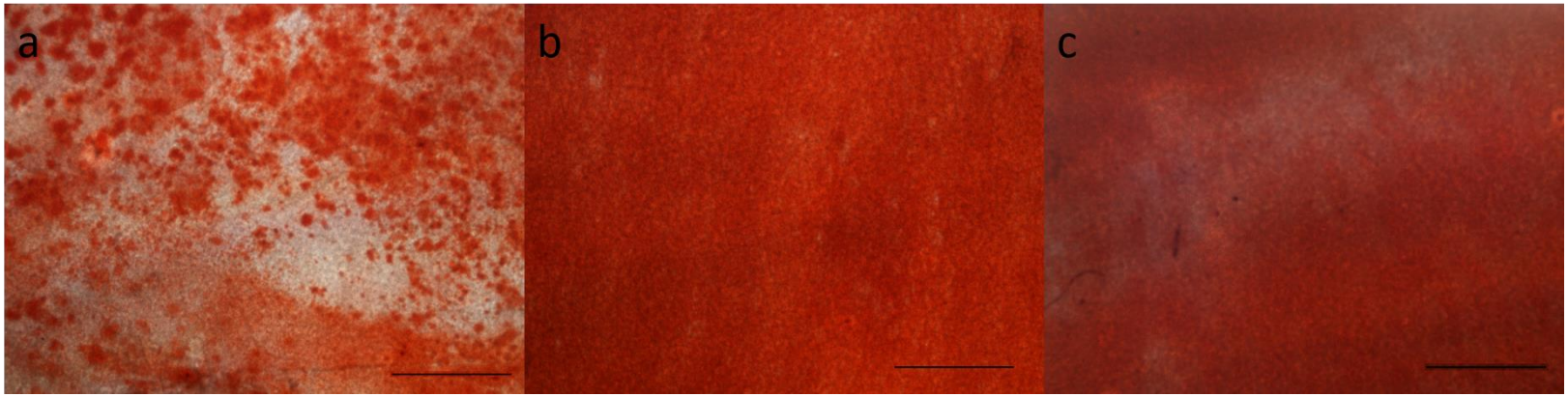

Figure S2.5. Histology images of human MSCs cultured on electrospun PCL scaffolds with various applied scaffold displacements. (a) 0 mm static samples were stained with Alizarin red and were noticeably absent of osteogenic ECM, unlike samples grown in (b) rising dynamic strain and (c)falling dynamic strain, which revealed enhanced osteogenic ECM deposition.

References

1. Higuchi, A.; Ling, Q.-D.; Chang, Y.; Hsu, S.-T.; Umezawa, A., Physical cues of biomaterials guide stem cell differentiation fate. *Chemical reviews* **2013,** *113* (5), 3297-3328.

2. Nam, J.; Johnson, J.; Lannutti, J. J.; Agarwal, S., Modulation of embryonic mesenchymal progenitor cell differentiation via control over pure mechanical modulus in electrospun nanofibers. *Acta Biomater* **2011,** *7* (4), 1516-1524.

3. Berrier, A. L.; Yamada, K. M., Cell–matrix adhesion. *Journal of cellular physiology* **2007,** *213* (3), 565-573.

4. Huebsch, N.; Arany, P. R.; Mao, A. S.; Shvartsman, D.; Ali, O. A.; Bencherif, S. A.; Rivera-Feliciano, J.; Mooney, D. J., Harnessing traction-mediated manipulation of the cell/matrix interface to control stem-cell fate. *Nature materials* **2010,** *9* (6), 518-526.

5. Lim, Y. B.; Kang, S. S.; An, W. G.; Lee, Y. S.; Chun, J. S.; Sonn, J. K., Chondrogenesis induced by actin cytoskeleton disruption is regulated via protein kinase C-dependent p38 mitogen-activated protein kinase signaling. *Journal of cellular biochemistry* **2003,** *88* (4), 713-718.

6. Woods, A.; Wang, G.; Beier, F., RhoA/ROCK signaling regulates Sox9 expression and actin organization during chondrogenesis. *Journal of Biological Chemistry* **2005,** *280* (12), 11626-11634.

7. Haudenschild, D. R.; Chen, J.; Pang, N.; Lotz, M. K.; D'Lima, D. D., Rho kinase–dependent activation of SOX9 in chondrocytes. *Arthritis & Rheumatology* **2010,** *62* (1), 191-200.

8. Shih, Y. R. V.; Tseng, K. F.; Lai, H. Y.; Lin, C. H.; Lee, O. K., Matrix stiffness regulation of integrin-mediated mechanotransduction during osteogenic differentiation of human mesenchymal stem cells. *Journal of Bone and Mineral Research* **2011,** *26* (4), 730-738.

9. Maldonado, M.; Wong, L. Y.; Echeverria, C.; Ico, G.; Low, K.; Fujimoto, T.; Johnson, J. K.; Nam, J., The effects of electrospun substrate-mediated cell colony morphology on the self-renewal of human induced pluripotent stem cells. *Biomaterials* **2015,** *50*, 10-19.

10. Horner, C. B.; Hirota, K.; Liu, J.; Maldonado, M.; Park, B. H.; Nam, J., Magnitude-Dependent and Inversely-related Osteogenic/Chondrogenic

Differentiation of Human Mesenchymal Stem Cells Under Dynamic Compressive Strain. *Journal of Tissue Engineering and Regenerative Medicine* **2016**.

11. Yim, E. K.; Sheetz, M. P., Force-dependent cell signaling in stem cell differentiation. *Stem cell research & therapy* **2012,** *3* (5), 41.

12. Maldonado, M.; Ico, G.; Low, K.; Luu, R. J.; Nam, J., Enhanced Lineage-Specific Differentiation Efficiency of Human Induced Pluripotent Stem Cells by Engineering Colony Dimensionality Using Electrospun Scaffolds. *Advanced healthcare materials* **2016,** *5* (12), 1408-1412.

13. Nam, J.; Perera, P.; Rath, B.; Agarwal, S., Dynamic regulation of bone morphogenetic proteins in engineered osteochondral constructs by biomechanical stimulation. *Tissue engineering. Part A* **2013,** *19* (5-6), 783-92.

14. Livak, K. J.; Schmittgen, T. D., Analysis of relative gene expression data using real-time quantitative PCR and the 2(-Delta Delta C(T)) Method. *Methods* **2001,** *25* (4), 402-8.

15. Schmittgen, T. D.; Livak, K. J., Analyzing real-time PCR data by the comparative CT method. *Nature protocols* **2008,** *3* (6), 1101-1108.

16. Wall, A.; Board, T., Mesenchymal Cell-Based Repair of Large Full Thickness Defects of Articular Cartilage. In *Classic Papers in Orthopaedics*, Springer: **2014**, pp 441-443.

17. Nam, J.; Huang, Y.; Agarwal, S.; Lannutti, J., Improved cellular infiltration in electrospun fiber via engineered porosity. *Tissue engineering* **2007,** *13* (9), 2249-2257.

18. Huang, C. H.; Chen, M. H.; Young, T. H.; Jeng, J. H.; Chen, Y. J., Interactive effects of mechanical stretching and extracellular matrix proteins on initiating osteogenic differentiation of human mesenchymal stem cells. *Journal of cellular biochemistry* **2009,** *108* (6), 1263-1273.

BIBLIOGRAPHY

Achilli, M. and D. Mantovani (2010). "Tailoring mechanical properties of collagen-based scaffolds for vascular tissue engineering: the effects of pH, temperature and ionic strength on gelation." Polymers **2**(4): 664-680.

Adelöw, C., T. Segura, et al. (2008). "The effect of enzymatically degradable poly (ethylene glycol) hydrogels on smooth muscle cell phenotype." Biomaterials **29**(3): 314-326.

Aguilar, M., C. Elvira, et al. (2007). "Smart polymers and their applications as biomaterials." Topics in tissue engineering **3**(6).

Ahmed, E. M. (2015). "Hydrogel: Preparation, characterization, and applications: A review." Journal of Advanced Research **6**(2): 105-121.

Alexander, A., J. Khan, et al. (2014). "Polyethylene glycol (PEG)–Poly (N-isopropylacrylamide)(PNIPAAm) based thermosensitive injectable hydrogels for biomedical applications." European Journal of Pharmaceutics and Biopharmaceutics **88**(3): 575-585.

Angele, P., D. Schumann, et al. (2004). "Cyclic, mechanical compression enhances chondrogenesis of mesenchymal progenitor cells in tissue engineering scaffolds." Biorheology **41**(3-4): 335-346.

Anseth, K. S., C. M. Wang, et al. (1994). "Kinetic evidence of reaction diffusion during the polymerization of multi (meth) acrylate monomers." Macromolecules **27**(3): 650-655.

Anton, F. (1934). Process and apparatus for preparing artificial threads, Google Patents.

Asma, C., E. Meriem, et al. (2014). "Physicochemical characterization of gelatin-cmc composite edibles films from polyion-complex hydrogels." Journal of the Chilean Chemical Society **59**(1): 2279-2283.

Baier Leach, J., K. A. Bivens, et al. (2003). "Photocrosslinked hyaluronic acid hydrogels: natural, biodegradable tissue engineering scaffolds." Biotechnology and bioengineering **82**(5): 578-589.

Bakshi, A., O. Fisher, et al. (2004). "Mechanically engineered hydrogel scaffolds for axonal growth and angiogenesis after transplantation in spinal cord injury." Journal of Neurosurgery: Spine **1**(3): 322-329.

Balke, S. and A. Hamielec (1973). "Bulk polymerization of methyl methacrylate." Journal of Applied Polymer Science **17**(3): 905-949.

Balke, S. T. and A. E. Hamielec (1973). "Bulk polymerization of methyl methacrylate." Journal of Applied Polymer Science **17**(3): 905-949.

Bartnikowski, M., R. M. Wellard, et al. (2015). "Tailoring hydrogel viscoelasticity with physical and chemical crosslinking." Polymers **7**(12): 2650-2669.

Benoit, D. S., M. P. Schwartz, et al. (2008). "Small functional groups for controlled differentiation of hydrogel-encapsulated human mesenchymal stem cells." Nature materials **7**(10): 816-823.

Berrier, A. L. and K. M. Yamada (2007). "Cell–matrix adhesion." Journal of cellular physiology **213**(3): 565-573.

Bhattarai, N., J. Gunn, et al. (2010). "Chitosan-based hydrogels for controlled, localized drug delivery." Advanced drug delivery reviews **62**(1): 83-99.

Bianco, P. and P. G. Robey (2001). "Stem cells in tissue engineering." Nature **414**(6859): 118-121.

Bosnakovski, D., M. Mizuno, et al. (2006). "Chondrogenic differentiation of bovine bone marrow mesenchymal stem cells (MSCs) in different hydrogels: influence of collagen type II extracellular matrix on MSC chondrogenesis." Biotechnology and bioengineering **93**(6): 1152-1163.

Bourke, S. L., M. Al-Khalili, et al. (2003). "A photo-crosslinked poly (vinyl alcohol) hydrogel growth factor release vehicle for wound healing applications." The AAPS Journal **5**(4): 101-111.

Boutris, C., E. Chatzi, et al. (1997). "Characterization of the LCST behaviour of aqueous poly (N-isopropylacrylamide) solutions by thermal and cloud point techniques." Polymer **38**(10): 2567-2570.

Brannigan, R. P. and A. P. Dove (2017). "Synthesis, properties and biomedical applications of hydrolytically degradable materials based on aliphatic polyesters and polycarbonates." Biomaterials Science **5**(1): 9-21.

Brannon-Peppas, L. and N. A. Peppas (1991). "Equilibrium swelling behavior of pH-sensitive hydrogels." Chemical Engineering Science **46**(3): 715-722.

Brazel, C. S. and N. A. Peppas (1995). "Synthesis and characterization of thermo- and chemomechanically responsive poly (N-isopropylacrylamide-co-methacrylic acid) hydrogels." Macromolecules **28**(24): 8016-8020.

Broz, M., D. L. VanderHart, et al. (2003). "Structure and mechanical properties of poly (D, L-lactic acid)/poly (ε-caprolactone) blends." Biomaterials **24**(23): 4181-4190.

Bryant, S. J., T. T. Chowdhury, et al. (2004). "Crosslinking density influences chondrocyte metabolism in dynamically loaded photocrosslinked poly (ethylene glycol) hydrogels." Annals of biomedical engineering **32**(3): 407-417.

Bryant, S. J., C. R. Nuttelman, et al. (2000). "Cytocompatibility of UV and visible light photoinitiating systems on cultured NIH/3T3 fibroblasts in vitro." Journal of Biomaterials Science, Polymer Edition **11**(5): 439-457.

Burdick, J. A. and K. S. Anseth (2002). "Photoencapsulation of osteoblasts in injectable RGD-modified PEG hydrogels for bone tissue engineering." Biomaterials **23**(22): 4315-4323.

Cao, H. and N. Kuboyama (2010). "A biodegradable porous composite scaffold of PGA/β-TCP for bone tissue engineering." Bone **46**(2): 386-395.

Carter, D. R., G. S. Beaupré, et al. (2004). "The mechanobiology of articular cartilage development and degeneration." Clinical orthopaedics and related research **427**: S69-S77.

Casper, C. L., J. S. Stephens, et al. (2004). "Controlling surface morphology of electrospun polystyrene fibers: effect of humidity and molecular weight in the electrospinning process." Macromolecules **37**(2): 573-578.

Caycik, S. and R. Jagger (1992). "The effect of cross-linking chain length on mechanical properties of a dough-molded poly (methylmethacrylate) resin." Dental Materials **8**(3): 153-157.

Cellesi, F. and N. Tirelli (2005). "A new process for cell microencapsulation and other biomaterial applications: Thermal gelation and chemical cross-linking in “tandem”." Journal of materials science: materials in medicine **16**(6): 559-565.

Cellesi, F., N. Tirelli, et al. (2004). "Towards a fully-synthetic substitute of alginate: development of a new process using thermal gelation and chemical cross-linking." Biomaterials **25**(21): 5115-5124.

Cha, C., J. H. Jeong, et al. (2011). "Tuning the dependency between stiffness and permeability of a cell encapsulating hydrogel with hydrophilic pendant chains." Acta biomaterialia **7**(10): 3719-3728.

Cha, C., R. H. Kohman, et al. (2009). "Biodegradable polymer crosslinker: independent control of stiffness, toughness, and hydrogel degradation rate." Advanced Functional Materials **19**(19): 3056-3062.

Chen, J. P. and T. H. Cheng (2006). "Thermo-Responsive Chitosan-graft-poly (N-isopropylacrylamide) Injectable Hydrogel for Cultivation of Chondrocytes and Meniscus Cells." Macromolecular bioscience **6**(12): 1026-1039.

Chen, M., M. Dong, et al. (2010). "Thermo-responsive core− sheath electrospun nanofibers from poly (N-isopropylacrylamide)/polycaprolactone blends." Chemistry of Materials **22**(14): 4214-4221.

Chou, A. I., S. O. Akintoye, et al. (2009). "Photo-crosslinked alginate hydrogels support enhanced matrix accumulation by nucleus pulposus cells in vivo." Osteoarthritis and cartilage **17**(10): 1377-1384.

Chu, C. (1981). "The in-vitro degradation of poly (glycolic acid) sutures—effect of pH." Journal of Biomedical Materials Research Part A **15**(6): 795-804.

Chu, C. R., R. D. Coutts, et al. (1995). "Articular cartilage repair using allogeneic perichondrocyteseeded biodegradable porous polylactic acid (PLA): A tissue-engineering study." Journal of biomedical materials research **29**(9): 1147-1154.

Colombani, D. (1997). "Chain-growth control in free radical polymerization." Progress in polymer science **22**(8): 1649-1720.

Comolli, N., B. Neuhuber, et al. (2009). "In vitro analysis of PNIPAAm-PEG, a novel, injectable scaffold for spinal cord repair." Acta Biomater **5**(4): 1046-1055.

Conova, L., J. Vernengo, et al. (2011). "A pilot study of poly (N-isopropylacrylamide)-g-polyethylene glycol and poly (N-isopropylacrylamide)-g-methylcellulose branched copolymers as injectable scaffolds for local delivery of neurotrophins and cellular transplants into the injured spinal cord: Laboratory investigation." Journal of Neurosurgery: Spine **15**(6): 594-604.

Cooperstein, M. A. and H. E. Canavan (2013). "Assessment of cytotoxicity of (N-isopropyl acrylamide) and Poly (N-isopropyl acrylamide)-coated surfaces." Biointerphases **8**(1): 19.

Cowan, P. J. and A. J. Tector (2017). "The Resurgence of Xenotransplantation." American Journal of transplantation.

Cukierman, E., R. Pankov, et al. (2001). "Taking cell-matrix adhesions to the third dimension." Science **294**(5547): 1708-1712.

Damink, L. O., P. Dijkstra, et al. (1995). "Glutaraldehyde as a crosslinking agent for collagen-based biomaterials." Journal of materials science: materials in medicine **6**(8): 460-472.

Deitzel, J., J. Kleinmeyer, et al. (2001). "Controlled deposition of electrospun poly (ethylene oxide) fibers." Polymer **42**(19): 8163-8170.

Derwent, J. J. K. and W. F. Mieler (2008). "Thermoresponsive hydrogels as a new ocular drug delivery platform to the posterior segment of the eye." Transactions of the American Ophthalmological Society **106**: 206.

Devine, D. M. and C. L. Higginbotham (2005). "Synthesis and characterisation of chemically crosslinked N-vinyl pyrrolidinone (NVP) based hydrogels." European Polymer Journal **41**(6): 1272-1279.

Doshi, J. and D. H. Reneker (1995). "Electrospinning process and applications of electrospun fibers." Journal of electrostatics **35**(2-3): 151-160.

Drapala, P. W., E. M. Brey, et al. (2011). "Role of thermo-responsiveness and poly (ethylene glycol) diacrylate cross-link density on protein release from poly (N-isopropylacrylamide) hydrogels." Journal of Biomaterials Science, Polymer Edition **22**(1-3): 59-75.

Drury, J. L. and D. J. Mooney (2003). "Hydrogels for tissue engineering: scaffold design variables and applications." Biomaterials **24**(24): 4337-4351.

Duan, Y., Z. Wang, et al. (2007). "Preparation of collagen-coated electrospun nanofibers by remote plasma treatment and their biological properties." Journal of Biomaterials Science, Polymer Edition **18**(9): 1153-1164.

Eichhorn, S. J. and W. W. Sampson (2005). "Statistical geometry of pores and statistics of porous nanofibrous assemblies." Journal of the Royal Society Interface **2**(4): 309-318.

El-Sherbiny, I. M. and M. H. Yacoub (2013). "Hydrogel scaffolds for tissue engineering: Progress and challenges." Global Cardiology Science and Practice: 38.

Elisseeff, J., K. Anseth, et al. (1999). "Transdermal photopolymerization for minimally invasive implantation." Proceedings of the National Academy of Sciences **96**(6): 3104-3107.

Elisseeff, J., W. McIntosh, et al. (2000). "Photoencapsulation of chondrocytes in poly (ethylene oxide)-based semi-interpenetrating networks." Journal of biomedical materials research **51**(2): 164-171.

Eljarrat-Binstock, E., A. Bentolila, et al. (2007). "Preparation, characterization, and sterilization of hydrogel sponges for iontophoretic drug-delivery use." Polymers for Advanced Technologies **18**(9): 720-730.

Engelberg, I. and J. Kohn (1991). "Physico-mechanical properties of degradable polymers used in medical applications: a comparative study." Biomaterials **12**(3): 292-304.

Fedorovich, N. E., M. H. Oudshoorn, et al. (2009). "The effect of photopolymerization on stem cells embedded in hydrogels." Biomaterials **30**(3): 344-353.

Fernández de La Mora, J. (2007). "The fluid dynamics of Taylor cones." Annu. Rev. Fluid Mech. **39**: 217-243.

Fisher, J. P., D. Dean, et al. (2001). "Photoinitiated polymerization of biomaterials." Annual review of materials research **31**(1): 171-181.

Fong, H., I. Chun, et al. (1999). "Beaded nanofibers formed during electrospinning." Polymer **40**(16): 4585-4592.

Fridrikh, S., J. Yu, et al. (2003). Nonlinear whipping behavior of electrified fluid jets, ACS Publications.

Fukamachi, K., D. J. Horvath, et al. (2010). "An innovative, sensorless, pulsatile, continuous-flow total artificial heart: device design and initial in vitro study." The Journal of Heart and Lung Transplantation **29**(1): 13-20.

Garg, K. and G. L. Bowlin (2011). "Electrospinning jets and nanofibrous structures." Biomicrofluidics **5**(1): 013403.

Geever, L. M., D. M. Devine, et al. (2006). "Lower critical solution temperature control and swelling behaviour of physically crosslinked thermosensitive copolymers based on N-isopropylacrylamide." European Polymer Journal **42**(10): 2540-2548.

Gentile, P., V. Chiono, et al. (2014). "An overview of poly (lactic-co-glycolic) acid (PLGA)-based biomaterials for bone tissue engineering." International journal of molecular sciences **15**(3): 3640-3659.

Giancotti, F. G. and E. Ruoslahti (1999). "Integrin signaling." Science **285**(5430):

1028-1033.

Gomoll, A. H. and T. Minas (2014). "The quality of healing: articular cartilage." Wound Repair and Regeneration **22**(S1): 30-38.

Grayson, W. L., T. Ma, et al. (2004). "Human mesenchymal stem cells tissue development in 3D PET matrices." Biotechnology progress **20**(3): 905-912.

Grinberg, V. Y., A. S. Dubovik, et al. (2000). "Studies of the thermal volume transition of poly (N-isopropylacrylamide) hydrogels by high-sensitivity differential scanning microcalorimetry. 2. Thermodynamic functions." Macromolecules **33**(23): 8685-8692.

Gu, B. K., D. J. Choi, et al. (2016). "3-dimensional bioprinting for tissue engineering applications." Biomaterials research **20**(1): 12.

Guilak, F., D. L. Butler, et al. (2001). "Functional tissue engineering: the role of biomechanics in articular cartilage repair." Clinical orthopaedics and related research **391**: S295-S305.

Gunatillake, P. A. and R. Adhikari (2003). "Biodegradable synthetic polymers for tissue engineering." Eur Cell Mater **5**(1): 1-16.

Hamidi, M., A. Azadi, et al. (2008). "Hydrogel nanoparticles in drug delivery." Advanced drug delivery reviews **60**(15): 1638-1649.

Haraguchi, K., H.-J. Li, et al. (2005). "Mechanism of forming organic/inorganic network structures during in-situ free-radical polymerization in PNIPA− clay nanocomposite hydrogels." Macromolecules **38**(8): 3482-3490.

Haudenschild, D. R., J. Chen, et al. (2010). "Rho kinase–dependent activation of SOX9 in chondrocytes." Arthritis & Rheumatology **62**(1): 191-200.

He, J.-H., Y. Wu, et al. (2005). "Critical length of straight jet in electrospinning." Polymer **46**(26): 12637-12640.

Helary, C., I. Bataille, et al. (2010). "Concentrated collagen hydrogels as dermal substitutes." Biomaterials **31**(3): 481-490.

Hench, L. L. (1991). "Bioceramics: from concept to clinic." Journal of the american ceramic society **74**(7): 1487-1510.

Hench, L. L. and E. Ethridge (1972). "Biomaterials: an interfacial approach." Academic Press, Inc., 1972: 385.

Hennink, W. and C. F. Van Nostrum (2012). "Novel crosslinking methods to design

hydrogels." Advanced drug delivery reviews **64**: 223-236.

Heydarkhan-Hagvall, S., K. Schenke-Layland, et al. (2008). "Three-dimensional electrospun ECM-based hybrid scaffolds for cardiovascular tissue engineering." Biomaterials **29**(19): 2907-2914.

Higuera, F. (2003). "Flow rate and electric current emitted by a Taylor cone." Journal of Fluid Mechanics **484**: 303-327.

Holzwarth, J. M. and P. X. Ma (2011). "Biomimetic nanofibrous scaffolds for bone tissue engineering." Biomaterials **32**(36): 9622-9629.

Hood, J. D. and D. A. Cheresh (2002). "Role of integrins in cell invasion and migration." Nature Reviews Cancer **2**(2): 91-100.

Horner, C. B., K. Hirota, et al. (2016). "Magnitude-Dependent and Inversely-related Osteogenic/Chondrogenic Differentiation of Human Mesenchymal Stem Cells Under Dynamic Compressive Strain." Journal of Tissue Engineering and Regenerative Medicine.

Horner, C. B., G. Ico, et al. (2016). "Microstructure-dependent mechanical properties of electrospun core–shell scaffolds at multi-scale levels." journal of the mechanical behavior of biomedical materials **59**: 207-219.

Hoyle, C. E. and J. F. Kinstle (1990). Radiation curing of polymeric materials, ACS Publications.

Huang, M.-H., S. Li, et al. (2004). "Synthesis and degradation of PLA–PCL–PLA triblock copolymer prepared by successive polymerization of ε-caprolactone and dl-lactide." Polymer **45**(26): 8675-8681.

Huang, X. and T. L. Lowe (2005). "Biodegradable thermoresponsive hydrogels for aqueous encapsulation and controlled release of hydrophilic model drugs." Biomacromolecules **6**(4): 2131-2139.

Huebsch, N., P. R. Arany, et al. (2010). "Harnessing traction-mediated manipulation of the cell/matrix interface to control stem-cell fate." Nature materials **9**(6): 518-526.

Hwang, N. S., S. Varghese, et al. (2006). "Chondrogenic differentiation of human embryonic stem cell–derived cells in arginine-glycine-aspartate–modified hydrogels." Tissue engineering **12**(9): 2695-2706.

Ico, G., A. Showalter, et al. (2016). "Size-dependent piezoelectric and mechanical properties of electrospun P (VDF-TrFE) nanofibers for enhanced energy

harvesting." Journal of Materials Chemistry A **4**(6): 2293-2304.

Iooss, P., A.-M. Le Ray, et al. (2001). "A new injectable bone substitute combining poly (ε-caprolactone) microparticles with biphasic calcium phosphate granules." Biomaterials **22**(20): 2785-2794.

Ishii, O., M. Shin, et al. (2005). "In vitro tissue engineering of a cardiac graft using a degradable scaffold with an extracellular matrix–like topography." The Journal of thoracic and cardiovascular surgery **130**(5): 1358-1363.

Islamova, R., Y. I. Puzin, et al. (2006). "A ternary initiating system for free-radical polymerization of methyl methacrylate." Polymer Science Series B **48**(3): 130-133.

Itskovitz-Eldor, J., M. Schuldiner, et al. (2000). "Differentiation of human embryonic stem cells into embryoid bodies compromising the three embryonic germ layers." Molecular medicine **6**(2): 88.

Jeong, B., Y. H. Bae, et al. (1997). "Biodegradable block copolymers as injectable drug-delivery systems." Nature **388**(6645): 860-862.

Jeong, B., S. W. Kim, et al. (2012). "Thermosensitive sol–gel reversible hydrogels." Advanced drug delivery reviews **64**: 154-162.

Jiang, B., J. C. Larson, et al. (2012). "Investigation of lysine acrylate containing poly (N-isopropylacrylamide) hydrogels as wound dressings in normal and infected wounds." Journal of Biomedical Materials Research Part B: Applied Biomaterials **100**(3): 668-676.

Jiang, Y., B. N. Jahagirdar, et al. (2002). "Pluripotency of mesenchymal stem cells derived from adult marrow." Nature **418**(6893): 41-49.

Jin, K., J. W. Simpkins, et al. (2015). "The critical need to promote research of aging and aging-related diseases to improve health and longevity of the elderly population." Aging and disease **6**(1): 1.

Jin, R., L. M. Teixeira, et al. (2009). "Injectable chitosan-based hydrogels for cartilage tissue engineering." Biomaterials **30**(13): 2544-2551.

Kai, D., M. P. Prabhakaran, et al. (2012). "Mechanical properties and in vitro behavior of nanofiber–hydrogel composites for tissue engineering applications." Nanotechnology **23**(9): 095705.

Kang, H.-W., S. J. Lee, et al. (2016). "A 3D bioprinting system to produce human-scale tissue constructs with structural integrity." Nature biotechnology **34**(3):

312-319.

Kang, H.-W., Y. Tabata, et al. (1999). "Fabrication of porous gelatin scaffolds for tissue engineering." Biomaterials **20**(14): 1339-1344.

Kang, X., Y. Xie, et al. (2007). "Adipogenesis of murine embryonic stem cells in a three-dimensional culture system using electrospun polymer scaffolds." Biomaterials **28**(3): 450-458.

Karp, J. M., M. S. Shoichet, et al. (2003). "Bone formation on two-dimensional poly (DL-lactide-co-glycolide)(PLGA) films and three-dimensional PLGA tissue engineering scaffolds in vitro." Journal of Biomedical Materials Research Part A **64**(2): 388-396.

Khan, M. Z. I., Ž. Prebeg, et al. (1999). "A pH-dependent colon targeted oral drug delivery system using methacrylic acid copolymers: I. Manipulation of drug release using Eudragit® L100-55 and Eudragit® S100 combinations." Journal of Controlled Release **58**(2): 215-222.

Kiatkamjornwong, S. (2007). "Superabsorbent polymers and superabsorbent polymer composites." Science Asia **33**(S1): 39-43.

Kim, M. S., S. J. Park, et al. (2011). "Thermosensitive hydrogels for tissue engineering." Tissue Engineering and Regenerative Medicine **8**(2): 117-123.

Kim, T. G., D. S. Lee, et al. (2007). "Controlled protein release from electrospun biodegradable fiber mesh composed of poly (ε-caprolactone) and poly (ethylene oxide)." International journal of pharmaceutics **338**(1): 276-283.

Klouda, L. and A. G. Mikos (2008). "Thermoresponsive hydrogels in biomedical applications." European journal of pharmaceutics and biopharmaceutics **68**(1): 34-45.

Kong, H. J., E. Alsberg, et al. (2004). "Controlling degradation of hydrogels via the size of crosslinked junctions." Advanced materials **16**(21): 1917-1921.

Koombhongse, S., W. Liu, et al. (2001). "Flat polymer ribbons and other shapes by electrospinning." Journal of Polymer Science Part B: Polymer Physics **39**(21): 2598-2606.

Kraeutler, M. J., J. T. Bravman, et al. (2013). "Bone–patellar tendon–bone autograft versus allograft in outcomes of anterior cruciate ligament reconstruction: a meta-analysis of 5182 patients." The American journal of sports medicine **41**(10): 2439-2448.

Kuo, C. K. and P. X. Ma (2001). "Ionically crosslinked alginate hydrogels as scaffolds for tissue engineering: part 1. Structure, gelation rate and mechanical properties." Biomaterials **22**(6): 511-521.

L'heureux, N., S. Pâquet, et al. (1998). "A completely biological tissue-engineered human blood vessel." The FASEB Journal **12**(1): 47-56.

Lee, J. H., R. K. Prud'Homme, et al. (2001). "Cure depth in photopolymerization: experiments and theory." Journal of Materials Research **16**(12): 3536-3544.

Lee, K., H. Kim, et al. (2003). "The change of bead morphology formed on electrospun polystyrene fibers." Polymer **44**(14): 4029-4034.

Lee, K. Y. and D. J. Mooney (2001). "Hydrogels for tissue engineering." Chemical reviews **101**(7): 1869-1880.

Lim, Y. B., S. S. Kang, et al. (2003). "Chondrogenesis induced by actin cytoskeleton disruption is regulated via protein kinase C-dependent p38 mitogen-activated protein kinase signaling." Journal of cellular biochemistry **88**(4): 713-718.

Lin, T., H. Wang, et al. (2004). "The charge effect of cationic surfactants on the elimination of fibre beads in the electrospinning of polystyrene." Nanotechnology **15**(9): 1375.

Lin, Y.-H., H.-F. Liang, et al. (2005). "Physically crosslinked alginate/N, O-carboxymethyl chitosan hydrogels with calcium for oral delivery of protein drugs." Biomaterials **26**(14): 2105-2113.

Liu, S. Q., R. Tay, et al. (2010). "Synthetic hydrogels for controlled stem cell differentiation." Soft matter **6**(1): 67-81.

Liu, W., J. Zhan, et al. (2014). "Injectable hydrogel incorporating with nanoyarn for bone regeneration." Journal of Biomaterials Science, Polymer Edition **25**(2): 168-180.

Liu, X. Y., J.-M. Nothias, et al. (2010). "Biocompatibility investigation of polyethylene glycol and alginate-poly-L-lysine for islet encapsulation." ASAIO journal **56**(3): 241-245.

Livak, K. J. and T. D. Schmittgen (2001). "Analysis of relative gene expression data using real-time quantitative PCR and the 2(-Delta Delta C(T)) Method." Methods **25**(4): 402-408.

Long, J. L., P. Zuk, et al. (2010). "Epithelial differentiation of adipose-derived stem

cells for laryngeal tissue engineering." The Laryngoscope **120**(1): 125-131.

Lu, Z., B. Z. Doulabi, et al. (2009). "Collagen type II enhances chondrogenesis in adipose tissue–derived stem cells by affecting cell shape." Tissue Engineering Part A **16**(1): 81-90.

Luyn, M., P. Wachem, et al. (1995). "Calcification of subcutaneously implanted collagens in relation to cytotoxicity, cellular interactions and crosslinking." Journal of materials science: materials in medicine **6**(5): 288-296.

Maldonado, M., G. Ico, et al. (2016). "Enhanced Lineage-Specific Differentiation Efficiency of Human Induced Pluripotent Stem Cells by Engineering Colony Dimensionality Using Electrospun Scaffolds." Advanced healthcare materials **5**(12): 1408-1412.

Maldonado, M., L. Y. Wong, et al. (2015). "The effects of electrospun substrate-mediated cell colony morphology on the self-renewal of human induced pluripotent stem cells." Biomaterials **50**: 10-19.

Mansur, H. S., C. M. Sadahira, et al. (2008). "FTIR spectroscopy characterization of poly (vinyl alcohol) hydrogel with different hydrolysis degree and chemically crosslinked with glutaraldehyde." Materials Science and Engineering: C **28**(4): 539-548.

Marklein, R. A. and J. A. Burdick (2010). "Controlling stem cell fate with material design." Advanced materials **22**(2): 175-189.

Marletta, G., G. Ciapetti, et al. (2007). "Improved osteogenic differentiation of human marrow stromal cells cultured on ion-induced chemically structured poly-ε-caprolactone." Biomaterials **28**(6): 1132-1140.

Martens, P. J., S. J. Bryant, et al. (2003). "Tailoring the degradation of hydrogels formed from multivinyl poly (ethylene glycol) and poly (vinyl alcohol) macromers for cartilage tissue engineering." Biomacromolecules **4**(2): 283-292.

Megelski, S., J. S. Stephens, et al. (2002). "Micro-and nanostructured surface morphology on electrospun polymer fibers." Macromolecules **35**(22): 8456-8466.

Mehta, S. and K. Powale (2013). "Organ-on-A-Chip." The Bombay Technologist **62**: 44-53.

Mironi-Harpaz, I., D. Y. Wang, et al. (2012). "Photopolymerization of cell-encapsulating hydrogels: crosslinking efficiency versus cytotoxicity." Acta

biomaterialia **8**(5): 1838-1848.

Mohabatpour, F., A. Karkhaneh, et al. (2016). "A hydrogel/fiber composite scaffold for chondrocyte encapsulation in cartilage tissue regeneration." RSC Advances **6**(86): 83135-83145.

Moore, W. R., S. E. Graves, et al. (2001). "Synthetic bone graft substitutes." ANZ journal of surgery **71**(6): 354-361.

Morimoto, N., A. Mahara, et al. (2016). "An evaluation of the engraftment and the blood flow of porcine skin autografts inactivated by high hydrostatic pressure." Journal of Biomedical Materials Research Part B: Applied Biomaterials.

Munton, T. and A. Russell (1973). "Effect of glutaraldehyde on cell viability, triphenyltetrazolium reduction, oxygen uptake, and β-galactosidase activity in Escherichia coli." Applied microbiology **26**(4): 508-511.

Murphy, S. V. and A. Atala (2014). "3D bioprinting of tissues and organs." Nature biotechnology **32**(8): 773-785.

Nam, J., Y. Huang, et al. (2007). "Improved cellular infiltration in electrospun fiber via engineered porosity." Tissue engineering **13**(9): 2249-2257.

Nam, J., Y. Huang, et al. (2008). "Materials selection and residual solvent retention in biodegradable electrospun fibers." Journal of Applied Polymer Science **107**(3): 1547-1554.

Nam, J., J. Johnson, et al. (2011). "Modulation of embryonic mesenchymal progenitor cell differentiation via control over pure mechanical modulus in electrospun nanofibers." Acta Biomater **7**(4): 1516-1524.

Nam, J., P. Perera, et al. (2012). "Dynamic regulation of bone morphogenetic proteins in engineered osteochondral constructs by biomechanical stimulation." Tissue Engineering Part A **19**(5-6): 783-792.

Nam, J., P. Perera, et al. (2013). "Dynamic regulation of bone morphogenetic proteins in engineered osteochondral constructs by biomechanical stimulation." Tissue Eng Part A **19**(5-6): 783-792.

Nam, J., B. Rath, et al. (2008). "Novel electrospun scaffolds for the molecular analysis of chondrocytes under dynamic compression." Tissue Engineering Part A **15**(3): 513-523.

Neergaard-Petersen, S., R. Ajjan, et al. (2013). "Fibrin clot structure and platelet

aggregation in patients with aspirin treatment failure." PloS one **8**(8): e71150.

Neffe, A. T., T. Gebauer, et al. (2013). Tailoring of mechanical properties of diisocyanate crosslinked gelatin-based hydrogels. MRS Proceedings, Cambridge Univ Press.

Nguyen, K. T. and J. L. West (2002). "Photopolymerizable hydrogels for tissue engineering applications." Biomaterials **23**(22): 4307-4314.

Nichol, J. W. and A. Khademhosseini (2009). "Modular tissue engineering: engineering biological tissues from the bottom up." Soft matter **5**(7): 1312-1319.

Nijenhuis, A., D. Grijpma, et al. (1992). "Lewis acid catalyzed polymerization of L-lactide. Kinetics and mechanism of the bulk polymerization." Macromolecules **25**(24): 6419-6424.

Nishi, C., N. Nakajima, et al. (1995). "In vitro evaluation of cytotoxicity of diepoxy compounds used for biomaterial modification." Journal of Biomedical Materials Research Part A **29**(7): 829-834.

Noble, B., V. Dean, et al. (1995). "Dextran sulfate promotes the rapid aggregation of porcine bone-marrow stromal cells." Bone **17**(4): 375-382.

Okuzaki, H., K. Kobayashi, et al. (2009). "Non-woven fabric of poly (N-isopropylacrylamide) nanofibers fabricated by electrospinning." Synthetic metals **159**(21): 2273-2276.

Okuzaki, H., K. Kobayashi, et al. (2009). "Thermo-responsive nanofiber mats." Macromolecules **42**(16): 5916-5918.

Omidian, H. and K. Park (2012). Hydrogels. Fundamentals and applications of controlled release drug delivery, Springer**:** 75-105.

Park, H., J. S. Temenoff, et al. (2007). "Injectable biodegradable hydrogel composites for rabbit marrow mesenchymal stem cell and growth factor delivery for cartilage tissue engineering." Biomaterials **28**(21): 3217-3227.

Park, J. (2012). Biomaterials science and engineering, Springer Science & Business Media.

Patrick Jr, C., P. Chauvin, et al. (1999). "Preadipocyte seeded PLGA scaffolds for adipose tissue engineering." Tissue engineering **5**(2): 139-151.

Peng, C. K., S. H. Yu, et al. (2006). "Polysaccharide-based artificial extracellular

matrix: Preparation and characterization of three-dimensional, macroporous chitosan and chondroitin sulfate composite scaffolds." Journal of Applied Polymer Science **99**(5): 2091-2100.

Pilipchuk, S. P., M. K. Vaicik, et al. (2013). "Influence of crosslinking on the stiffness and degradation of dermis-derived hydrogels." Journal of Biomedical Materials Research Part A **101**(10): 2883-2895.

Pitt, C. G., F. Chasalow, et al. (1981). "Aliphatic polyesters. I. The degradation of poly (ϵ-caprolactone) in vivo." Journal of Applied Polymer Science **26**(11): 3779-3787.

Pitt, G., M. Gratzl, et al. (1981). "Aliphatic polyesters II. The degradation of poly (DL-lactide), poly (ε-caprolactone), and their copolymers in vivo." Biomaterials **2**(4): 215-220.

Place, E. S., J. H. George, et al. (2009). "Synthetic polymer scaffolds for tissue engineering." Chemical Society Reviews **38**(4): 1139-1151.

Platt, J. L., R. J. Fischel, et al. (1991). "Immunopathology of hyperacute xenograft rejection in a swine-to-primate model." Transplantation **52**(2): 214-220.

Port, F. K., D. M. Dykstra, et al. (2005). "Trends and results for organ donation and transplantation in the United States, 2004." American Journal of transplantation **5**(4p2): 843-849.

Porter, J. R., A. Henson, et al. (2009). "Biocompatibility and Mesenchymal Stem Cell Response to Poly (ε-Caprolactone) Nanowire Surfaces for Orthopedic Tissue Engineering." Tissue Engineering Part A **15**(9): 2547-2559.

Probes, M. (2005). LIVE/DEAD® Viability/Cytotoxicity Kit* for mammalian cells*, MP.

Qiu, Y. and K. Park (2001). "Environment-sensitive hydrogels for drug delivery." Advanced drug delivery reviews **53**(3): 321-339.

Qu, X., A. Wirsen, et al. (2000). "Novel pH-sensitive chitosan hydrogels: swelling behavior and states of water." Polymer **41**(12): 4589-4598.

Rajzer, I., E. Menaszek, et al. (2014). "Electrospun gelatin/poly (ε-caprolactone) fibrous scaffold modified with calcium phosphate for bone tissue engineering." Materials Science and Engineering: C **44**: 183-190.

Ramanan, R. M. K., P. Chellamuthu, et al. (2006). "Development of a temperature-sensitive composite hydrogel for drug delivery applications." Biotechnology

progress **22**(1): 118-125.

Rault, I., V. Frei, et al. (1996). "Evaluation of different chemical methods for cros-linking collagen gel, films and sponges." Journal of materials science: materials in medicine **7**(4): 215-221.

Rawlinson, J. (1994). "Morbidity after anterior cervical decompression and fusion. The influence of the donor site on recovery, and the results of a trial of surgibone compared to autologous bone." Acta neurochirurgica **131**(1): 106-118.

Reneker, D. H. and I. Chun (1996). "Nanometre diameter fibres of polymer, produced by electrospinning." Nanotechnology **7**(3): 216.

Reneker, D. H., A. L. Yarin, et al. (2000). "Bending instability of electrically charged liquid jets of polymer solutions in electrospinning." Journal of Applied physics **87**(9): 4531-4547.

Rockwood, D. N., D. B. Chase, et al. (2008). "Characterization of electrospun poly (N-isopropyl acrylamide) fibers." Polymer **49**(18): 4025-4032.

Sabnis, A., M. Rahimi, et al. (2009). "Cytocompatibility studies of an in situ photopolymerized thermoresponsive hydrogel nanoparticle system using human aortic smooth muscle cells." Journal of Biomedical Materials Research Part A **91**(1): 52-59.

Saghafi, H., R. Palazzetti, et al. (2013). "Impact response of glass/epoxy laminate interleaved with nanofibrous mats." Engineering Solid Mechanics **1**(3): 85-90.

Schmaljohann, D. (2006). "Thermo-and pH-responsive polymers in drug delivery." Advanced drug delivery reviews **58**(15): 1655-1670.

Schmaljohann, D., J. Oswald, et al. (2003). "Thermo-responsive PNiPAAm-g-PEG films for controlled cell detachment." Biomacromolecules **4**(6): 1733-1739.

Schmittgen, T. D. and K. J. Livak (2008). "Analyzing real-time PCR data by the comparative CT method." Nature protocols **3**(6): 1101-1108.

Schuurman, W., V. Khristov, et al. (2011). "Bioprinting of hybrid tissue constructs with tailorable mechanical properties." Biofabrication **3**(2): 021001.

Shim, W. S., J.-H. Kim, et al. (2006). "Biodegradability and biocompatibility of a pH-and thermo-sensitive hydrogel formed from a sulfonamide-modified poly (ε-caprolactone-co-lactide)–poly (ethylene glycol)–poly (ε-caprolactone-co-

lactide) block copolymer." Biomaterials **27**(30): 5178-5185.

Smith, C. M., A. L. Stone, et al. (2004). "Three-dimensional bioassembly tool for generating viable tissue-engineered constructs." Tissue engineering **10**(9-10): 1566-1576.

Solursh, M., T. F. Linsenmayer, et al. (1982). "Chondrogenesis from single limb mesenchyme cells." Developmental biology **94**(1): 259-264.

Son, W. K., J. H. Youk, et al. (2004). "The effects of solution properties and polyelectrolyte on electrospinning of ultrafine poly (ethylene oxide) fibers." Polymer **45**(9): 2959-2966.

Son, W. K., J. H. Youk, et al. (2004). "Electrospinning of ultrafine cellulose acetate fibers: studies of a new solvent system and deacetylation of ultrafine cellulose acetate fibers." Journal of Polymer Science Part B: Polymer Physics **42**(1): 5-11.

Sophia Fox, A. J., A. Bedi, et al. (2009). "The basic science of articular cartilage: structure, composition, and function." Sports health **1**(6): 461-468.

Stanishevsky, A., J. Wetuski, et al. (2015). "Ribbon-like and spontaneously folded structures of tungsten oxide nanofibers fabricated via electrospinning." RSC Advances **5**(85): 69534-69542.

Sun, D., C. Chang, et al. (2006). "Near-field electrospinning." Nano letters **6**(4): 839-842.

Sun, G., X. Zhang, et al. (2011). "Dextran hydrogel scaffolds enhance angiogenic responses and promote complete skin regeneration during burn wound healing." Proceedings of the National Academy of Sciences **108**(52): 20976-20981.

Sun, H., L. Mei, et al. (2006). "The in vivo degradation, absorption and excretion of PCL-based implant." Biomaterials **27**(9): 1735-1740.

Sun, H. W., R. Feigal, et al. (1990). "Cytotoxicity of glutaraldehyde and formaldehyde in relation to time of exposure and concentration." Pediatr Dent **12**(5): 303-307.

Sung, H. W., D. M. Huang, et al. (1999). "Evaluation of gelatin hydrogel crosslinked with various crosslinking agents as bioadhesives: in vitro study." Journal of Biomedical Materials Research Part A **46**(4): 520-530.

Swift, T., L. Swanson, et al. (2016). "The pH-responsive behaviour of poly (acrylic

acid) in aqueous solution is dependent on molar mass." Soft matter **12**(9): 2542-2549.

Takahashi, K., K. Tanabe, et al. (2007). "Induction of pluripotent stem cells from adult human fibroblasts by defined factors." cell **131**(5): 861-872.

Tallawi, M., E. Rosellini, et al. (2015). "Strategies for the chemical and biological functionalization of scaffolds for cardiac tissue engineering: a review." Journal of the Royal Society Interface **12**(108): 20150254.

Tan, H. and K. G. Marra (2010). "Injectable, biodegradable hydrogels for tissue engineering applications." Materials **3**(3): 1746-1767.

Taylor, M., A. Daniels, et al. (1994). "Six bioabsorbable polymers: in vitro acute toxicity of accumulated degradation products." Journal of applied biomaterials **5**(2): 151-157.

Teo, W. E., W. He, et al. (2006). "Electrospun scaffold tailored for tissue-specific extracellular matrix." Biotechnology journal **1**(9): 918-929.

Toh, W. S., E. H. Lee, et al. (2010). "Cartilage repair using hyaluronan hydrogel-encapsulated human embryonic stem cell-derived chondrogenic cells." Biomaterials **31**(27): 6968-6980.

Tomazic, B., W. Brown, et al. (1994). "Physicochemical properties of calcific deposits isolated from porcine bioprosthetic heart valves removed from patients following 2–13 years function." Journal of biomedical materials research **28**(1): 35-47.

Tong, X., J. Zheng, et al. (2007). "Swelling and mechanical behaviors of carbon nanotube/poly (vinyl alcohol) hybrid hydrogels." Materials Letters **61**(8): 1704-1706.

Turner, D. (1977). "Autoacceleration of free-radical polymerization. 1. The critical concentration." Macromolecules **10**(2): 221-226.

Turturro, S. B., M. J. Guthrie, et al. (2011). "The effects of cross-linked thermo-responsive PNIPAAm-based hydrogel injection on retinal function." Biomaterials **32**(14): 3620-3626.

Vernengo, J., G. Fussell, et al. (2008). "Evaluation of novel injectable hydrogels for nucleus pulposus replacement." Journal of Biomedical Materials Research Part B: Applied Biomaterials **84**(1): 64-69.

Villasante, A. and G. Vunjak-Novakovic (2015). "Tissue-engineered models of

human tumors for cancer research." Expert opinion on drug discovery **10**(3): 257-268.

Wakitani, S., T. Goto, et al. (1994). "Mesenchymal cell-based repair of large, full-thickness defects of articular cartilage." J Bone Joint Surg Am **76**(4): 579-592.

Wall, A. and T. Board (2014). Mesenchymal Cell-Based Repair of Large Full Thickness Defects of Articular Cartilage. Classic Papers in Orthopaedics, Springer**:** 441-443.

Wang, J., J. Zhang, et al. (2013). "A protein-based hydrogel for in vitro expansion of mesenchymal stem cells." PloS one **8**(9): e75727.

Wang, L. S., J. Boulaire, et al. (2010). "The role of stiffness of gelatin-hydroxyphenylpropionic acid hydrogels formed by enzyme-mediated crosslinking on the differentiation of human mesenchymal stem cell." Biomaterials **31**(33): 8608-8616.

Wannatong, L., A. Sirivat, et al. (2004). "Effects of solvents on electrospun polymeric fibers: preliminary study on polystyrene." Polymer International **53**(11): 1851-1859.

Ward, M. A. and T. K. Georgiou (2011). "Thermoresponsive polymers for biomedical applications." Polymers **3**(3): 1215-1242.

Webb, A. R., J. Yang, et al. (2004). "Biodegradable polyester elastomers in tissue engineering." Expert opinion on biological therapy **4**(6): 801-812.

Wong, S. (2010). "An investigation of process parameters to optimize the fiber diameter of electrospun vascular scaffolds through experimental design."

Woods, A., G. Wang, et al. (2005). "RhoA/ROCK signaling regulates Sox9 expression and actin organization during chondrogenesis." Journal of Biological Chemistry **280**(12): 11626-11634.

Woodward, S. C., P. Brewer, et al. (1985). "The intracellular degradation of poly (ε-caprolactone)." Journal of Biomedical Materials Research Part A **19**(4): 437-444.

Wu, X., L. Black, et al. (2007). "Preparation and assessment of glutaraldehyde-crosslinked collagen–chitosan hydrogels for adipose tissue engineering." Journal of Biomedical Materials Research Part A **81**(1): 59-65.

Xu, T., K. W. Binder, et al. (2012). "Hybrid printing of mechanically and biologically

improved constructs for cartilage tissue engineering applications." Biofabrication **5**(1): 015001.

Yakushiji, T., K. Sakai, et al. (1999). "Effects of cross-linked structure on temperature-responsive hydrophobic interaction of poly (N-isopropylacrylamide) hydrogel-modified surfaces with steroids." Analytical Chemistry **71**(6): 1125-1130.

Yan, D., J. Jones, et al. (2013). "Plasma treatment of random and aligned electrospun pcl nanofibers." Journal of Medical and Biological Engineering **33**(2): 171-178.

Yang, G.-Z., H.-P. Li, et al. (2017). "Influence of Working Temperature on The Formation of Electrospun Polymer Nanofibers." Nanoscale research letters **12**(1): 55.

Yao, J., C. W. Bastiaansen, et al. (2014). "High strength and high modulus electrospun nanofibers." Fibers **2**(2): 158-186.

Yarin, A. L., S. Koombhongse, et al. (2001). "Taylor cone and jetting from liquid droplets in electrospinning of nanofibers." Journal of Applied physics **90**(9): 4836-4846.

Yoo, H. S., E. A. Lee, et al. (2005). "Hyaluronic acid modified biodegradable scaffolds for cartilage tissue engineering." Biomaterials **26**(14): 1925-1933.

Yost, M. J., C. M. Gore, et al. (2011). Apparatus for producing tissue scaffold having aligned fibrils, Google Patents.

Yu, L. and J. Ding (2008). "Injectable hydrogels as unique biomedical materials." Chemical Society Reviews **37**(8): 1473-1481.

Zampetti, E., A. Muzyczuk, et al. (2011). "Effects of temperature and humidity on electrospun conductive nanofibers based on polyaniline blends." Journal of Nanoparticle Research **13**(11): 6193-6200.

Zanetti, N. C. and M. Solursh (1984). "Induction of chondrogenesis in limb mesenchymal cultures by disruption of the actin cytoskeleton." The Journal of cell biology **99**(1): 115-123.

Zhang, J., Z. Yang, et al. (2013). "Cells behave distinctly within sponges and hydrogels due to differences of internal structure." Tissue Engineering Part A **19**(19-20): 2166-2175.

Zhang, Y., H. Ouyang, et al. (2005). "Electrospinning of gelatin fibers and

gelatin/PCL composite fibrous scaffolds." Journal of Biomedical Materials Research Part B: Applied Biomaterials **72**(1): 156-165.

Zhao, W., X. Jin, et al. (2013). "Degradable natural polymer hydrogels for articular cartilage tissue engineering." Journal of Chemical Technology and Biotechnology **88**(3): 327-339.

Zhao, X., X. Sun, et al. (2017). "Cell infiltrative hydrogel fibrous scaffolds for accelerated wound healing." Acta biomaterialia **49**: 66-77.